



LUND UNIVERSITY

Cerebrospinal fluid circulation and the glymphatic system in health and disease

Kritsilis, Marios

2025

Document Version:

Publisher's PDF, also known as Version of record

[Link to publication](#)

Citation for published version (APA):

Kritsilis, M. (2025). *Cerebrospinal fluid circulation and the glymphatic system in health and disease*. [Doctoral Thesis (compilation), Department of Experimental Medical Science]. Lund University, Faculty of Medicine.

Total number of authors:

1

General rights

Unless other specific re-use rights are stated the following general rights apply:

Copyright and moral rights for the publications made accessible in the public portal are retained by the authors and/or other copyright owners and it is a condition of accessing publications that users recognise and abide by the legal requirements associated with these rights.

- Users may download and print one copy of any publication from the public portal for the purpose of private study or research.
- You may not further distribute the material or use it for any profit-making activity or commercial gain
- You may freely distribute the URL identifying the publication in the public portal


Read more about Creative commons licenses: <https://creativecommons.org/licenses/>

Take down policy

If you believe that this document breaches copyright please contact us providing details, and we will remove access to the work immediately and investigate your claim.

LUND UNIVERSITY

PO Box 117
221 00 Lund
+46 46-222 00 00



The illustration depicts a human brain at the top and a heart at the bottom, connected by a thick, braided red structure representing the glymphatic system. Red vessels indicate arterial blood flow, while blue vessels indicate venous blood flow. The brain's surface is covered with a network of these vessels, and the heart shows its own internal circulation. The background is a light blue gradient.

Cerebrospinal fluid circulation and the glymphatic system in health and disease

MARIOS KRITSILIS

EXPERIMENTAL MEDICAL SCIENCE | FACULTY OF MEDICINE | LUND UNIVERSITY



About the author

MARIOS KRITSILIS studied Medicine at the National and Kapodistrian University of Athens, Greece. His interest in neuroscience led him to Lund, where he joined the Glia-Immune Interactions lab. During his doctoral studies, Marios investigated the mechanisms of cerebrospinal fluid circulation and the glymphatic system in different disease models.



Cerebrospinal fluid circulation
and the glymphatic system in health and disease

Cerebrospinal fluid circulation and the glymphatic system in health and disease

Marios Kriksilis



LUND
UNIVERSITY

DOCTORAL DISSERTATION

Doctoral dissertation for the degree of Doctor of Philosophy (PhD) at the
Faculty of Medicine, Lund University, Sweden.

To be publicly defended on 7th of May 2025 at 13:15 in Belfragesalen,
BMC D15, Lund University, Lund, Sweden

Faculty opponent

Rune Enger

Professor of Neuroscience
University of Oslo, Norway

Organization: LUND UNIVERSITY Department of Experimental Medical Science, Faculty of Medicine

Document name: Doctoral Dissertation

Date of issue: 7 May 2025

Author: Marios Kritsilis

Title and subtitle: Cerebrospinal fluid circulation and the glymphatic system in health and disease

Abstract:

Cerebrospinal fluid (CSF) circulation is a complex process that is still not fully understood. Despite decades of research on CSF and its distinct functions, there still remain a number of open questions regarding the mechanisms that govern its circulation. The recently discovered glymphatic system, which is mostly active during sleep, clears the brain from extracellular metabolites and waste products. Yet many parameters of these functions have not been investigated in several disease conditions, while the methods to study them are also constantly evolving.

This thesis aims to elucidate some of the mechanisms of CSF circulation and the glymphatic system in health and disease. The first study investigated how the glymphatic system is affected by heart failure (HF). The study found evidence of dysregulation of brain fluid dynamics in mice with HF, while cerebral blood flow emerged as a potential new regulator of glymphatic clearance. The second study compared the efficacy of different lectins and staining methods in labeling cerebral vasculature as an important step for aquaporin 4 polarization studies, which is a crucial component of glymphatic function. The third study investigated the main pathways through which CSF leaves the central nervous system and confirmed that the nasal pathway is a major CSF efflux route that can readily adapt to different pathophysiological challenges. The fourth study looked at the interaction of amyloid beta (A β) in the CSF with glymphatic function using a pig model developed in our lab. The study found that CSF distribution and glymphatic influx were impaired in pigs injected with A β in the CSF, while A β was found to co-localize with elastin elements across the cerebral arterial walls.

Overall, these studies highlight the importance of understanding the mechanisms behind the glymphatic system and CSF circulation, and how they relate to various diseases.

Key words: neurodegeneration, cardiovascular diseases, neurofluids, MRI, microscopy, animal models

Classification system and/or index terms (if any)

Supplementary bibliographical information

Language: English, with popular summaries in Swedish and Greek

Number of pages: 92

ISSN and key title: 1652-8220

ISBN: 978-91-8021-712-5

Recipient's notes

Price

Security classification

I, the undersigned, being the copyright owner of the abstract of the above-mentioned dissertation, hereby grant to all reference sources permission to publish and disseminate the abstract of the above-mentioned dissertation.

Signature

Date 2024-03-24

Cerebrospinal fluid circulation and the glymphatic system in health and disease

Marios Kriksilis



LUND
UNIVERSITY

Cover art © Maria Carlos Oliveira

Copyright pp 1-92 Marios Kritsilis

Paper 1 © Oxford University Press

Paper 2 © MDPI

Paper 3 © by the Authors (Manuscript unpublished)

Paper 4 © by the Authors (Manuscript unpublished)

Faculty of Medicine

Department of Experimental Medical Science

ISBN 978-91-8021-712-5

ISSN 1652-8220

Printed in Sweden by Media-Tryck, Lund University

Lund 2025



Media-Tryck is a Nordic Swan Ecolabel
certified provider of printed material.
Read more about our environmental
work at www.mediatryck.lu.se

MADE IN SWEDEN 

Table of Contents

| | |
|---|-----------|
| List of original papers and manuscripts..... | 9 |
| Published papers and manuscripts not included in the thesis..... | 10 |
| Popular summary | 11 |
| Populärvetenskaplig sammanfattning | 13 |
| Περίληψη..... | 15 |
| Abbreviations..... | 17 |
| Introduction | 19 |
| Cerebrospinal fluid circulation..... | 19 |
| Cerebrospinal fluid production..... | 19 |
| The ventricular system and the subarachnoid space..... | 20 |
| Cerebrospinal fluid efflux | 21 |
| The nasal efflux pathway..... | 21 |
| Other cranial and spinal nerves | 22 |
| Meningeal lymphatics | 23 |
| The glymphatic system..... | 25 |
| The perivascular spaces | 26 |
| Aquaporin-4..... | 27 |
| Drivers of the glymphatic system..... | 28 |
| Models to study the glymphatic system | 32 |
| The glymphatic system and neurodegeneration | 37 |
| Aims of the thesis | 39 |
| Key Methods | 41 |
| Animals | 41 |
| Mice (Papers I -III)..... | 41 |
| Pigs (Papers III – IV)..... | 41 |
| Surgery and disease models | 42 |
| CM injection in mice (Papers I, III and IV) | 42 |
| CM injection in pigs (Papers III and IV)..... | 42 |
| Intraparenchymal tracer injection (Paper I)..... | 43 |
| Cranial window preparation (Paper I) | 43 |

| | |
|---|-----------|
| Heart failure mouse model (Paper I) | 44 |
| Transient middle cerebral artery occlusion (tMCAo) (Paper II) | 44 |
| Ablation of olfactory sensory neurons (Paper III) | 44 |
| In vivo imaging and analysis..... | 44 |
| MRI (Papers I and III) | 44 |
| In vivo two-photon imaging of arterial pulsatility (Paper I)..... | 46 |
| In vivo transcranial fluorescence imaging (Papers III and IV)..... | 47 |
| Tissue processing, imaging and analysis..... | 47 |
| Ex vivo fluorescence imaging (Papers I, III and IV)..... | 47 |
| Immunohistochemistry (Papers I, II and IV)..... | 48 |
| Tissue clearing and light-sheet microscopy (Papers I, III and IV) | 48 |
| Summary of Results and Discussion | 51 |
| Dysregulation of brain fluid dynamics in heart failure (Paper I) | 51 |
| HF leads to increased glymphatic influx by enhancing arterial pulsatility | 51 |
| Glymphatic mismatch between influx and clearance leads to a relative increase in brain parenchyma volume | 52 |
| CBF emerges as a potentially new regulator of the glymphatic system | 54 |
| Differential efficacy of lectins in cerebral blood vessel labeling (Paper II).56 | |
| Superior efficacy of LEA lectin in labeling cerebral vasculature..... | 56 |
| Reduced labeling specificity in ischemic stroke..... | 56 |
| Functional characteristics of the nasal CSF efflux pathway. (Paper III)..... | 60 |
| Nasal efflux adapts to changes in CM injection rate | 60 |
| The nasal efflux pathway remains active in aging | 60 |
| Circulating A β ₁₋₄₂ leads to reduced nasal efflux | 62 |
| Ablation of olfactory sensory neurons impairs nasal efflux | 63 |
| A β ₁₋₄₂ clearance pathways in the gyrencephalic brain (Paper IV)..... | 65 |
| Circulating A β ₁₋₄₂ causes global impairment in glymphatic influx..... | 65 |
| A β ₁₋₄₂ is retained at the proximal PVS influx sites | 65 |
| A β ₁₋₄₂ co-localizes with elastin across the cerebral arterial wall | 68 |
| Conclusions and Future perspectives | 71 |
| Reflection on methods and final remarks | 73 |
| References | 75 |
| Acknowledgements | 91 |

List of original papers and manuscripts

This thesis is based on the following papers and manuscripts:

I. Loss of glymphatic homeostasis in heart failure

Kritsilis M, Vanherle L, Rosenholm M, in 't Zandt R, Yao Y, Swanberg KM, Weikop P, Gottschalk M, Shanbhag NC, Luo J, Boster K, Nedergaard M, Meissner A, Lundgaard I

Brain. 2024 Dec 18;awae411. doi: 10.1093/brain/awae411

II. Not All Lectins Are Equally Suitable for Labeling Rodent Vasculature

Battistella R, **Kritsilis M**, Matuskova H, Haswell D, Cheng AX, Meissner A, Nedergaard M, Lundgaard I

Int J Mol Sci. 2021 Oct 26;22(21):11554. doi: 10.3390/ijms222111554.

III. Functional aspects of CSF efflux dynamics (manuscript)

Shanbhag NC*, **Kritsilis M***, Jukkola J*, Bèchet NB, Swanberg KM, Liu C, Liu X, Liu N, Johansson E, Sime W, Massoumi R, in 't Zandt R and Lundgaard I

IV. An arterial transmural entrapment system prevents amyloid recirculation into the brain (manuscript)

Bèchet NB, Shanbhag NC, **Kritsilis M**, Liu C, Leon F, Meissner A and Lundgaard I

Published papers and manuscripts not included in the thesis

I. DNase Treatment Prevents Cerebrospinal Fluid Block in Early Experimental Pneumococcal Meningitis

Pavan C*, L R Xavier A*, Ramos M, Fisher J, **Kritsilis M**, Linder A, Bentzer P, Nedergaard M and Lundgaard I

Ann Neurol. 2021 Oct;90(4):653-669. doi: 10.1002/ana.26186.

II. Impaired cerebrospinal fluid transport due to idiopathic subdural hematoma in pig: an unusual case

Shanbhag NC, Bèchet NB, **Kritsilis M** and Lundgaard I

BMC Vet Res. 2021 Jul 20;17(1):250. doi: 10.1186/s12917-021-02954-2.

III. Effect of systemic hypothermia on glymphatic function (manuscript)

Liu C, Liu N, Shanbhag NC, Kritsilis M, Bèchet NB, Battistella R and Lundgaard I

Popular summary

Our brain bathes in a transparent liquid called cerebrospinal fluid (CSF). This fluid is of vital importance for the brain's health as it not only protects the brain, acting as a cushion against mechanical injuries, but it also mediates the delivery of essential nutrients to the brain's cells. Only a few years ago it was found that CSF has another important function, to clean the brain from metabolic by-products and protein waste that accumulate over time. This function is necessary for maintaining brain health, since the brain, unlike other organs in the body, does not have its own lymphatic vessels to clean itself. Getting rid of this waste is necessary to prevent the accumulation of certain toxic proteins that are implicated in the development and progression of neurodegenerative diseases such as Alzheimer's and Parkinson's.

This cleaning system relies on the CSF flowing around the cerebral arteries and entering the brain parenchyma through specialized water channels called aquaporin-4. The CSF then mixes with the fluid between brain cells, picking up waste that accumulates there and finally carries them around the cerebral veins to exit the brain. Because of its dependence on the glial cells of the brain that express the aquaporin-4 water channels and due to its lymphatic-like function, this drainage system of the brain was named "glymphatic system". Interestingly, it was found that this drainage system of the brain is mostly active during sleep, revealing that this fundamental part of life where we spend approximately one third of our lifetime also serves to keep our brains clean.

However, there are still a number of unanswered questions regarding the mechanisms of the glymphatic system and CSF circulation, especially in the context of diseases. Much like CSF research extends to several different directions, this thesis also touched upon various topics; from the investigation of disease models and their impact on the glymphatic system to comparative studies and methodological refinement and from the pathways that CSF uses to leave the brain to alternative clearance mechanisms of amyloid.

In Paper I, we studied how the glymphatic system is affected in heart failure, a cardiovascular disease where the heart does not pump blood effectively and found that heart failure causes dysregulation of brain fluid homeostasis. We also found that blood flow to the brain might be another factor regulating glymphatic clearance, highlighting the complex interaction between cardiovascular function and brain health. In Paper II, we compared different ways to stain and visualize the blood

vessels of the brain, providing a guide for selecting the most appropriate methods for different experimental applications. In Paper III, we looked into the pathways that CSF uses to exit the brain. We confirmed that the route through the nose and towards the lymphatic vessels of the neck is an important drainage route, which can quickly adapt to different challenges, while it remains active in aging. Finally, in Paper IV, we observed that the glymphatic system is impaired by the introduction of amyloid beta in the CSF and also found an alternative clearance pathway for this toxic protein through the vascular wall of cerebral arteries.

The findings in this thesis indicate the need to better understand how brain fluids circulate and how they relate to various diseases. As we continue to uncover more about the glymphatic system and CSF circulation, we may discover new targets for therapies that could protect against neurological disorders.

Populärvetenskaplig sammanfattning

Vår hjärna badar i en genomskinlig vätska som kallas ryggmärgsvätska (CSV). Denna vätska är livsviktig för hjärnans hälsa eftersom den inte bara skyddar hjärnan genom att fungera som en stötdämpare mot mekaniska skador, utan också levererar viktiga näringsämnen till hjärncellerna. För bara några år sedan upptäcktes att CSV har ytterligare en viktig funktion, nämligen att rengöra hjärnan från metaboliska biprodukter och proteinskräp som ansamlas över tid. Denna funktion är nödvändig för att upprätthålla hjärnans hälsa, eftersom hjärnan, till skillnad från andra organ i kroppen, inte har egna lymfkärl för att rengöra sig själv. Att bli av med avfall är nödvändigt för att förhindra ansamlingen av vissa giftiga proteiner som bidrar till utvecklingen och progressionen av neurodegenerativa sjukdomar som Alzheimers och Parkinsons.

Detta rengöringssystem förlitar sig på att CSV flödar runt de cerebrala artärerna och tränger in i hjärnvävnaden genom specialiserade vattenkanaler som kallas aquaporin-4. CSV blandas sedan med vätskan mellan hjärncellerna, plockar upp avfall som ansamlas där och transporterar det slutligen runt de cerebrala venerna för att lämna hjärnan. På grund av att systemet är beroende av hjärnans gliaceller som uttrycker aquaporin-4 vattenkanalerna och har samma funktion som det lymfatiska systemet, kallades detta dräneringssystem i hjärnan för "det glymfatiska systemet". Intressant nog upptäcktes att detta dräneringssystem i hjärnan är som mest aktivt under sömnen, vilket visar att denna grundläggande del av livet, där vi tillbringar ungefär en tredjedel av vår livstid, också hjälper till att hålla hjärnan ren.

Det finns dock fortfarande ett antal obesvarade frågor gällande mekanismerna bakom det glymfatiska systemet och CSV-cirkulationen, särskilt i samband med sjukdomar. Precis som CSF-forskningen sträcker sig i flera olika riktningar, berör denna avhandling också olika ämnen; från undersökning av sjukdomsmodeller och deras påverkan på det glymfatiska systemet till jämförande studier och metodologisk förfining, och från de vägar som CSV använder för att lämna hjärnan till alternativa mekanismer för borttransport av amyloid.

I Artikel I studerade vi hur det glymfatiska systemet påverkas vid hjärtsvikt, en kardiovaskulär sjukdom där hjärtat inte pumpar blod effektivt, och fann att hjärtsvikt orsakar dysreglering av hjärnans vätskebalans. Vi fann också att blodflödet till hjärnan kan vara ytterligare en faktor som reglerar glymfatisk rensning, vilket belyser den komplexa interaktionen mellan kardiovaskulär funktion

och hjärnhälsa. I Artikel II jämförde vi olika sätt att färga och visualisera hjärnans blodkärl, vilket ger en guide för att välja de mest lämpliga metoderna för olika experimentella tillämpningar. I Artikel III tittade vi på de vägar som CSV använder för att lämna hjärnan. Vi bekräftade att vägen genom näsan och mot halsens lymfkärl är en viktig dräneringsväg, som snabbt kan anpassa sig till olika utmaningar och förblir aktiv under åldrandet. Slutligen, i Artikel IV, observerade vi att det glymfatiska systemet försämras av introduktionen av amyloid beta i CSV och fann också väg för borttransport av detta giftiga protein genom kärlväggen i cerebrala artärer.

Resultaten i denna avhandling tyder på att det finns ett behov av att bättre förstå hur hjärnvätskor cirkulerar och hur de relaterar till olika sjukdomar. I takt med att vi avslöjar mer om det glymfatiska systemet och CSV-cirkulationen kan vi identifiera nya terapeutiska mål som potentiellt kan skydda mot neurologiska sjukdomar.

Περίληψη

Ο εγκέφαλός μας περιβάλλεται από ένα διαυγές υγρό που ονομάζεται εγκεφαλονωτιαίο υγρό (ΕΝΥ). Αυτό το υγρό είναι ζωτικής σημασίας για την υγεία του εγκεφάλου, καθώς όχι μόνο τον προστατεύει, λειτουργώντας ως μαξιλάρι ενάντια σε μηχανικούς τραυματισμούς, αλλά επίσης διευκολύνει τη μεταφορά απαραίτητων θρεπτικών συστατικών στα κύτταρα του εγκεφάλου. Μόλις πριν από λίγα χρόνια ανακαλύφθηκε ότι το ΕΝΥ έχει ακόμα μία σημαντική λειτουργία, να καθαρίζει τον εγκέφαλο από μεταβολικά παραπροϊόντα και πρωτεϊνικά απόβλητα που συσσωρεύονται με την πάροδο του χρόνου. Αυτή η λειτουργία είναι απαραίτητη για τη διατήρηση της υγείας του εγκεφάλου, δεδομένου ότι ο εγκέφαλος, σε αντίθεση με άλλα όργανα του σώματος, δεν διαθέτει δικά του λεμφαγγεία για να καθαρίζεται. Η απομάκρυνση αυτών των αποβλήτων είναι απαραίτητη για την πρόληψη της συσσώρευσης ορισμένων τοξικών πρωτεϊνών που εμπλέκονται στην ανάπτυξη και εξέλιξη νευροεκφυλιστικών ασθενειών όπως η νόσος του Αλτσχάιμερ και η νόσος του Πάρκινσον.

Αυτό το σύστημα καθαρισμού βασίζεται στη ροή του ΕΝΥ γύρω από τις εγκεφαλικές αρτηρίες και την είσοδό του στο εγκεφαλικό παρέγχυμα μέσω εξειδικευμένων καναλιών νερού που ονομάζονται ακουαπορίνη-4. Το ΕΝΥ στη συνέχεια αναμιγνύεται με το υγρό μεταξύ των εγκεφαλικών κυττάρων, συλλέγοντας τα απόβλητα που συσσωρεύονται εκεί και τελικά τα μεταφέρει γύρω από τις εγκεφαλικές φλέβες για να εξέλθουν από τον εγκέφαλο. Λόγω της εξάρτησής του από τα γλοιακά κύτταρα του εγκεφάλου που εκφράζουν τα κανάλια νερού ακουαπορίνη-4 και λόγω της λειτουργείας του που προσομοιάζει αυτή των λεμφαγγείων, αυτό το σύστημα καθαρισμού του εγκεφάλου ονομάστηκε «γλυμφατικό σύστημα». Παρουσιάζει ενδιαφέρον ότι αυτό το «αποχετευτικό σύστημα του εγκεφάλου» είναι κυρίως ενεργό κατά τη διάρκεια του ύπνου, αποκαλύπτοντας ότι αυτό το θεμελιώδες μέρος της ζωής, όπου περνάμε περίπου το ένα τρίτο του χρόνου μας, χρησιμεύει επίσης για να διατηρεί τον εγκέφαλό μας καθαρό.

Ωστόσο, εξακολουθούν να υπάρχουν αρκετά αναπάντητα ερωτήματα σχετικά με τους μηχανισμούς του γλυμφατικού συστήματος και την κυκλοφορία του ΕΝΥ, ιδιαίτερα στο πλαίσιο διαφόρων ασθενειών. Αυτή η διατριβή αγγίζει διάφορα θέματα: από τη διερεύνηση μοντέλων ασθενειών και τις επιπτώσεις τους στο γλυμφατικό σύστημα μέχρι συγκριτικές μελέτες και μεθοδολογική βελτίωση, και

από τις οδούς που χρησιμοποιεί το ENY για να εγκαταλείψει τον εγκέφαλο μέχρι εναλλακτικούς μηχανισμούς καθαρισμού του αμυλοειδούς.

Στο Άρθρο I, μελετήσαμε πώς επηρεάζεται το γλυμφατικό σύστημα στην καρδιακή ανεπάρκεια, μια καρδιαγγειακή νόσο όπου η καρδιά δεν αντλεί αποτελεσματικά το αίμα, και διαπιστώσαμε ότι η καρδιακή ανεπάρκεια προκαλεί απορρύθμιση της ομοιόστασης των εγκεφαλικών υγρών. Διαπιστώσαμε επίσης ότι η ροή αίματος στον εγκέφαλο μπορεί να είναι ένας άλλος παράγοντας που ρυθμίζει τη γλυμφατική κάθαρση, υπογραμμίζοντας την πολύπλοκη αλληλεπίδραση μεταξύ καρδιαγγειακής λειτουργίας και εγκεφαλικής υγείας. Στο Άρθρο II, συγκρίναμε διαφορετικούς τρόπους χρώσης και απεικόνισης των αιμοφόρων αγγείων του εγκεφάλου, παρέχοντας έναν οδηγό για την επιλογή των καταλληλότερων μεθόδων για διαφορετικές πειραματικές εφαρμογές. Στο Άρθρο III, εξετάσαμε τις οδούς που χρησιμοποιεί το ENY για να εξέλθει από τον εγκέφαλο. Επιβεβαιώσαμε ότι η διαδρομή μέσω της μύτης και προς τα λεμφικά αγγεία του λαιμού είναι μια σημαντική οδός κάθαρσης, η οποία μπορεί να προσαρμοστεί γρήγορα σε διαφορετικές προκλήσεις, ενώ παραμένει ενεργή κατά τη γήρανση. Τέλος, στο Άρθρο IV, παρατηρήσαμε ότι το γλυμφατικό σύστημα επηρεάζεται αρνητικά από την εισαγωγή βήτα-αμυλοειδούς στο ENY και επίσης βρήκαμε μια εναλλακτική οδό κάθαρσης για αυτή την τοξική πρωτεΐνη μέσω του αγγειακού τοιχώματος των εγκεφαλικών αρτηριών.

Τα ευρήματα αυτής της διατριβής υποδεικνύουν την ανάγκη για καλύτερη κατανόηση του τρόπου κυκλοφορίας των εγκεφαλικών υγρών και πώς αυτά σχετίζονται με διάφορες ασθένειες. Καθώς συνεχίζουμε να ανακαλύπτουμε περισσότερα για το γλυμφατικό σύστημα και την κυκλοφορία του ENY, μπορεί να ανακαλύψουμε νέους στόχους για θεραπείες που θα μπορούσαν να προστατεύσουν από νευρολογικές παθήσεις.

Abbreviations

| | |
|-----------|--|
| AD | Alzheimer's disease |
| AQP4 | Aquaporin-4 |
| A β | Amyloid beta |
| BBB | Blood-brain barrier |
| CBF | Cerebral blood flow |
| CM | Cisterna magna |
| CNS | Central nervous system |
| CSF | Cerebrospinal fluid |
| DCLNs | Deep cervical lymph nodes |
| EF | Ejection fraction |
| GBCA | Gadolinium-based contrast agent |
| HF | Heart failure |
| HFREF | Heart failure with reduced ejection fraction |
| i.p. | Intraperitoneal |
| ISF | Interstitial fluid |
| KO | Knockout |
| K/X | Ketamine/Xylazine |
| LAD | Left anterior descending |
| LEA | Lycopersicon esculentum agglutinin |
| MI | Myocardial infarction |
| MRI | Magnetic resonance imaging |
| PVS | Perivascular space(s) |
| SCLNs | Superficial cervical lymph nodes |
| WGA | Wheat germ agglutinin |

Introduction

Cerebrospinal fluid circulation

Cerebrospinal fluid (CSF) is a clear liquid similar to plasma that circulates around the brain and fills the cerebral ventricles. It has a vital role in homeostasis of the central nervous system (CNS) as it not only provides protection from mechanical injuries to the brain, but also acts as a medium for the transfer of nutrients and waste to and from the brain¹.

The history of the fluid circulating around the brain can be traced all the way back to 3000 B.C., where the Egyptian physician and architect Imhotep described the fluid coming out of an open head trauma². In the millennia that passed, a fascinating series of discoveries better described the presence of this fluid around the brain, the spinal cord and inside the cerebral ventricles, while giving it a number of different names³. It was only in 1842 when the French physician, François Magendie introduced the term “cerebrospinal fluid” which has been universally used ever since³.

Cerebrospinal fluid production

Today, the CSF is known to be secreted at a rate of approximately 500 mL per day in the adult human⁴. CSF production mainly takes place at the secretory epithelium of the choroid plexus, which is a specialization of the ependymal cells lining the ventricles⁵, where CSF is secreted from the basolateral compartment and into the ventricles, against an osmotic gradient⁶.

Evidence that CSF production occurred at the choroid plexus of the cerebral ventricles had already emerged in the 1850s^{7,8}. However, it was experimental studies in the 1910s that confirmed the continuous secretion of CSF by the choroid plexus, by documenting the development of hydrocephalus when the flow downstream of the lateral ventricles was obstructed^{9,10}. Later studies showed that CSF sampled directly from the choroid plexus had a different ionic concentration than a serum ultrafiltrate but similar to the one found in the cisterna magna (CM)¹¹.

Experimental evidence has also supported the idea of extrachoroidal CSF secretion^{12–14}, suggesting the blood brain barrier (BBB), the interstitial fluid (ISF) of the brain and even the ependymal layer lining the ventricular walls as potential

contributors to CSF secretion¹⁵. While the extrachoroidal contribution to CSF secretion remains a matter of debate up to this date^{6,16–18}, the mechanisms behind choroidal secretion are also being revisited. The water channel aquaporin-1, which is highly expressed in the luminal membrane of the choroid plexus, has long been considered an important contributor to CSF secretion¹⁹. However, recent evidence suggests that is in fact not required for CSF secretion²⁰. Instead, the membrane transporters that can couple fluid transport to ionic translocation emerge as the molecular drivers of CSF secretion and as promising pharmacological targets against brain pathologies such as hydrocephalus^{6,20,21}.

The ventricular system and the subarachnoid space

The first description of the brain's ventricular system can be traced back to Aristotle and the 4th century B.C.^{17,22}. Interestingly, the ventricles were believed to house the life-giving vapor known as *spiritus animalis* for over a millennium, based on the views of Galen^{23,24}. It was only in 1664 when Thomas Willis described the presence of fluid in the ventricles and the cerebral aqueduct³. Later on, the Italian physician Domenico Felice Cotugno described the presence of clear fluid not only within the ventricles but also around the spinal cord, the cerebral hemispheres and in the subarachnoid space^{3,25}. However, the ventricular system was considered a distinct closed compartment until the discovery of the foramina of Magendie and Luschka^{17,26}. These discoveries provided the necessary pieces for Harvey Cushing to describe the unidirectional flow of CSF from the choroid plexus to the ventricular system and then into the CM, the central canal of the spinal cord, the subarachnoid space, and finally into the dural sinuses as the third circulation^{17,27}.

Cerebrospinal fluid efflux

The constant production of CSF inevitably requires an efficient way of fluid drainage so that brain fluid homeostasis is maintained. For several decades, Cushing's description of the third circulation shaped the understanding of CSF circulation and efflux. According to this model, the CSF exits the subarachnoid space and drains directly into the bloodstream through specialized structures called arachnoid villi or granulations^{8,28}. This was supported by previous findings by Key and Retzius who injected blue-colored gelatin into the CSF compartment of human cadavers and found it accumulating in arachnoid granulations²⁹. These projections of the arachnoid mater into the venous sinuses that lie within the dura mater were first illustrated by Vesalius and later described by Pacchioni^{30–32} and are separated based on their size into microscopic villi and larger granulations that are visible to the naked eye^{33,34}. Despite contemporary reports of CSF drainage through the perineural sheath of the olfactory nerve and towards the lymphatic network of the nasal mucosa³⁵, the view of Weed and Cushing regarding the central role of arachnoid granulations in CSF drainage was established and largely persisted to this day^{36,37}. However, the lack of in vivo evidence of CSF efflux through the arachnoid granulations has shifted the researchers' interest towards other efflux routes that have long been overlooked³⁸.

The nasal efflux pathway

While the first description of passage through the cribriform plate and towards the nasal area can be traced all the way back to Galen, it was Schwalbe's tracer experiments in 1869 that revealed a connection between the subarachnoid space and nasal lymphatics³⁹. Since then, a large number of in vivo and ex vivo studies have confirmed that tracers injected in the CSF can be found in the nasal lymphatics, having passed through the cribriform plate³⁸. However, the exact anatomical pathway that CSF uses to cross the cribriform plate remains a matter of debate. One reason for this lack of clarity is the difficulty in accessing the microscopic components in question with the current imaging methods³⁸. Despite important advancements in imaging techniques that have contributed to the characterization of the lymphatic network around the cribriform plate, these are in most cases ex vivo studies, that cannot accurately capture the dynamic flow of CSF⁴⁰. At the same time, in vivo techniques such as magnetic resonance imaging (MRI) lack the resolution to identify the exact anatomical pathway that CSF uses to exit through the cribriform plate⁴¹. The three most probable such pathways supported by the literature are briefly summarized in (*Figure 1*). The dense lymphatic network of the nasal turbinates then converges into collecting lymphatic vessels that drain to the superficial cervical lymph nodes (SCLNs) with potential additional connections to other lymphatic networks of the cervical region^{40,42,43}.

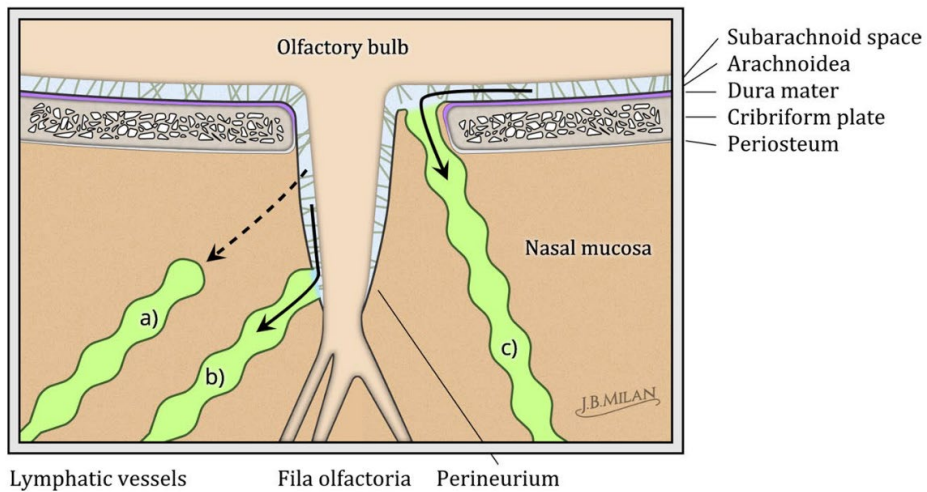


Figure 1. CSF efflux through the cribriform plate.

Schematic representation of the three experimentally supported models of the anatomical routes for CSF outflow along the olfactory nerves that cross the cribriform plate. In model (a), the perineurium of the olfactory nerve bundles is a continuation of the arachnoid mater (light blue) although, it does not form a barrier outside the skull or is only weakly attached to the nerve. Thereby, fluid and solutes have unrestricted access to the interstitial space of the nasal (sub)mucosa (brown) where they can enter the lymphatic vasculature of the tissue (green). In model (b), CSF again crosses the plate within the perineural space but this time it has a direct pathway to lymphatic capillaries that surround the nerve. Model (c) shows lymphatic vessels crossing the cribriform plate and having direct access to the CSF already on the CNS side. In this model the arachnoid mater would not form a barrier in the region around the cribriform plate. Scheme by Joachim Birch Milan. Adapted from Proulx, 2021³⁸, under a CC BY license.

Other cranial and spinal nerves

The presence of CSF along the optic nerve has also been well documented over the years, although interspecies differences have made it difficult to reach a consensus regarding the downstream drainage of this route and therefore its relative importance compared to the olfactory route³⁸. At least in mice, lymphatics from the ocular region seem to drain into nasolacrimal lymphatics and towards the SCLNs⁴⁰. Lymphatic vessels have also been identified within the trigeminal and facial nerves, although tracer outflow has not been demonstrated past the respective ganglia^{38,44–46}. Tracer has also been demonstrated to flow within lymphatic vessels through the jugular foramina, where the glossopharyngeal, vagus and accessory nerves exit the skull, and towards the deep cervical lymph nodes (DCLNs)⁴⁵.

Although substantially less studied, lymphatic CSF efflux along the dorsal nerve roots of the spinal nerves has been known to occur for several decades^{29,38}. However, in most studies the injected tracers could not be found further than the dorsal root ganglia, with the exception of the lumbo-sacral region, where tracers were shown to drain towards sacral and iliac lymph nodes^{38,47}.

Meningeal lymphatics

While lymphatic vessels in the dura mater were first described by Paolo Mascagni in 1787^{48,49}, it was two studies in 2015 that reawakened the interest in these meningeal lymphatic vessels and their role in CSF efflux^{46,50}. These vessels were found to run in close proximity to the venous sinuses of the dura as well as the meningeal arteries. Together with the lymphatic vessels found at the base of the skull they were shown to drain CSF and macromolecules to the DCLNs^{46,50,51}. However, the exact anatomical pathway of tracer uptake by the dorsal meningeal lymphatics quickly became a matter of controversy when researchers reported the presence of CSF-injected tracers inside the dorsal meningeal lymphatics, postulating the existence of specific “hot spots” where the meningeal lymphatics have direct access to CSF^{40,52}. Other groups were able to confirm tracer uptake only in the skull base lymphatics and not in the dorsal lymphatics^{45,46,51}. Recently, it was found that bridging veins create discontinuities in the arachnoid mater, and the arachnoid cuff exits that form around them can allow the exchange of CSF and solutes between the subarachnoid space and the dura⁵³. This finding is also in line with human MRI data showing the accumulation of CSF-injected tracer in the parasagittal space^{54–57}.

Despite the increasing number of studies on CSF efflux through lymphatic pathways in recent years, only a few of them have tried to comprehensively assess more than one of these pathways at the same time^{42,45,51,58}. As the complementary nature of these pathways becomes increasingly apparent, future studies should address their relative importance both in physiological and pathological conditions (*Figure 2*). Additionally, it should be noted that we cannot be certain about whether the tracers used to visualize CSF circulation and efflux reflect actual CSF movement or if the CSF, mainly composed of water, has in fact access to more pathways than we can see using tracers. Finally, future studies should investigate the similarities and differences in these pathways between various animal species and humans to unlock their therapeutic potential for maintaining CNS homeostasis.

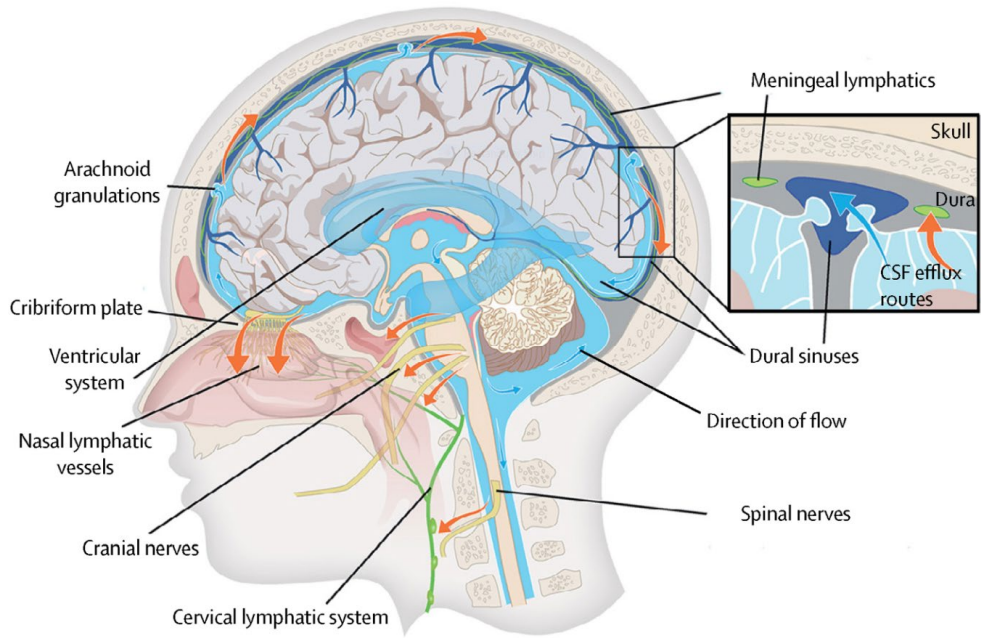


Figure 2. CSF efflux pathways.

Schematic representation of the main pathways that CSF uses to exit the skull. While experimental evidence exists for all these pathways, their relative contribution to CSF efflux remains a matter of debate. Reprinted from Rasmussen et al., © 2018⁵⁹, with permission from Elsevier.

The glymphatic system

All biological processes in an organism require energy, and the metabolic processes to generate that energy inevitably produce by-products. These by-products or metabolic waste need to be efficiently cleared from the tissue to maintain its homeostasis. In peripheral tissues, excess interstitial fluid (ISF) and metabolic waste that accumulates in the extracellular space are removed by the lymphatic system. The lymphatic system that runs in parallel with the blood circulation, carries all the waste from the different organs and finally drains it in the venous circulation⁶⁰.

Despite the presence of various lymphatic networks that contribute to CSF drainage around the CNS, the brain itself has been known to be devoid of lymphatic vessels^{61,62}. This has been considered rather strange given that the brain receives about 12% of the cardiac output while only weighing 2% of the body weight^{63,64}. At the same time, it is a high energy-demanding organ, thereby having a high rate of metabolic waste generation.

In the absence of conventional lymphatic vessels, the brain has developed a system where the CSF that circulates around it, penetrates into the tissue and drives the export of metabolic waste⁶⁵ (*Figure 3*). While evidence of CSF-mediated clearance of the CNS had been present in the past^{66–70}, it was only in 2012 when Iliff et al. defined and described this brain-wide flow of CSF into and through the brain parenchyma⁷¹. The researchers in Maiken Nedergaard's group injected fluorescent tracers into the CSF compartment and using in vivo two-photon imaging, they were able to visualize the tracer movement along the perivascular space (PVS) of cerebral arteries. They also found that this influx of CSF into the brain was facilitated by the aquaporin-4 (AQP4) water channels found along the endfeet of astrocytes that form the outer boundary of the PVS. Finally, they reported that this AQP4-dependent water flux contributed to the clearance of intraparenchymally-injected soluble amyloid beta (A β) from the brain, along cerebral veins⁷¹. Due to the system's dependence on the astrocytic (glial) water channels and the lymphatic-like clearance function that it serves, it was termed "glymphatic"^{71,72}. Briefly, the glymphatic system can be summarized as follows:

CSF enters the perivascular spaces of cerebral arteries, penetrates into the brain parenchyma and mixes with the ISF, and ultimately carries solutes to perivenous spaces to exit the brain⁶⁵.

To understand more about the glymphatic system, as well as its implication in health and disease, we will dive into the main components and drivers of glymphatic flow.

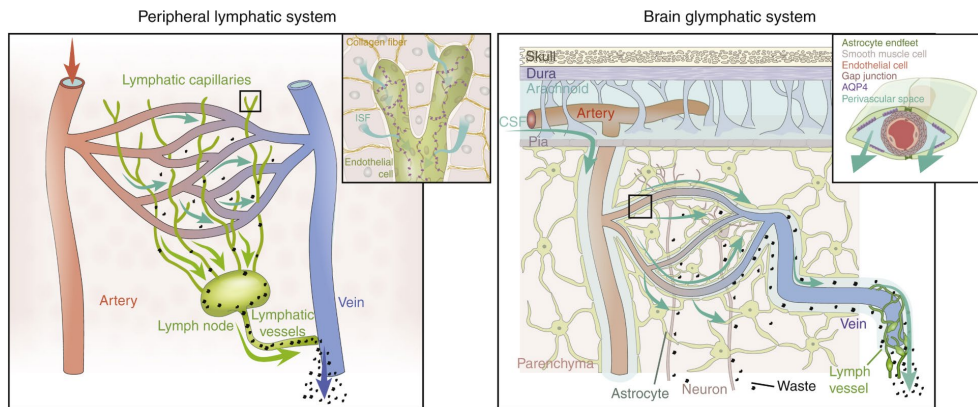


Figure 3. Comparison of peripheral lymphatic and the brain's glymphatic system.

(Left) In peripheral tissues, plasma ultrafiltrate enters lymphatic capillaries and is ultimately returned to the venous system. (Right) Due to the lack of conventional lymphatic vessels, the brain relies on the glymphatic system to clean its ISF. CSF enters the brain parenchyma alongside the arteries, penetrates into the tissue through the AQP4 water channels that are polarized to the astrocytic endfeet, mixes with the ISF and ultimately carries solutes to the perivenous spaces to exit the brain. Reprinted from Hablitz and Nedergaard, © 2021⁶⁵, with permission from Elsevier.

The perivascular spaces

The spaces around cerebral vessels, or Virchow-Robin spaces as often referred to, have always been regarded as an important site for fluid flow in the brain^{73,74}. These PVS are fluid-containing channels that surround cerebral vasculature and are ensheathed by the astrocytic endfeet⁶⁵. Ever since their first description in the 19th century, several controversies have risen regarding the extent of these spaces as penetrating arteries turn into capillaries, the presence of pia mater within the space and whether CSF can pass through it and finally whether the PVS is in direct connection with the subarachnoid space. These controversies have been fueled by the difficulty in accessing this space in deeper brain regions, especially in vivo, the artefacts introduced by tissue fixation methods causing collapse of the PVS and finally regional and interspecies differences in the anatomy of the PVS^{17,74–77}. However, recent studies have tried to shed light on some of these matters^{75,78}, and advancements in imaging techniques are expected to provide more definite answers in the future.

Regarding their role in the glymphatic system, the PVS of the arteries or periarterial spaces constitute low-resistance pathways for CSF flow from the subarachnoid space to deeper sites within the parenchyma^{71,72}. Accordingly, the PVS of cerebral veins or perivenous spaces are the site where extracellular fluid and protein waste are transported to before they ultimately exit the brain through various CSF efflux routes^{53,71}. Both of these components of glymphatic flux are dependent on AQP4 channels lining the astrocytic endfeet that form the outer boundary of PVS^{71,79}.

Aquaporin-4

The water channel AQP4 was only discovered in 1994 by the independent groups of Peter Agre and Alan Verkman and was later found to be expressed in astrocytes throughout the brain⁸⁰⁻⁸². It favors a polarized expression at the astrocytic endfeet ensheathing cerebral vasculature⁸³. Using immunogold analyses, it has been found that its endfoot expression is up to ten times higher compared to the non-perivascular membrane expression in rodents and about two to three times higher in humans⁸⁴. Being a member of the aquaporin family, it is an integral membrane protein, selectively permeable to water⁸⁵, and comprised of several isoforms, with M1 and M23 being the most prominent⁸⁶⁻⁸⁸. AQP4 is a tetrameric protein, with each monomer forming a pore where water can pass through⁸⁹. These channels are not just randomly scattered around the plasma membrane of astrocytic endfeet but highly organized in structures known as orthogonal arrays of particles (OAP)⁹⁰⁻⁹². Within the OAP, M1 and M23 isoforms of AQP4 assemble in heterotetramers, and the ratio between them greatly affects the stability and anchorage of OAP to the membrane⁹³⁻⁹⁵.

The important role of AQP4 in relation to the glymphatic system lies on its polarized expression at the astrocytic endfeet and its ability to permit free passage of water, thereby facilitating the flow of CSF from the periarterial space to the brain parenchyma and from the parenchyma to the perivenous space^{71,72}. The dependence of the glymphatic system on AQP4 was reported already in the first glymphatic study when researchers found diminished glymphatic influx and clearance in AQP4 knockout (KO) mice compared to the wild-type ones⁷¹ (*Figure 4A*). A later study challenged the necessity of AQP4 for this process, reporting that their KO model of AQP4 did not exhibit impaired tracer movement from the CSF to the brain or reduced clearance of intraparenchymally-injected A β ⁹⁶. However, a follow-up study combining the results from several independent labs, including four different AQP4 KO models and different imaging modalities such as in vivo fluorescence imaging and MRI, reaffirmed that lack of AQP4 impaired glymphatic influx⁷⁹ (*Figure 4B*). The disparity in findings was attributed to the choice of anesthetic and the invasiveness of intraparenchymal injection of tracer, both of which can greatly affect normal glymphatic function^{79,97,98}. Emerging evidence has increased our understanding of the effect of AQP4 deletion on the glymphatic system. Lack of AQP4 along the perivenous space could result in increased resistance to glymphatic clearance. Accordingly, the fluid accumulation in the interstitial space could cause enlargement of the extracellular space and increased resistance towards periarterial influx, thereby explaining the overall impairment of glymphatic transport^{99,100}.

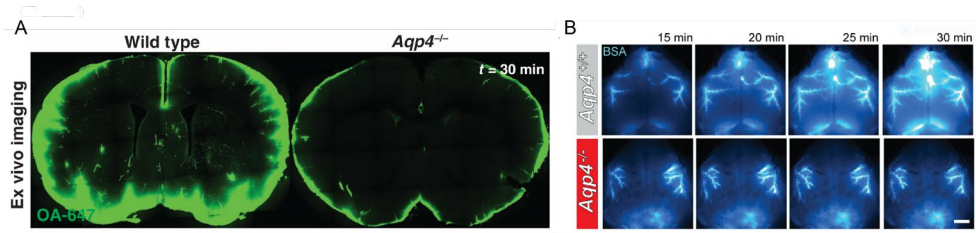


Figure 4. Glymphatic influx is impaired in AQP4 KO mice.

(A) Ex vivo coronal brain slice images from wild type and AQP4 KO mice 30 min after the CM injection of ovalbumin-647 (OA-647). Reprinted from Iliff et al., © 2012⁷¹, with permission from AAAS. (B) Representative images from in vivo transcranial optical imaging of wildtype mice (Aqp4+/+) and Aqp4 KO (Aqp4-/-) mice starting at 15 min after CM delivery of bovine serum albumin-647 (BSA-647). Scale bar: 2 mm. Adapted from Mestre et al., 2018⁷⁹.

Except for the overall expression of AQP4 in astrocytes, its polarized localization and anchorage to the astrocytic endfeet are of equal importance for glymphatic homeostasis⁷⁹, while it has a greater impact on the clearance of larger molecules¹⁰¹. The ratio of M1 to M23 isoforms affects the intramembrane organization of AQP4 and can also be used to assess its polarization^{102–106}. Additionally, the dystroglycan-associated protein complex and its components such as dystroglycan, dystrophin, dystrobrevin and α -syntrophin are crucial for AQP4 stabilization to the membrane, and lack of these proteins has been found to cause reduced AQP4 polarization which could lead to reduced glymphatic influx^{79,92,103,107–109}.

Drivers of the glymphatic system

Following the discovery of the glymphatic system, several studies identified a number of factors regulating glymphatic flow. Evidence for some of these drivers of the glymphatic system will be discussed in the following paragraphs. It is important to note that since most of these studies have investigated the various glymphatic drivers in isolation, it is still difficult to estimate their relative importance and contribution to glymphatic system regulation. Additionally, given the growing interest in glymphatic research, it is certain that more such drivers will emerge in the future.

Sleep and anesthesia

Early after the discovery of the glymphatic system a study by Xie et al. reported that CSF-injected tracers penetrated deeper along the PVS in mice that were sleeping or anesthetized with K/X compared to awake mice¹¹⁰. Using in vivo two-photon microscopy, the study reported a dramatic reduction of CSF influx of up to 90% in awake mice compared to naturally sleeping ones¹¹⁰. The effect was largely attributed to the expansion of interstitial space volume that occurs during sleep and anesthesia, while it also hinted at the role of norepinephrine, which will be discussed later on¹¹⁰.

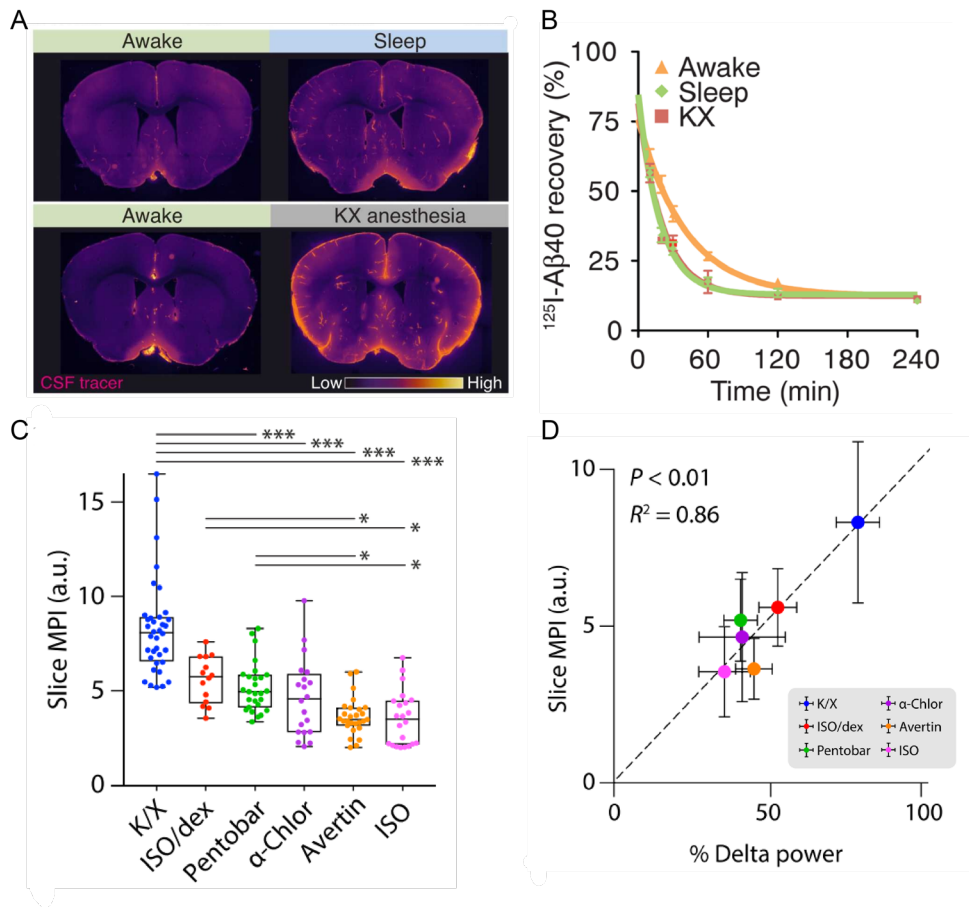


Figure 5. Effect of sleep and anesthesia on glymphatic function.

(A) Representative ex vivo coronal brain slice images from awake, sleeping and K/X-anesthetized mice 30 min after the CM injection of ovalbumin-555. Reprinted from Miyakoshi et al., © 2023¹¹¹, with permission from Elsevier. **(B)** Time-disappearance curves of ^{125}I -A β_{1-40} after its injection into the frontal cortex in awake (orange triangles), sleeping (green diamonds), and K/X-anesthetized (red squares) mice. Reprinted from Xie et al., © 2013¹¹⁰, with permission from AAAS. **(C)** Quantification of mean pixel intensity (MPI) across all coronal brain slices (each dot represents the average of one brain) from the six groups of anesthetized mice. Adapted from Hablitz et al., 2019⁹⁷, under a CC BY-NC license. **(D)** Scatterplot showing the correlation between MPI in coronal slices and the prevalence of delta band power. Each dot represents the group mean for each anesthetic (whiskers, SD). Adapted from Hablitz et al., 2019⁹⁷, under a CC BY-NC license.

This study soon became the cornerstone for the idea that glymphatic function might constitute an integral component of sleep^{107,110}. Therefore, the biological need for sleep, which is conserved in all species and whose neurobiological role has long been eluded, could now serve an additional purpose: to give the brain the chance to clear its waste via the glymphatic system^{65,107,110}. A later study reported that pial and penetrating arterioles exhibited sleep cycle-dependent vascular dynamics, which are

reflected in PVS size and glymphatic influx¹¹², while several other studies confirmed that sleep and anesthesia lead to increased glymphatic influx and clearance of not only tracers but also proteins such as A β and tau, compared to the awake state^{110,111,113,114} (*Figure 5A-B*). Accordingly, sleep disturbances were reported to result in reduced brain clearance, with further evidence coming from human studies^{115–117}.

A recent study brought into question the idea that the glymphatic system is predominantly active during sleep and anesthesia, suggesting that tracer movement within the brain is instead enhanced in awake mice¹¹⁸. However, a later report using a multimodal in vivo and ex vivo approach in awake, sleeping and anesthetized mice was able to reaffirm that brain clearance (out of the brain and not from one point in the brain to another) is indeed enhanced during sleep and anesthesia¹¹⁹.

The mechanisms behind this effect are only recently being elucidated. A study in humans revealed that neuronal activity is coupled to CSF and hemodynamic oscillations in sleep¹²⁰. Additionally, mouse studies showed that glymphatic function is under circadian control and that during sleep or ketamine anesthesia, neurons generate large-amplitude, rhythmic ionic oscillations in the ISF that drive CSF movement through the parenchyma^{103,121}. In anesthetized animals, neuronal activity and specifically, the power of slow wave delta oscillations (1-4 Hz) was correlated to increased CSF tracer influx⁹⁷ (*Figure 5C-D*). Interestingly, when neuronal activity was induced by multisensory 40 Hz (gamma) stimulation, glymphatic clearance was potentiated in the cerebral cortex, further validating the central role of neurons in regulating the brain's clearing mechanism¹²².

Arterial pulsations

Evidence that cerebral arterial pulsations drive CSF flow in the PVS existed already before the discovery of the glymphatic system¹²³. Blocking these cardiac-generated pulsations at the level of the ascending aorta or the brachiocephalic artery was shown to diminish the perivascular distribution of intraventricularly-injected tracer^{69,124}. Following the characterization of the glymphatic system, studies showed that increasing or reducing cerebral arterial pulsations induced a corresponding effect on glymphatic influx¹²⁵. In vivo particle tracking in the PVS confirmed that CSF flow is driven by arterial pulsations⁷⁷. This perivascular pumping mechanism was found to be impaired in hypertension, likely due to arterial wall stiffening, resulting in reduced glymphatic transport^{77,126}. However, later modeling studies have suggested that arterial pulsatility alone might serve more of a mixing effect in the PVS and may not be sufficient to drive unidirectional fluid flow^{127–129}.

Vasomotion

Except for the cardiac-generated arterial pulsations, brain clearance has also been associated with vasomotion, derived from the spontaneous vasoconstriction and vasodilation caused by the vascular smooth muscle cells^{112,130}. Vasomotion is

associated with slow neuronal oscillations (centered around ~ 0.1 Hz) that occur independently of pulsatile blood flow¹³¹. Mouse studies using in vivo two-photon microscopy showed that spontaneous vasomotion propagated along pial arterioles and correlated with clearance of intraparenchymally-injected tracers^{130,132}. Additionally, evoked vascular reactivity (functional hyperemia) was reported to increase both glymphatic influx and clearance^{130,133}. On the other hand, progressive loss of vascular smooth muscle cells that occurs in the APP/PS1 mouse model was shown to result in reduced brain clearance¹³⁰. Further support for the role of vasomotion has come from human studies reporting the presence of these infraslow pulsations, which are enhanced during sleep^{134–136}.

Norepinephrine

Over the last few years of glymphatic research, the hormone and neurotransmitter norepinephrine has subtly emerged as an important molecule that ties together some of the aforementioned drivers of glymphatic activity^{110,137}. Norepinephrine from the locus coeruleus has been previously postulated to be responsible for the suppression of the glymphatic system during wakefulness by reducing the interstitial volume fraction and thereby increasing tissue resistance to glymphatic flow^{107,110,138}. A recent study expanded our understanding of the role of norepinephrine, showing that locus coeruleus-derived noradrenergic oscillations drive arterial vasomotion during sleep and thereby control glymphatic influx and clearance¹³⁷ (Figure 6).

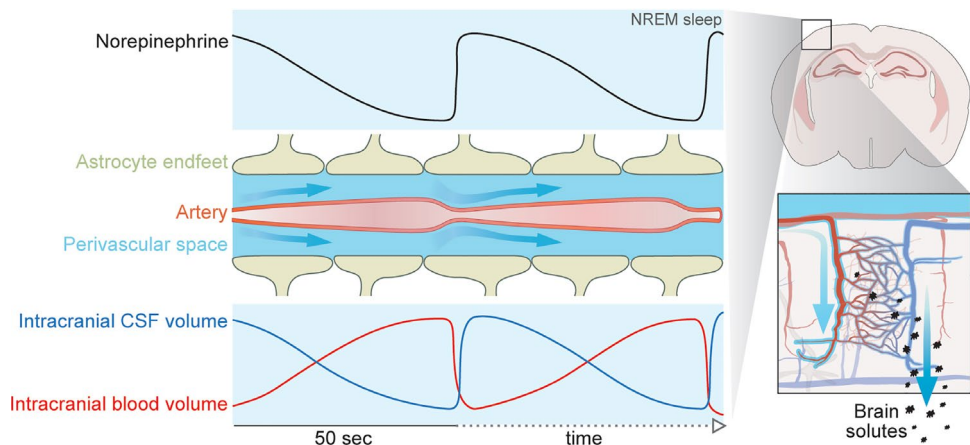


Figure 6. Infraslow oscillations in norepinephrine release drive vascular volume dynamics and control glymphatic flow during sleep.

Schematic representation of the mechanisms behind glymphatic brain clearance during sleep. Infraslow oscillations in norepinephrine release drive slow, rhythmic constrictions and dilations of the cerebral arteries, which, in turn, promote CSF flow along the PVS and through the brain parenchyma. Since cerebral blood volume and CSF volume are constricted to the confined space of the skull, vascular tone dynamics induce an anti-correlated infraslow oscillatory pattern in blood volume and CSF volume within the intracranial space. The directional flow of CSF and ISF promotes the removal of waste from the brain tissue toward draining lymph nodes in the periphery. Reprinted from Hauglund et al., © 2025¹³⁷, with permission from Elsevier.

Models to study the glymphatic system

Since the discovery of the glymphatic system, it was evident that it constitutes a complex brain-wide biological system. This meant that the intricate interplay between its various components could not be comprehensively studied *in silico* or *in vitro*. Today, after more than a decade of intense glymphatic research, except for a number of modeling studies that have greatly contributed to explaining different parts of the system, the field still heavily relies on experimentation on living organisms¹³⁹.

Rodent models

Like most recent studies in biomedicine, rodents have been the main animal model that has been used in glymphatic studies. The cornerstone experiment for studying the glymphatic system involves the introduction of tracers into the CSF^{71,140,141}. The tracers are typically introduced *in vivo* in the CM, a CSF space downstream of the 4th ventricle, from where the tracer can then circulate towards the subarachnoid space and the spinal canal. This route is typically preferred compared to intraventricular injection as it avoids damage to the brain tissue, which has been shown to result in impaired glymphatic function^{79,96,98}. The tracers used are typically fluorescent, radioactive or gadolinium-based contrast agents (GBCAs) for use in MRI. The tracers are then allowed to circulate and enter the PVS of the brain while imaged *in vivo* with various techniques, such as two-photon microscopy, transcranial imaging, single-photon emission computed tomography (SPECT/CT), positron emission tomography–computed tomography (PET/CT) and dynamic contrast-enhanced MRI (DCE-MRI)^{41,71,142–145}. The flow in the PVS has been criticized to be an artifact of injection, due to increased intracranial pressure (ICP)^{96,146–148}. However, an elegant study by Raghunandan et al. using a dual-syringe protocol where CSF was withdrawn at the same volumetric flow rate as the CM injection confirmed that ICP elevation was mild and transient as previously reported¹²⁵, while flow measurements in the PVS were similar to those reported in single-syringe experiments^{77,149,150}. Following tracer circulation, the brain and other tissues relevant for CSF efflux pathways can be dissected and imaged using epifluorescence, confocal and light-sheet microscopy to extract useful measurements of tracer distribution^{71,151}.

Intraparenchymal injection of tracers has also been widely used in rodents to measure glymphatic clearance from the brain. Fluorescent or radioactive molecules are injected into the brain parenchyma through a burr hole in the skull, and the tracer remaining in the brain or the tracer accumulated along efflux pathways are typically used as measures of glymphatic clearance^{110,137,144,152–154}. A recent study also proposed an *in vivo* assay where glymphatic clearance, following an intraparenchymal injection, can be visualized and measured in real time using fluorescence microscopy at the level of the femoral vein⁹⁸.

While a lot of our knowledge on glymphatic flow mechanisms has come from two-photon microscopy and transcranial imaging techniques, it is important to keep in mind that these methods can only capture phenomena taking place on the dorsal brain surface^{59,139}. Light-sheet fluorescence microscopy has emerged as a promising technique to help visualize tracer distribution in the whole brain or even the whole mouse with high spatial resolution^{111,151}. While this method cannot provide dynamic in vivo data, it can be leveraged to investigate CSF efflux pathways and their connection to the glymphatic system^{40,58,111,139}. The development of MRI-based methods to study the glymphatic system in rodents has provided invaluable insights into the brain-wide nature of glymphatic circulation^{41,139,144,155,156} (Figure 7). The continuous development of contrast-enhanced and contrast-free MRI sequences is expected to help bridge the translational gap between rodent and human glymphatic research.

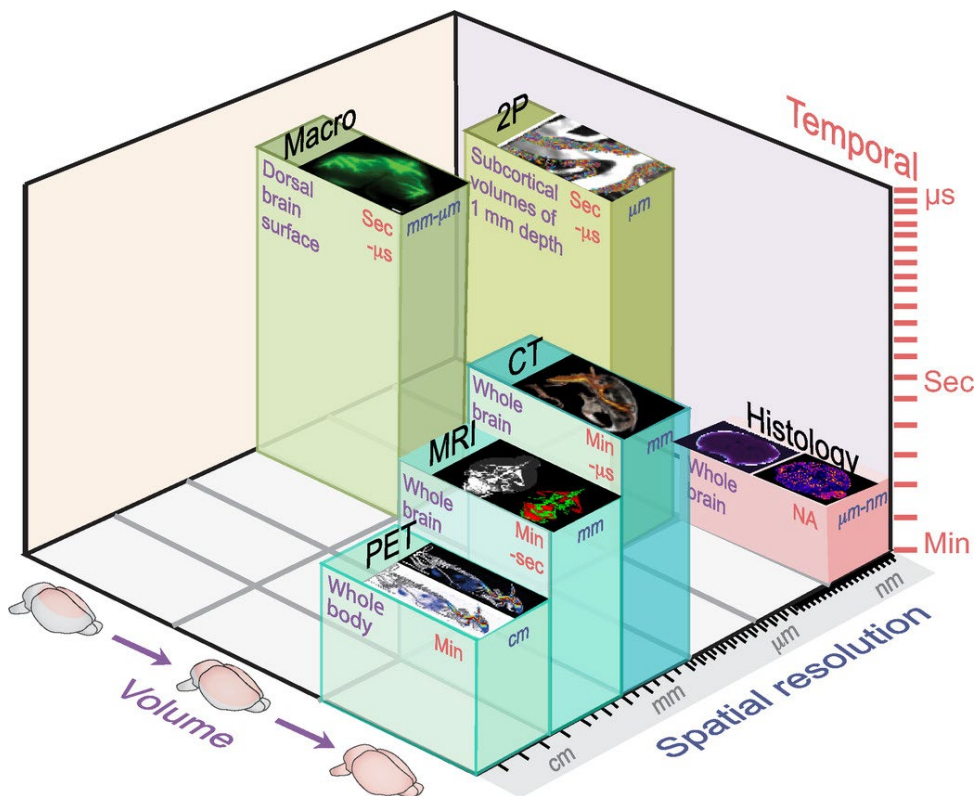


Figure 7. Methods to image the glymphatic system.

Different techniques used to image the glymphatic system plotted in a 3D plot depicting the typical qualities of each imaging modality in three different measures, namely temporal resolution, spatial resolution, and volume imaging. CT, computed topography; Macro, macroscopic transcranial imaging; PET, positron emission tomography; MRI, magnetic resonance imaging; 2p, two-photon microscopy. Reprinted from Rasmussen et al., © 2022¹⁷, with permission from The American Physiological Society.

Given the vast number of glymphatic studies that emerged over the past decade, it was inevitable that methodological discrepancies would result in conflicting results. One prominent example involved the different anesthetics used to study the glymphatic system. While Xie et al. had shown that sleep and K/X anesthesia similarly promote glymphatic function, a number of later studies using different anesthetics failed to observe glymphatic influx^{96,157–159}. Since then, several studies have showcased the reduction in glymphatic influx that occurs when animals are anesthetized with other anesthetics compared to K/X, thereby likely explaining the previous opposing results^{41,79,97,151}.

A recent study in mice also identified key differences between natural sleep and anesthesia with regard to vascular dynamics and the relative influence of different glymphatic drivers¹³⁷. Locus coeruleus-derived noradrenergic oscillations have been shown to control slow vasomotion during sleep and constitute the main driving force for glymphatic transport¹³⁷. On the other hand, slow wave delta oscillations and heart rate were correlated with glymphatic influx in mice anesthetized with different anesthetic regimes⁹⁷. While both sleep and anesthesia have been shown to promote glymphatic activity¹¹⁰, the suppression of norepinephrine and vasomotion during anesthesia suggests that under these two different conditions the primary drivers of glymphatic activity might differ¹³⁷. This greatly increases our understanding of glymphatic regulation as a whole and should be taken into account when designing future glymphatic studies.

The development of methods to introduce, modify or delete specific genes in rodents has allowed researchers to study the genetic basis of various diseases and gain insights into complex biological processes. Several transgenic models of various diseases have been used to study the mechanisms of disease development and progression in the context of the glymphatic system^{160–162}. However, it was only via the use of AQP4 KO mice that we were able to gain an understanding of the crucial role of this protein and characterize the glymphatic system as a whole^{71,79}.

Large mammals

Despite the many advantages of studying the glymphatic system in rodents, the potential translation of findings to humans would require several assumptions regarding the conservation of the mechanisms involved. The invasive nature of most glymphatic experiments at the moment does not allow for a wide range of human experimental studies. Therefore, investigations in large mammals provide a valuable translational step for elucidating the mechanisms of glymphatic flow in more complex systems.

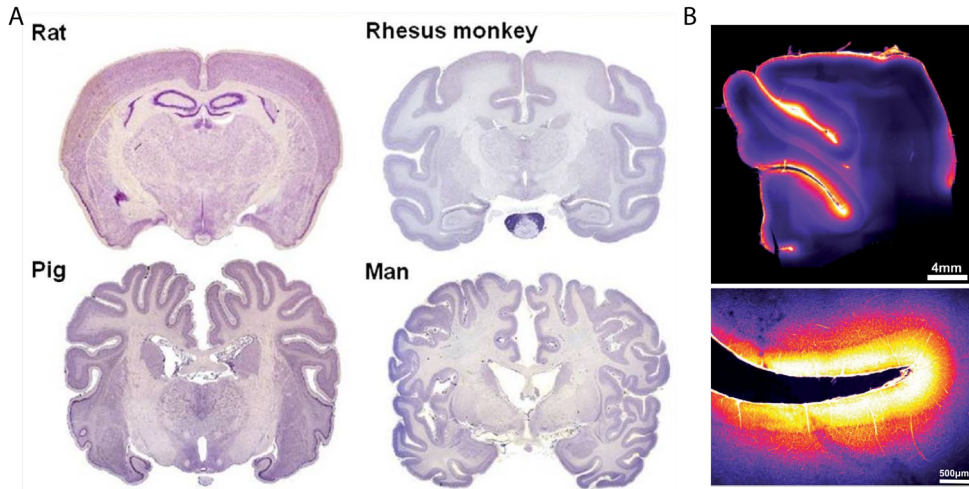


Figure 8. The effect of sulci on glymphatic influx.

(A) Coronal brain sections from various species showcasing the difference between the lissencephalic brain of rats compared to the gyrencephalic brains of monkeys, pigs and humans. Reprinted from Howells et al., © 2010¹⁶³, with permission from Sage Publications. (B) Confocal images of pig cortical slices showing robust tracer distribution in the sulci of the pig brain. Adapted from Bèchet et al., 2021¹⁶⁴, under a CC BY license.

While the groundwork of CSF circulation in the PVS and along efflux routes had been laid by experiments in large mammals, including non-human primates even before the first description of the glymphatic system, similar work has been very limited in the last few decades^{69,165,166}. A single study in non-human primates using DCE-MRI found that contrast agent had penetrated most of the brain within 2 h from the injection, while subarachnoid hemorrhage significantly impaired this glymphatic influx¹⁶⁷. However, important ethical considerations regarding research use of non-human primates make the expansion of glymphatic research in these species far less likely in the future. Recently, our lab developed a pig model to study the glymphatic system¹⁶⁸. Compared to the smooth lissencephalic rodent brain, the gyrencephalic brain of pigs closely relates to human anatomy (*Figure 8A*). This model allowed us to identify that the glymphatic system not only exists in pigs, but its microarchitecture is more complex compared to mice and rats¹⁶⁴. The sulci of the brain were reported to facilitate CSF distribution (*Figure 8B*), while PVS density was four times higher in pigs compared to mice¹⁶⁴. A recent study in ferrets, whose brain is also gyrencephalic, confirmed that glymphatic influx is enhanced in the sulci and that this sulcus-dominant influx is mediated by increased AQP4 expression in those regions¹⁶⁹. Although limited in number, these studies have provided valuable insights into how evolutionary changes in brain structure coincide with changes in glymphatic system physiology.

Human studies

The first study that confirmed the existence of the glymphatic system in humans was performed by Eide and Rigstad in 2015¹⁷⁰. A GBCA was injected intrathecally in a patient with suspected intracranial hypotension, followed by MRI at one timepoint before and two timepoints after the injection¹⁷⁰. The study revealed the transport of tracer into the brain, confirming that the glymphatic system is conserved from rodents to humans. Since then, a number of studies by the same group expanded on previous findings and provided a more comprehensive view of glymphatic enhancement dynamics, while also confirming the important role of sleep for glymphatic homeostasis^{117,171–175} (Figure 9).

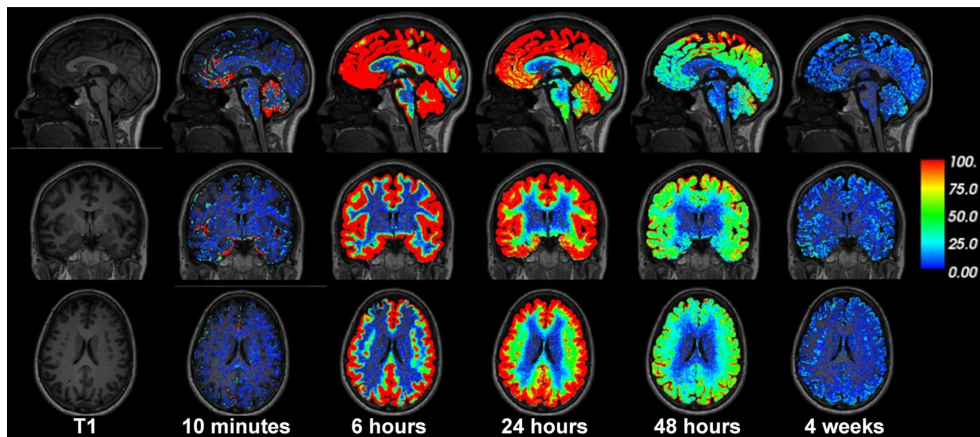


Figure 9. Brain-wide signal enhancement of time in the human brain.

Standardized T₁-weighted MRI obtained at different time points before and after intrathecal administration of the GBCA gadobutrol in a human subject. The images show tracer enhancement within the brain tissue, while tracer in CSF spaces has been subtracted. Percentage T₁ signal increase from tracer enrichment in brain tissue is illustrated by the color scale. After 4 weeks, there was no sign of residual tracer in the brain tissue. Reprinted from Eide et al., © 2021¹¹⁷, with permission from Oxford University Press.

While the above-mentioned studies involved the introduction of GBCAs in the CSF, in recent years there has been an increasing interest in non-invasive assessments of glymphatic function. One such method that has been commonly used relies on the detection and measurement of enlarged PVS in the brain, which have been associated with impaired glymphatic function¹⁷⁶. PVS enlargement is typically measured using a variety of visual rating scales or automated programs based on machine learning^{176,177}. Although PVS enlargement could be caused by fluid stagnation and disruption of CSF flow, the pathophysiological basis of its association with glymphatic dysfunction is still unclear^{176,178}. Another very popular method for non-invasive assessment of glymphatic function in humans relies on the diffusion tensor imaging analysis along the perivascular space (DTI-ALPS)

index¹⁷⁹. This technique uses diffusion MRI to evaluate the diffusivity along the direction of the PVS of medullary veins within the white matter of the brain^{179,180}. Due to the simplicity of the measurement and the possibility to calculate the index retrospectively in existing clinical datasets, it was quickly adopted by several researchers to look for correlations with various diseases^{178,180}. However, a number of limitations and the unclear pathophysiological processes that are reflected in the index have challenged the notion that this index can accurately encompass glymphatic function^{181–183}. These and other measures that correlated with disease conditions that had already been shown experimentally to be affected by the glymphatic system need further curation and thorough explanation of their potential applications and limitations^{180,181,183}. However, their quick adoption by a large number of researchers is indicative of the widespread need for reliable methods to assess glymphatic function in the clinical setting.

The glymphatic system and neurodegeneration

The glymphatic system has been recognized as an important contributor to the removal of toxic proteins from the brain^{71,72,184}. Up to this day, several studies have investigated its interaction with various neurodegenerative diseases, such as Alzheimer's (AD) and Parkinson's (PD), where the accumulation of toxic proteins is part of the pathophysiology of the disease. A β and tau have central role in the pathophysiology of AD^{185,186}. Therefore, the ability of the glymphatic system to clear these proteins from the brain has made it a potential therapeutic target for novel AD treatments^{71,154,162}. Similarly, it has been shown that α -synuclein, which has been largely implicated in the pathophysiology of PD is cleared through the glymphatic system^{187,188}. Intriguingly, increasing evidence has shown that neurodegenerative diseases can cause loss of perivascular AQP4 polarization and glymphatic dysfunction, setting the stage for a vicious cycle where further neurodegeneration will follow^{59,104,160,188,189} (*Figure 10*). This can be further aggravated by aging and impaired sleep architecture, both of which are independently associated with glymphatic dysfunction^{117,152,184,190,191}.

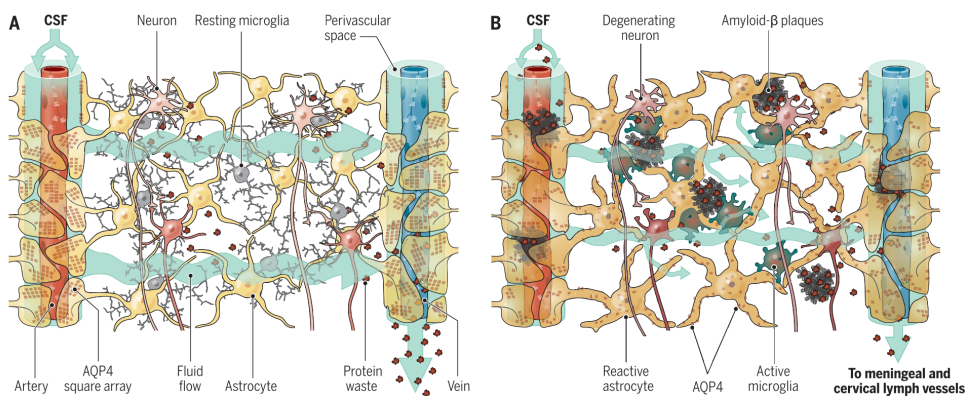


Figure 10. The glymphatic system in health and disease.

(A) A well-functioning glymphatic system contributes to the clearance of interstitial solutes and protein waste away from the brain. **(B)** A β plaque formation, astroglia, decrease in perivascular AQP4 polarization, vascular amyloidosis and age-related decline in CSF production can all impede glymphatic flow and thereby impair waste clearance. Reprinted from Nedergaard and Goldman, © 2020¹⁸⁴, with permission from AAAS.

Still several important questions regarding its role in other less-studied neurodegenerative diseases remain to be answered^{192–195}, as well as its implication on diseases that start far from the brain but lead to neurodegeneration, such as diabetes and heart failure (HF)^{196–198}. However, with an increasing number of studies looking into potential therapeutic strategies for neurodegeneration by leveraging the glymphatic system, the future of the field looks promising and exciting.

Aims of the thesis

Although CSF and its unique functions have been studied for several decades, there still remain a number of open questions regarding the mechanisms that govern its circulation. This thesis aims to elucidate some of the mechanisms of CSF circulation and the glymphatic system in health and disease using a variety of methods and animal models. The specific aims of the papers included in the thesis were:

- I. Investigate how the glymphatic system is affected in a mouse model of HF.
- II. Compare the efficacy of different lectins in labeling cerebral vasculature.
- III. Explore functional aspects of the nasal CSF efflux pathway.
- IV. Examine how A β (re)-circulation in the CSF affects the glymphatic system.

Key Methods

Key methods used in this thesis are briefly described below. For more details, please refer to the Materials and Methods section of the attached papers and manuscripts.

Animals

Mice (Papers I -III)

Adult male C57BL/6 mice were used for all experiments. Mice were housed in a climate-controlled animal facility with a 12 h dark-light cycle, in groups of 3-5 in ventilated cages with appropriate environmental enrichment. The mice had *ad libitum* access to normal chow and water. All experimental procedures performed in Lund were approved by the Malmö-Lund ethical Committee on Animal Research (Dnr 5.2.18-10992/18, 5.8.18-14734/2021, 5.8.18-20240/2021 and V 2023/1245, 5.8.18-08269/2019, 5.8.18-20241/2021, 5.8.18-08160/2021 and 5.8.18-04510/2024). Experiments performed at the Center for Translational Neuromedicine at the University of Copenhagen were approved by the Danish Animal Inspectorate and by the Department of Animal Experimental Medicine of the University of Copenhagen (2020-15-0201-00562). Experiments performed at the German Center for Neurodegenerative Diseases in Bonn, Germany were approved by the Landesamt für Natur-, Umwelt- und Verbraucherschutz (81-02.04.2019.A214/01).

Pigs (Papers III – IV)

Adult male pigs (*Sus scrofa domestica*) were purchased by an approved supplier and were used for all experiments. Pigs were housed in pens with a 12 h dark-light cycle and had *ad libitum* access to water and food. All experimental procedures were approved by the Malmö-Lund ethical Committee on Animal Research (Dnr 5.8.18-05527/2019).

Surgery and disease models

CM injection in mice (Papers I, III and IV)

Mice were anesthetized with an i.p. injection of K/X, administered in a volume of 10 mL/kg, and when the reflexes ceased, each mouse was positioned on a stereotactic frame. The procedure was then performed as previously described¹⁴¹. An incision was made on the skin, and the muscles at the back of the neck were reflected to expose the CM. The CM injection was performed using a 30 G dental needle (Carpule, Sopira) connected to a Hamilton syringe (Hamilton Company, Reno, NV, USA) via Polyethylene (PE) 10 tubing (AgnTho's AB, Lidingö, Sweden). Glue and dental cement were then used to secure the cannula to the skull.

Fluorescent tracers, BSA-647 (Alexa Fluor™ 647-conjugated BSA, A34785, Invitrogen/Thermo Fisher Scientific, CA, USA) and/or A β ₁₋₄₂ HiLyte-555 (HiLyte™ Fluor 555-labeled beta amyloid 1-42, AS-60480-01, Anaspec, CA, USA) were injected in the CM using a single infusion syringe pump (LEGATO® 100 Syringe pump, KD Scientific, Holliston, MA, USA) typically at a rate of 1 μ L/min, unless otherwise specified. The tracer was allowed to circulate for a variable amount of time according to the experimental design. Mice were then euthanized either by decapitation or by transcardial perfusion with PBS [sometimes containing wheat germ agglutinin (WGA) lectin] and 4% paraformaldehyde (PFA). Tissues of interest were then dissected and immersion-fixed in 4% PFA overnight before used for further processing.

For DCE-MRI experiments, a copper needle (0.32-mm outer diameter; Nippon Tokushukan MFG Co. Ltd., Tokyo, Japan) was used instead of the stainless-steel dental needle⁴¹. The GBCA Dotarem® (DOTA-Gd, 12.5 mM, Guerbet LLC, Princeton, NJ, USA) was injected into the CM using a remote-controlled pump (Harvard Apparatus PHD 2000, Holliston, MA, USA) typically at a rate of 1 μ L/min unless otherwise specified. Following the end of the experiment, the mice were euthanized by decapitation, and the brains were isolated and immersion-fixed in 4% PFA overnight before further processing.

CM injection in pigs (Papers III and IV)

Pigs were anesthetized as previously described¹⁶⁴. Briefly, they were first premedicated with an intramuscular injection of a mixture of tiletamine, zolazepam and dexmedetomidine. Once unconscious, they were intubated, and a 20 G cannula was inserted into the ear vein connected to a triple i.v. line that administered maintenance anesthesia (ketamine, fentanyl and midazolam). The CM injection surgery was then performed as previously described^{164,168}. Briefly, the skin overlying the back of the head and neck was resected, and the underlying muscle

layers were severed and retracted to reveal the CM. The CM injection was performed using an 18 G cannula and was secured in place with glue. Fluorescent tracers (BSA-647, A β ₁₋₄₂ HiLyte-555, A β ₁₋₄₀ HiLyte-555, 10,000 MW dextran-555) and aCSF were injected according to the experimental design using a 1 mL syringe connected to a 10 cm i.v. line at a rate of 100 μ L/min. Following tracer circulation, the pigs were euthanized by an i.v. injection of pentobarbital, and tissues of interest were extracted and fixed in 4% PFA.

Intraparenchymal tracer injection (Paper I)

Mice were anesthetized with isoflurane and placed on a stereotactic frame. The skin overlying the dorsal skull was locally anesthetized with bupivacaine before an incision was made along the midline. A burr hole was then drilled at the coordinates: AP +0.6 mm; ML -2.0 mm, relative to bregma. A glass capillary containing the fluorescent tracer BSA-647 connected to a 10 μ L Hamilton syringe (Hamilton Company, Reno, NV, USA) was slowly inserted at DV -3.3 mm from the skull. The tracer was injected at a rate of 0.2 μ L/min for 5 min (1 μ L volume). The capillary was left in place for 10 min to prevent backflow and was then slowly retracted. The incision was closed using surgical glue (Histoacryl[®], B. Braun Medical AB, Danderyd, Sweden), and bupivacaine was injected subcutaneously in the wound area. The mice were allowed to recover from the anesthesia, and 48 h after the injection, they were anesthetized with K/X and transcardially perfused with PBS and 4% PFA. The brains were then immersion-fixed overnight in 4% PFA before further analysis.

Cranial window preparation (Paper I)

Mice were anesthetized with isoflurane and fixed to a stereotactic frame. Their heads were shaved and cleaned with isopropyl alcohol. Lidocaine was administered subcutaneously at the incision site and carprofen was given i.p. for postoperative analgesia. A 1.3 cm-diameter piece of skin was removed to expose the dorsal skull, and the surface of the skull was cleaned and dried. An aluminum frame was attached to the skull of the mice using dental acrylic (Fuji LUTE BC, GC, Tokyo, Japan and Super Bond, Sun Medical, Shiga, Japan). A 4 mm-diameter craniotomy was then performed using a dental drill centered above the barrel-field cortex approximately 2.5 mm posterior to bregma. When sufficiently thinned, the bone was gently removed, and a thin circular 4-mm diameter glass coverslip was mounted in its place and fixed to the skull with dental cement (C&B Metabond[®], Parkell, NY, USA). Animals were allowed to recover for a minimum of 48 h before two-photon imaging. The mice were administered i.p. carprofen once every 24 hours for two days after the surgery.

Heart failure mouse model (Paper I)

HF was induced by permanent ligation of the left anterior descending (LAD) coronary artery as previously described¹⁹⁹. Mice were anesthetized with isoflurane, intubated, and ventilated. A lateral thoracotomy was then performed, the pericardium was opened, and the LAD was permanently ligated. Following ligation, the chest was closed, and the mice were extubated upon spontaneous respiration. For sham surgeries, the same procedure was performed without ligation of the LAD. Mice received buprenorphine for post-surgery analgesia.

Transient middle cerebral artery occlusion (tMCAo) (Paper II)

The left MCA was occluded in mice anesthetized with isoflurane. A monofilament (9–10 mm coating length, 0.19 ± 0.01 mm tip diameter; Doccol, Sharon, MA, US) was inserted through a microincision in the external carotid artery and further advanced to the internal carotid artery. Reperfusion was initiated after 60 min by removing the filament. The mice were euthanized 1 or 7 days after tMCAo.

Ablation of olfactory sensory neurons (Paper III)

Pharmacological ablation of olfactory sensory neurons was achieved by intranasal administration of zinc-sulfate (ZnSO_4)²⁰⁰. Mice were anesthetized with isoflurane and 10 μL of 10% v/w ZnSO_4 in sterile saline or vehicle (sterile saline) were administered onto each of the nostrils using a 10- μL pipette in an alternating droplet instillation method (2 x 2.5 μL dose/nostril, 5-minute break between rounds). Following the treatment, mice were kept in a prone position to allow for excess fluid to exit the nasal cavity.

In vivo imaging and analysis

MRI (Papers I and III)

MRI acquisitions were performed on a 9.4 Tesla preclinical MR scanner using an Agilent magnet (Agilent, Santa Clara, USA), Bruker BioSpec Avance III electronics (Bruker, Ettlingen, Germany), with actively shielded gradients (maximum 670 mT/m; rise time 130 μs) and integrated shims (BGA 12S HP, Bruker, BioSpin, Ettlingen, Germany) and operated via ParaVision 7.0.0. Complete details of image acquisition, reconstruction and analysis can be found in Papers I and III. Briefly, the following sequences were used:

Cardiac MRI

Cardiac function was assessed in mice anesthetized with isoflurane using a quadrature volume transmit coil (112/086) and a 20 mm linear surface loop receive coil (Bruker, Ettlingen, Germany). A modified Bruker 2D ultra-short echo time (UTE) imaging sequence [echo time (T_E) = 0.5 ms; repetition time (T_R) = 5 ms; slice thickness = 1 mm; matrix size 96 x 96; field of view (FOV) = 25x25 mm²; flip angle $\alpha = 7^\circ$] was used to acquire a total of 12064 spokes per slice within 1 min^{201,202}. To cover the left ventricle from base to apex, 9-11 slices were needed depending on its size. The reconstructed data was exported into digital imaging and communications in medicine (DICOM) format, and were used for the assessment of hemodynamic parameters using Segment (v.3.3, Medviso, <https://segment.heiberg.se>)²⁰³. The volume of the left ventricle was manually drawn at the end-systolic and end-diastolic phases of the cardiac cycle, and the stroke volume and ejection fraction (EF) were automatically calculated by the software. The average heart rate over all measured slices was estimated by the software and used to calculate the cardiac output.

Brain volumetry

To measure brain volume, mice were anesthetized with K/X and scanned using a quadrature volume transmit coil (112/086), and a mouse 2x2 phased array receive coil (Bruker, Ettlingen, Germany). High-resolution T_2 -weighted Rapid Acquisition by Refocused Echoes (RARE; T_E = 21.4 or 33 ms; T_R = 3550 ms; slice thickness = 0.5 mm; 30 slices; 120x150; resolution 0.1x0.1 mm²; α = 180°; echo train length = 8; number of averages N_A = 13) acquisitions were used. Manual ventricle segmentations were performed within a scripted MATLAB (2023b; MathWorks, MA, USA) environment. Brain and ventricle masks were visualized and summed for each slice in MATLAB. Parenchymal tissue volumes were calculated as total brain mask voxel counts minus ventricular mask counts over the brain slices, multiplied by the voxel volume (0.005 mm³). The percentage of ventricular volume normalized to whole brain volume was defined as relative ventricular volume, while the percentage of parenchymal volume normalized to whole brain volume was defined as relative parenchymal volume.

Regional cerebral blood flow

For regional cerebral blood flow (CBF) measurements, mice anesthetized with K/X were scanned using a quadrature volume transmit coil (112/086), and a mouse 2x2 phased array receive coil. Flow-sensitive Alternating Inversion Recovery Echo-Planar Imaging (FAIR-EPI; T_E = 13.27 ms; T_R = 2039.8 ms; spectral bandwidth = 320.175 kHz; slice thickness = 1.5 mm; image matrix 73x64; resolution 0.2344x0.2329 mm²; N_A = 4) acquisitions with global pre-saturation over 6 inversion times for slice-selective and global inversion conditions were localized to coronal slices in the striatum and hippocampus, respectively. Data were exported as

DICOMs and used to estimate CBF per voxel according to methods previously described²⁰⁴. CBF fit and group statistical analyses were scripted in MATLAB and are available online at <https://doi.org/10.5281/zenodo.11475856>²⁰⁵. Regional masks for ventral striatum and hypothalamus were segmented manually in Fiji²⁰⁶. Descriptive statistics for associated CBF values were then calculated over each regional mask.

DCE-MRI

For the DCE-MRI experiments, mice anesthetized with K/X were scanned using a transmit/receive cryocoil. The 3D Fast Low-Angle Shot (FLASH) sequence ($T_E = 1.5$ ms; $T_R = 10$ ms; $\alpha = 10^\circ$; 100 μm isotropic resolution; acquisition time = 2.5 min per timepoint) was used to acquire a total of 26 scans, including two baseline pre-contrast scans. Following the acquisition, images were exported to DICOM format and imported to MICE Toolkit (v2022.4.9, NONPI Medical, Umeå, Sweden), where the acquisitions were motion-corrected. Net signal enhancement was calculated at each timepoint by subtracting the average signal of the two baseline acquisitions, and denoising was applied using principal component analysis. The merged anatomical image from each mouse was then used to manually draw eight spherical volumes of interest (VOIs) at the coronal orientation (four on each hemisphere). The VOIs were placed in the brain parenchyma, right above the anterior cerebral artery and at the ventral hypothalamus, as well as 1 mm dorsally to each of these. These masks were then applied to the DCE-MRI timepoints to calculate the enhancement over time as a measure of glymphatic influx⁴¹. The signal enhancement measurements from each right and left pair of VOIs were averaged to generate a single time-enhancement curve per brain area as a measure of CSF tracer influx. For the measurement of nasal CSF efflux, a mask over the whole nasal turbinates area was manually drawn on each slice and filtered by Otsu multi-step thresholding to exclude the air cavities and isolate the nasal turbinate tissue. Within this nasal turbinate mask, only the voxels that enhanced more than three times the standard deviation of the background noise throughout the experiment were considered in the signal enhancement calculation.

In vivo two-photon imaging of arterial pulsatility (Paper I)

Animals were imaged under a two-photon microscope (Thorlabs Bergamo with a Spectra Physics InSight® DS+™ laser) using a 25x objective (25x Nikon CFI APO LWD Objective, 380-1050 nm, NA = 1.10, WD = 2.0 mm). Images were acquired using ThorImage®LS v3.0 software. For in vivo vasculature labeling, mice were briefly anesthetized with isoflurane and given a retro-orbital injection of FITC-dextran (150 μL , 2000 kDa, D7137, Invitrogen/Thermo Fisher Scientific, CA, USA). After at least 20 min of recovery, each mouse was positioned under the objective lens via the headplate. Imaging of pial arteries was first performed in the

awake state at 3-5 different locations in each mouse for 2 min in each location (frame rate = 30 Hz). For the excitation of FITC-dextran, an 805-910 nm laser wavelength at <10 mW laser power was used, and emission was collected by a 525/25 nm filter (Semrock). Following awake imaging, the mice were anesthetized with K/X, and vasculature imaging was repeated using the same parameters as in awake imaging. For the analysis of arterial pulsatility and vasomotion, the diameter of a vascular segment was first measured in sequential frames. Then, the time series of the vascular diameter measurement was subtracted by its mean value, and a bandpass filter was applied to isolate the diameter changes in the frequency range of interest. The frequency range was set to 0.05-0.2 Hz for slow vasomotion, 10-14 Hz for cardiac arterial pulsatility in awake mice, and 2-6 Hz for cardiac arterial pulsatility under K/X anesthesia. Vascular pulsatility was then quantified by calculating the interquartile range of the bandpass-filtered signal. To account for differences in diameter among different vascular segments, the relative amplitude was also calculated by dividing the interquartile range by the average diameter of the vessel across all frames and is reported as relative arterial pulsatility or relative slow vasomotion. The amplitude of three to five vascular segments was averaged into one biological replicate.

In vivo transcranial fluorescence imaging (Papers III and IV)

For in vivo transcranial fluorescence imaging, after the CM cannula was glued to the skull, mice were positioned under a Nikon SMZ25 stereomicroscope with a Plan Apo 0.5x objective (NA = 0.08) equipped with an Andor Zyla 4.2 Plus sCMOS camera (Mag = 0.75x, Zoom = 1.5x). The BSA-647 tracer was excited using 635 nm CoolLED pE4000 LED illumination, and the emission was collected using a quadruple bandpass filter. The tracer injection and imaging were started simultaneously, and in vivo images were acquired at 1-min intervals. For the quantification of tracer distribution, image series were imported in Fiji²⁰⁶, regions of interest (ROIs) were manually drawn, and mean fluorescence intensities were measured.

Tissue processing, imaging and analysis

Ex vivo fluorescence imaging (Papers I, III and IV)

Tissues of interest containing fluorescent tracers were imaged post-fixation using a Nikon SMZ25 stereomicroscope. Brain sections and dorsal dura from mice were mounted on slides and imaged using a Nikon Ti2 wide-field fluorescence

microscope. For the analysis of tracer distribution, ROIs were drawn in Fiji²⁰⁶ and mean fluorescence intensities were measured.

Immunohistochemistry (Papers I, II and IV)

Standard immunohistochemistry protocols were used to stain for a variety of target proteins. When needed, antigen retrieval was performed with sodium citrate buffer or pepsin. Following a blocking and permeabilization step, sections were incubated with primary antibodies at 4 °C (*Table 1*). After washing with PBS, secondary antibodies conjugated to different fluorophores were applied. After washing the excess antibodies, incubation with lectin and DAPI was performed before mounting the sections on glass slides.

Table 1. Primary antibodies used for immunohistochemistry. AQP4 = aquaporin-4, GLUT-1 = glucose transporter 1, GFAP = glial fibrillary acidic protein, CD = cluster of differentiation, α -SMA = alpha smooth muscle actin, Iba1 = ionized calcium-binding adaptor molecule 1.

| Antibody | Source | Catalogue number | Company |
|--------------------|--------|------------------|-----------------|
| AQP4 | Rabbit | AB3594 | Merck Millipore |
| Laminin | Rabbit | ab7463 | Abcam |
| Collagen IV | Rabbit | ab6586 | Abcam |
| Cy3-conjugated IgG | Donkey | 715-165-150 | Nordic Biosite |
| GLUT-1 | Mouse | ab40084 | Abcam |
| | Mouse | MABS132 | Merck Millipore |
| GFAP | Rabbit | Z033429 | Dako/Agilent |
| CD31 | Rabbit | ab28364 | Abcam |
| α -SMA | Rabbit | ab5694 | Abcam |
| Iba1 | Rabbit | 019-19741 | Wako |
| Elastin | Rabbit | ab23747 | Abcam |

Images were acquired using a Nikon Ti2 wide-field fluorescence microscope and/or a Nikon A1RHD confocal scanning microscope. Image analysis was performed in Fiji²⁰⁶ and specific details for each quantification can be found in the respective papers.

Tissue clearing and light-sheet microscopy (Papers I, III and IV)

Mouse brains, mouse head and spine samples, and pig brain pieces were optically cleared using the iDISCO+ protocol as previously described²⁰⁷. Bone-containing samples were first decalcified in 10% ethylenediaminetetraacetic acid (EDTA) for 24 h. Samples were then washed in PBS, dehydrated in increasing methanol/H₂O solutions (20%, 40%, 60%, 80%, 100%, 1 h each and 100% overnight), delipidated with methanol/dichloromethane (33% / 66% for 3 h) and 100% dichloromethane (2 x 15 min), and finally immersed in ethyl cinnamate (ECi, 100%) for at least seven

days prior to imaging. Optically cleared samples were imaged using a LaVision UltraMicroscope Blaze light-sheet microscope (Miltenyi Biotec, Bergisch Gladbach, Germany) controlled by ImSpectorPro software (Miltenyi Biotec, Bergisch Gladbach, Germany), while immersed in ECI.

The image stacks were imported into Arivis Vision4D v3.5 (Zeiss Arivis, Rostock, Germany) for 3D reconstruction. Tiled images of the head-spine samples were manually aligned in the XY axes based on visual inspection, using the Tile Sorter function of Arivis Vision4D. Representative images and videos of the reconstructed samples were then acquired. The 3D reconstructed brains were analyzed using the built-in Analysis Pipeline of Arivis Vision4D. For the CM-injected brains, the Intensity Threshold Segmenter tool was used for each brain image set, and the sum voxel intensity of all the voxels with an intensity value above the threshold was then calculated and used as a measure of CSF tracer influx. For the intraparenchymally-injected brains, the sum intensity and sum volume of the voxels continuous to the injection site were calculated and used to assess glymphatic clearance from the brain. For tracer penetration depth analysis, image stacks were imported into Fiji²⁰⁶ and the maximum intensity projections were generated. The penetration depth of six vessels from the dorsolateral brain (three from each hemisphere) was measured and averaged into one biological replicate.

Summary of Results and Discussion

In this section, the main results from the papers included in the thesis are summarized and discussed. However, the reader is encouraged to refer to the final version of the papers and manuscripts attached at the end of this book.

Dysregulation of brain fluid dynamics in heart failure (Paper I)

The glymphatic system plays a crucial role in clearing waste products from the brain, and its dysfunction has been linked to various neurodegenerative conditions^{72,184}. HF is known to affect brain function and increase the risk of cognitive decline and AD^{208–210}, however, the mechanisms behind this interaction are not fully understood. Cerebral arterial pulsations originating in the heart have been reported to be a major driver of the glymphatic system^{77,125}. Therefore, this study aimed to investigate the impact of heart failure with reduced ejection fraction (HFrEF) on the glymphatic system using a mouse model of MI.

HF leads to increased glymphatic influx by enhancing arterial pulsatility

To study the effect of HF on glymphatic function, mice subjected to MI or sham surgery were injected in the CM at 12 weeks post-surgery. HFrEF resulted in a significant increase in glymphatic influx at 12 weeks post MI. This increase was observed using both a small molecular weight GBCA and a larger fluorescent tracer (BSA-647). Interestingly, glymphatic influx was inversely correlated with the EF, suggesting a relationship between the degree of cardiac dysfunction and CSF influx into the brain parenchyma (*Figure 11A-J*).

To understand the mechanism behind this increased influx, we used two-photon microscopy to measure cerebral arterial pulsatility, which is a well-established driver of glymphatic influx, especially under anesthesia. Our results revealed a significant increase in arterial pulsatility in MI mice compared to sham at 12 weeks post-surgery, providing a plausible explanation for the observed enhancement in glymphatic influx (*Figure 11K-L*).

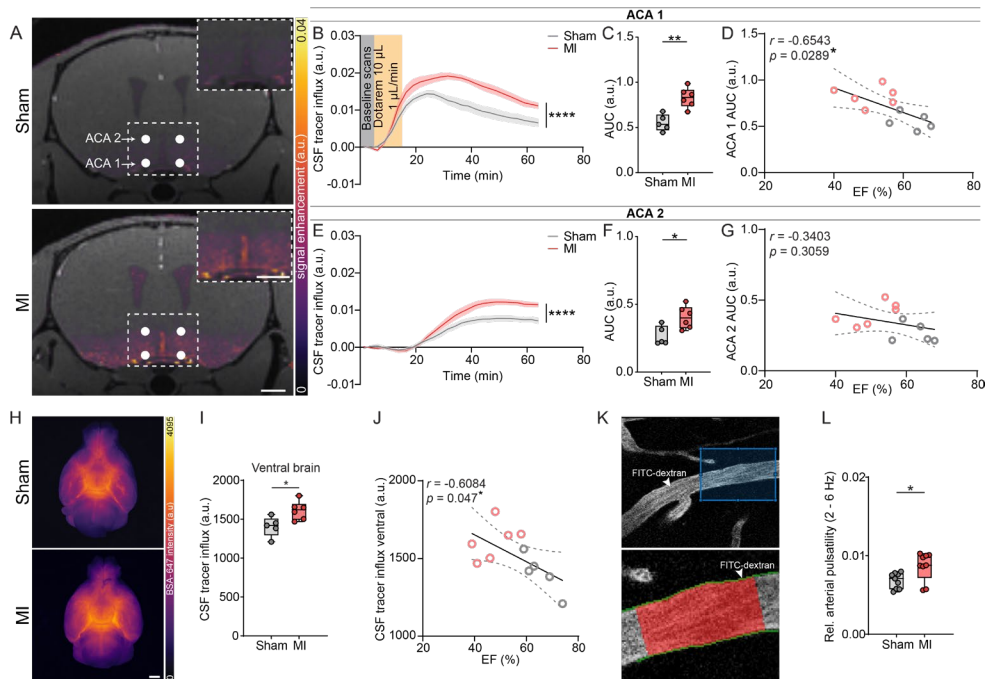


Figure 11. Glymphatic influx is increased at 12 weeks post MI due to enhanced arterial pulsatility. (A) Representative coronal images of parenchymal contrast agent infiltration 20 min after the end of the CM injection, at the level of the anterior cerebral artery (ACA) from a sham (top) and a MI (bottom) mouse. Signal enhancement was quantified by parenchymal volumes of interest (VOIs, white circles) positioned right above the ACA (ACA 1) and 1 mm dorsally (ACA 2). Scale bar: 1 mm; inset = 1 mm. (B-D) Characteristics of the CSF tracer influx at the ACA 1 VOI, including the time - mean enhancement curve (B), the area under the curve (AUC) (C) and the correlation between the AUC and the EF (D). (E-G) Characteristics of the CSF tracer influx at the ACA 2 VOI, including the time - mean enhancement curve (E), the AUC (F) and the correlation between the AUC and the EF (G). (H) Representative images of CSF tracer distribution at the ventral brain surface from a sham and a MI mouse. Scale bar: 2 mm. (I) Quantification of mean fluorescence intensity of CSF tracer influx at the ventral brain. (J) Correlation between EF and mean fluorescence intensity at the ventral brain surface. (K) Top: Representative in vivo two-photon fluorescence microscopy image of a pial artery after intravenous injection of FITC-dextran. The blue box indicates the vascular segment used for arterial pulsatility analysis. Bottom: The magnified vascular segment from which the vascular diameter oscillations were measured. (L) Arterial pulsatility amplitude, normalized to the vessel diameter, under K/X anesthesia. Adapted from Paper I¹⁹⁸.

Glymphatic mismatch between influx and clearance leads to a relative increase in brain parenchyma volume

Glymphatic clearance of intraparenchymally injected tracers is another method to assess glymphatic function, with reduced clearance considered to contribute to cognitive decline¹⁵². Here we found that clearance of intraparenchymally injected BSA-647 was not impaired at 12 weeks post-MI and did not correlate with the EF,

despite the increase in glymphatic influx (*Figure 12A-D*). This mismatch between influx and clearance suggests a dysregulation of the glymphatic system in HFrEF.

Further investigation using structural MRI scans showed that while whole brain volumes were similar between MI and sham groups at 12 weeks post-surgery, there was a significant reduction in ventricular volume in MI mice, which persisted even after normalizing for whole brain volume. Accordingly, the brain parenchyma of MI mice was proportionally increased compared to the sham group (*Figure 12E-I*).

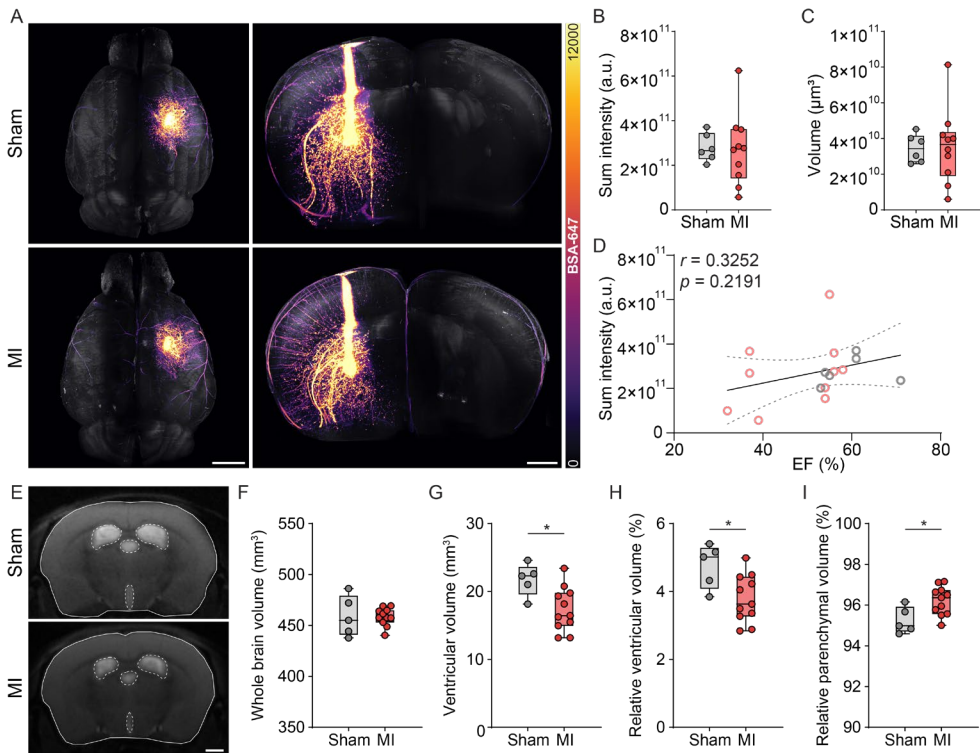


Figure 12. Glymphatic clearance is not affected by HF leading to proportionately larger brain parenchyma at 12 weeks post MI.

(A) Representative 3D reconstructed images of optically cleared brains isolated 48 h after fluorescent BSA-647 tracer was injected into the striatum of sham (top) and MI (bottom) mice; dorsal view (left) and close-up anterior view (right). Scale bar left: 2 mm; right: 1 mm. (B) Quantification of sum fluorescence intensity around the injection site of the tracer. (C) Quantification of interstitial tracer volume remaining around the injection site. (D) Correlation between EF and sum fluorescence intensity around the injection site. (E) Representative coronal brain images acquired using a RARE sequence from a sham (top) and a MI (bottom) mouse (brain masks marked with white lines and ventricular masks marked with white dashed lines). Scale bar: 1 mm. (F) Whole brain volume at 12 weeks post-MI or sham surgery. (G) Ventricular volume at 12 weeks post-MI or sham surgery. (H) Relative ventricular volume at 12 weeks post-MI or sham surgery. (I) Relative brain parenchymal volume at 12 weeks post-MI or sham surgery. Adapted from Paper I¹⁹⁸.

CBF emerges as a potentially new regulator of the glymphatic system

Finally, we investigated the relationship between CBF and glymphatic function. Using FAIR-EPI, we found a significant decrease in CBF in the hypothalamus of MI mice at 12 weeks post-surgery, while CBF in the striatum was not significantly affected. Intriguingly, the analysis also revealed an inverse correlation between CBF in the striatum and glymphatic clearance from that region (*Figure 13*). This finding suggests a previously unknown connection between CBF and the glymphatic system.

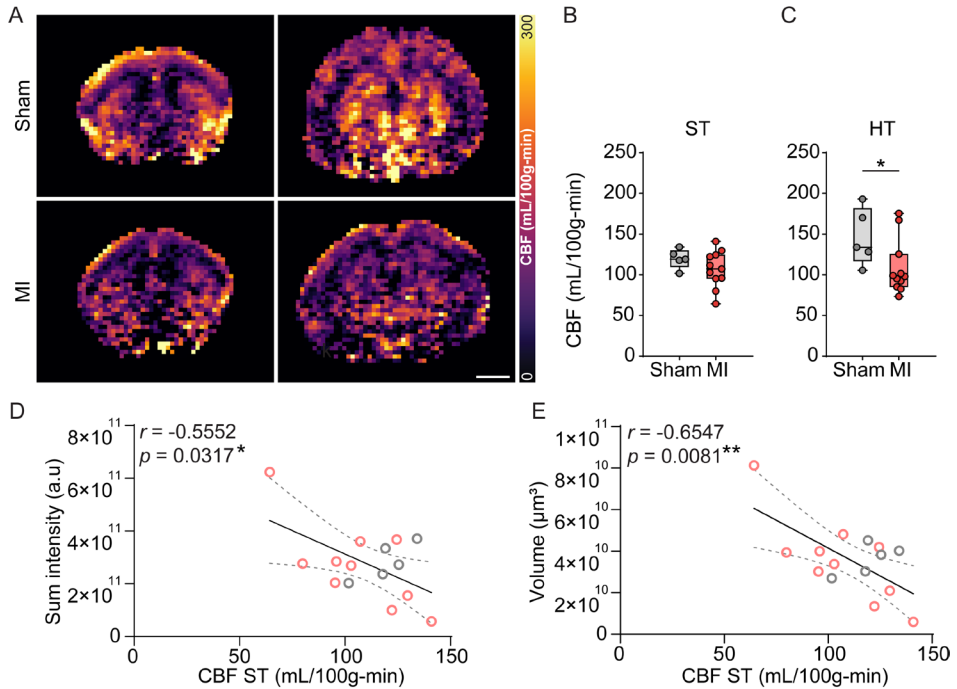


Figure 13. CBF inversely correlates with glymphatic clearance.

(A) Representative CBF maps acquired using a FAIR-EPI MRI sequence at 12 weeks post-surgery at the level of the striatum (ST, *left*) and the hypothalamus (HT, *right*) from sham (*top*) and MI (*bottom*) mice. Scale bar: 2 mm. (B) Mean CBF at the ventral striatum. (C) Mean CBF at the hypothalamus. (D) Correlation between mean CBF at the ventral striatum and sum fluorescence intensity around the injection site. (E) Correlation between mean CBF at the ventral striatum and tracer volume remaining around the injection site. Adapted from Paper I¹⁹⁸.

Overall, the results of **Paper I** show that HFrEF strongly affects glymphatic function. While glymphatic influx was shown to increase at 12 weeks post-MI, likely as a result of enhanced cerebral arterial pulsations, glymphatic clearance was not affected at that timepoint (*Figure 14*). This mismatch is consistent with dysregulation of brain fluid dynamics and potential fluid stagnation in the brain as indicated by the relative increase in brain parenchyma volume. This could explain

the increased CSF influx to the brain via perivascular pathways in HF, and why this was not associated with more solute clearance from the brain. We suggest that this fluid accumulation, whether intra- or extracellular, could be a source of further brain pathology in HF. The dysregulation of the glymphatic system in HF could contribute to the accumulation of neurotoxic waste products, potentially explaining the increased risk of cognitive impairment and AD in HF patients.

In search of mechanistic explanations for our results, we comprehensively examined various factors known to regulate glymphatic function. We found no significant differences in AQP4 polarization, extracellular matrix proteins, or BBB integrity between MI and sham mice. We also found no differences in CSF efflux through the nasal turbinates or in PVS size, thereby these factors are unlikely to influence our results.

In this study we also found that CBF might be a potential new regulator of glymphatic function, with reduced CBF correlating with impaired clearance. This observation adds CBF to the list of factors that can influence glymphatic function, paving the way for further research on this connection. As HFrEF progression eventually results in reduced CBF²¹¹, we speculate that glymphatic clearance may further deteriorate, potentially leading to neurodegeneration. Therefore, glymphatic dysfunction could be a mediator in the relationship between HF and neurodegeneration which is well-established both in humans and in animal models^{199,212,213}.

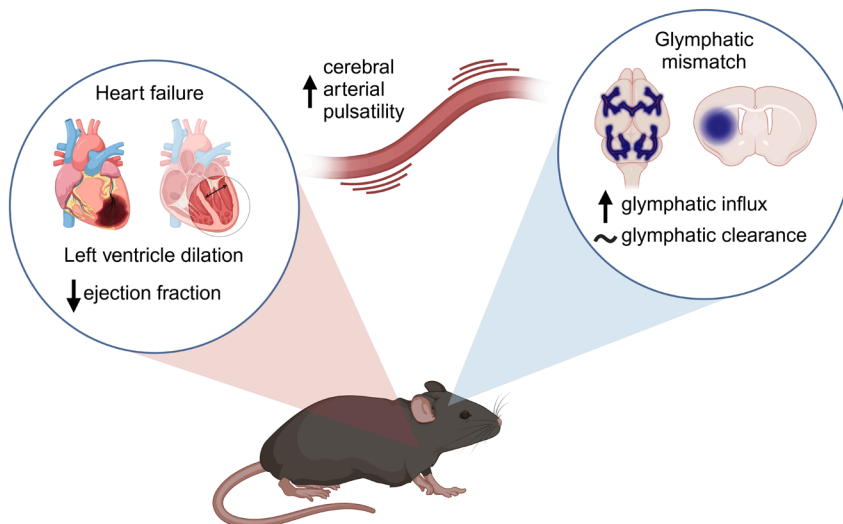


Figure 14. Glymphatic mismatch in HFrEF.

Schematic representation of the main findings of the study. MI-induced HF leads to left ventricle dilation and reduced EF. This gradually leads to increased glymphatic influx, supported by elevated cerebral arterial pulsatility. Glymphatic clearance, however, does not increase proportionately with influx, consistent with dysregulation of brain fluid dynamics. Created with BioRender.com.

Differential efficacy of lectins in cerebral blood vessel labeling (Paper II)

Cerebral blood vessels play a crucial role in maintaining brain homeostasis. Specifically in the context of the glymphatic system, cerebral blood vessels and the PVS that surrounds them constitute an integral part of the brain's clearing mechanism. AQP4 and specifically its polarized localization to the astrocytic endfeet that form the outer boundary of the PVS has been commonly used as an indicator of efficient glymphatic transport^{79,214,215}. Therefore, co-labeling of vasculature and AQP4 is essential for mapping perivascular pathways and assessing glymphatic function. Lectins are a class of carbohydrate-binding proteins that have long been used to label blood vessels due to their affinity for endothelial glycoproteins^{216,217}. However, the efficacy of different lectins in labeling cerebral vessels under different conditions has not been systematically compared. In this study we aimed to compare the efficacy of three commonly used lectins, *Griffonia simplicifolia* isolectin B4 (IB4), *wheat germ agglutinin* (WGA), and *Lycopersicon esculentum agglutinin* (LEA), in labeling mouse vasculature under physiological conditions and in a stroke model.

Superior efficacy of LEA lectin in labeling cerebral vasculature

The labeling efficacy of the different lectins was assessed in free-floating mouse brain sections, which are commonly used in glymphatic research. The efficacy was calculated by dividing the average peak signal at the vascular wall by the background signal of individual vessels (signal-to-noise ratio). LEA lectin showed a remarkably higher signal-to-noise ratio when compared to IB4 and WGA at equivalent concentrations (5 µg/mL) (*Figure 15A-D*).

Interestingly, while LEA excelled in histological applications, transcatheter perfusion with WGA lectin in high concentration (125 µg/mL) achieved similar vascular specificity (*Figure 15E-I*).

Reduced labeling specificity in ischemic stroke

We then tested how this lectin-based vascular labeling is affected in pathological conditions, specifically in a mouse model of ischemic stroke. For this we used a transient middle cerebral artery occlusion (tMCAo) model, that results in the formation of a necrotic core surrounded by a penumbra region.

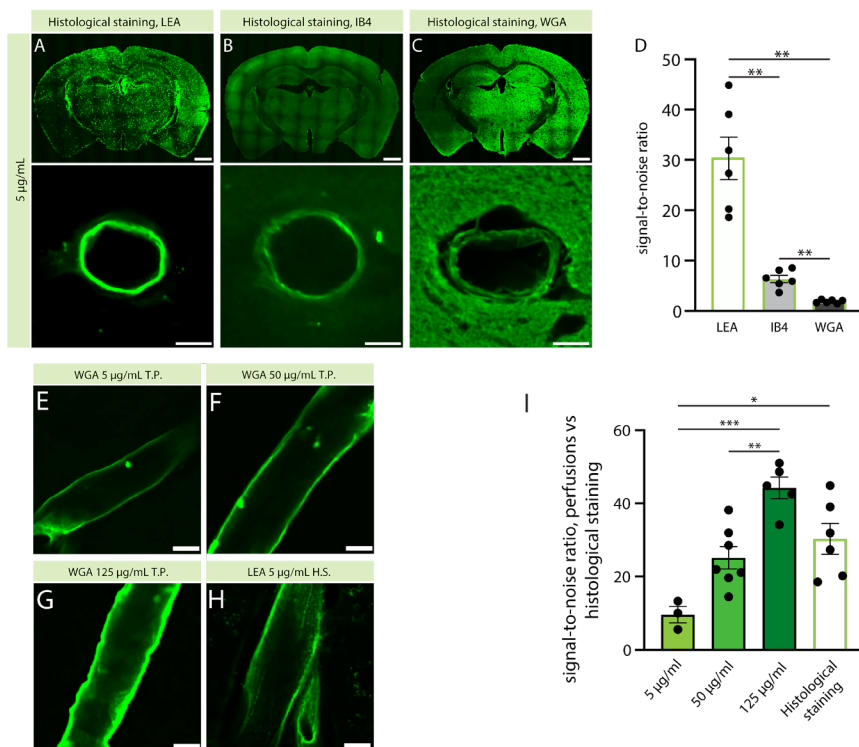


Figure 15. Efficacy of different lectins in labeling cerebral vasculature.

(A-C) Representative confocal images of coronal brain sections stained with LEA, IB4 and WGA lectins (top) and high magnification images of the blood vessels used for the quantification of the signal-to-noise ratio (bottom). Scale bars: 1 mm (top); 10 µm (bottom). (D) Quantification of the signal-to-noise ratio of the three lectins in labeling cerebral blood vessels. (E-H) Representative high magnification images of blood vessels stained with transcardial perfusion of increasing concentrations of WGA lectin (E-G) and with histological staining of LEA lectin (H). Scale bars: 10 µm. (I) Quantification of the signal-to-noise ratio of histological staining with LEA lectin vs transcardial perfusion of increasing concentrations of WGA lectin. Scale bars: 10 µm. T.P.= transcardial perfusion; H.S.= histological staining. Adapted from Paper II²¹⁸.

We found that 7 days post-stroke, LEA lectin's specificity for blood vessels dropped by 59% in the ischemic core and 69% in the penumbra. Further investigation revealed unspecific binding of LEA lectin to activated microglia (Iba1+ cells), likely due to altered glycoprotein expression during the inflammatory response (Figure 16). This off-target binding significantly compromised the utility of LEA for accurate vascular mapping in the post-stroke brain.

Taken together, the results of **Paper II** show that LEA is the optimal lectin for histological vascular labeling in healthy brain tissue. However, its utility diminishes significantly in pathological conditions such as stroke, where inflammatory responses can lead to unspecific binding.

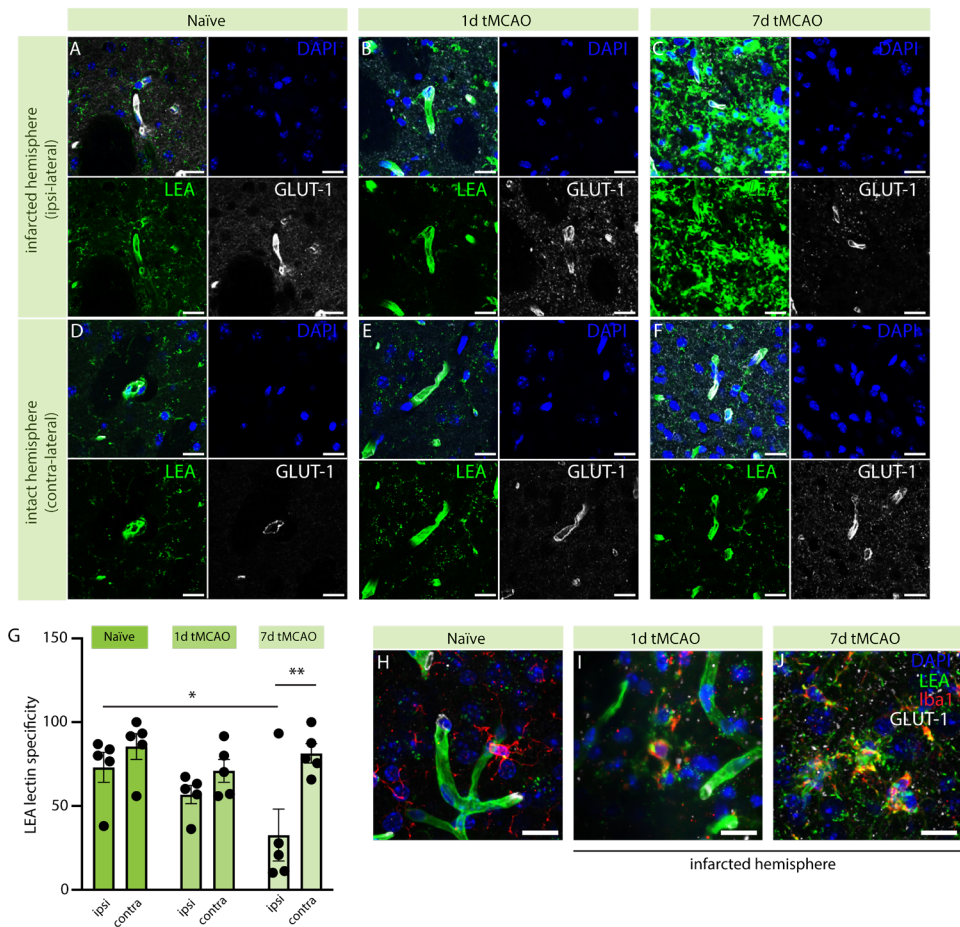


Figure 16. LEA lectin's specificity is reduced in ischemic stroke.

(A-F) Representative confocal images of blood vessels stained with LEA lectin, GLUT-1 and DAPI from the ipsilateral (A-C) and contralateral (D-F) hemispheres of naïve, 1d tMCAO and 7d tMCAO mice. Scale bars: 20 μ m. **(G)** Quantification of LEA lectin's specificity in labeling cerebral blood vessels from naïve, 1d tMCAO and 7d tMCAO mice. **(H-J)** Representative confocal images of blood vessels stained with LEA lectin, GLUT-1, Iba1 and DAPI showing the colocalization of LEA lectin and Iba1 staining in the infarcted hemisphere of the 1d tMCAO and 7d tMCAO mice compared to the naïve mice. Scale bars: 20 μ m. Adapted from Paper II²¹⁸.

These findings have important implications for glymphatic system research. Labeling the cerebral vasculature is crucial both for mapping the PVS and for assessing AQP4 polarization. The high specificity of LEA lectin in healthy brain tissue makes it an excellent choice for co-labeling with AQP4 in glymphatic studies. On the other hand, the increasing use of light-sheet microscopy of optically-cleared brains could benefit from the transcardial perfusion with WGA lectin which could

provide 3D labeling of the brain vasculature, while at the same time it bypasses the challenges of conventional antibody staining²¹⁹.

However, our study's results caution against over-reliance on lectin-based methods especially in disease models. The dramatic decline in LEA lectin's labeling efficacy within ischemic regions highlights the context-dependent nature of lectin binding and underscores the need for careful methodological validation in disease models where vascular and inflammatory changes occur.

Functional characteristics of the nasal CSF efflux pathway. (Paper III)

While the pathway that drains CSF through the cribriform plate and towards the nasal lymphatics and cervical lymph nodes has been known for several decades^{38,39}, its exact anatomical and functional characteristics are not clearly understood. A major reason for this is the difficulty in accessing this complex area, especially using in vivo imaging techniques. In this study we used a combination of in vivo and ex vivo imaging methods to elucidate functional aspects of the nasal efflux pathway.

Nasal efflux adapts to changes in CM injection rate

Using DCE-MRI, signal enhancement in the nasal turbinates of mice was measured in real time following CM injection of a GBCA at different injection rates. Compared to the commonly used injection rate of 1 $\mu\text{L}/\text{min}$, a lower injection rate of 0.4 $\mu\text{L}/\text{min}$ led to slower enhancement dynamics, with a slower enhancing slope and taking more time to reach maximum signal enhancement. Accordingly, a higher injection rate of 4 $\mu\text{L}/\text{min}$ yielded significantly faster enhancement dynamics with a steeper enhancing slope, while taking significantly less time to reach maximum signal enhancement (*Figure 17A-D*).

Similar results were observed following the injection of a larger fluorescent tracer in the CM at different injection rates. A progressive increase in tracer signal intensities in the nasal turbinates was found from lower to higher injection rates. The SCLNs, being the main downstream recipients of the nasal efflux pathway, reflected the result of the nasal turbinates, with reduced intensity in the low injection rate group and increased intensity in the high injection rate group. Interestingly, signal intensities in the DCLNs were not affected by the different injection rates (*Figure 17E-H*).

The nasal efflux pathway remains active in aging

Signal enhancement in the nasal turbinates of 2-year-old mice was not decreased compared to young adults. Real time in vivo signal enhancement revealed an increase in nasal turbinates signal during the last 20 min of circulation in the older mice, while the sum enhancement was not significantly different between the two groups (*Figure 18*).

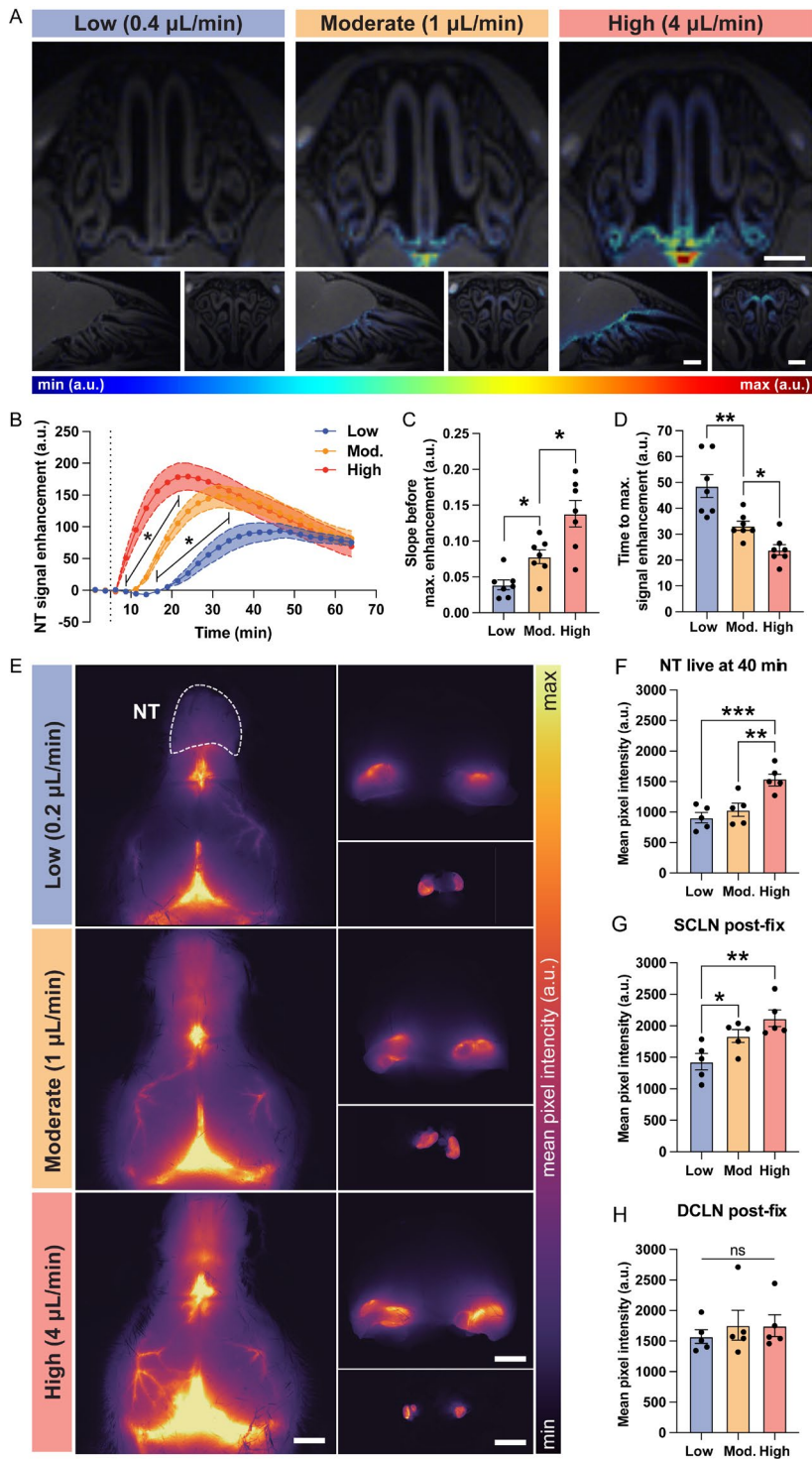


Figure 17. The nasal efflux pathway quickly responds to acute volumetric shifts of CSF.

(A) Representative images of the nasal turbinates (NT) at axial (*top*), sagittal (*left bottom*) and coronal (*right bottom*) views at timepoint 7 of the experiment. Scale bars: 1 mm. (B-D) Characteristics of tracer efflux to the nasal turbinates, including the time – enhancement curves (B), the slope before maximum enhancement (C) and the time to maximum enhancement (D). (E) Representative images of fluorescent in vivo tracer distribution on whole dorsal surface and nasal turbinates at 40 min from the beginning of tracer injection (*left*) and ex vivo imaging of SCLNs (*right top*) and DCLNs (*right bottom*) from mice injected at a low (*top*), moderate (*middle*) and high rate (*bottom*). Scale bars: 2 mm. (F) Quantification of mean fluorescence intensity at the nasal turbinates. (G) Quantification of mean fluorescence intensity at the SCLNs. (H) Quantification of mean fluorescence intensity at the DCLNs. Adapted from Paper III.

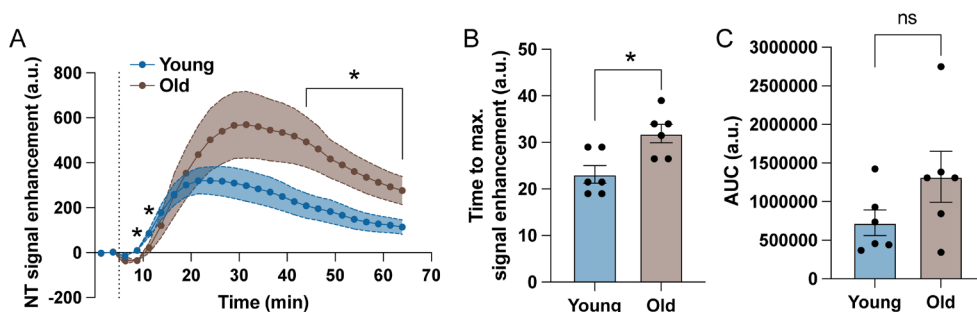


Figure 18. Nasal efflux is not impaired in aging.

(A) Time – enhancement curves of NT signal enhancement in young and 2-year-old mice. Dashed grey line indicates the start of tracer injection. (B) Time to maximum NT signal enhancement in young and 2-year-old mice. (C) Area under curve from NT signal enhancement at the last timepoint of the experiment in young and 2-year-old mice. Adapted from Paper III.

Circulating $A\beta_{1-42}$ leads to reduced nasal efflux

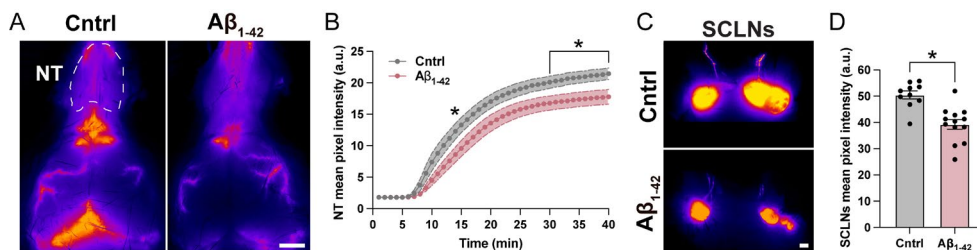


Figure 19. Nasal efflux is impaired by acute $A\beta$ exposure.

(A) Representative images of fluorescent in vivo tracer distribution on whole dorsal surface and nasal turbinates at 30 min from the end of tracer injection from mice co-injected with BSA-647 and $A\beta_{1-42}$ or BSA-647 and aCSF. Scale bar: 2 mm. (B) Time – intensity curves showing the mean fluorescence intensity at the nasal turbinates during the 40 min of the experiment. (C) Representative ex vivo images of SCLNs from mice co-injected with BSA-647 and $A\beta_{1-42}$ or BSA-647 and aCSF. Scale bar: 1 mm. (D) Quantification of mean fluorescence intensity at the SCLNs. Adapted from Paper III.

To demonstrate the effect of soluble A β_{1-42} on the nasal efflux pathway, A β_{1-42} was co-injected in the CM together with the fluorescent tracer BSA-647. The tracer signal in the nasal turbinates captured by in vivo transcranial imaging was progressively reduced over time in the A β_{1-42} co-injection group compared to the group co-injected with aCSF. Signal intensity in the SCLNs was also reduced, showing that acute exposure to A β_{1-42} in the CSF diminished tracer efflux through the nasal pathway (*Figure 19*).

Ablation of olfactory sensory neurons impairs nasal efflux

Intranasal treatment with ZnSO₄ was used in mice to cause degeneration of the olfactory sensory neurons that cross the cribriform plate, acting as conduits for the flow of CSF to the nasal turbinates. Seven days after the ZnSO₄ treatment, the olfactory epithelium and the olfactory sensory neurons were markedly damaged. Assessment of the signal enhancement in the nasal turbinates following the CM injection of a GBCA revealed that the area that enhanced significantly was reduced due to the ablation, leading to impaired signal enhancement dynamics in mice treated with ZnSO₄ compared to those treated with saline (*Figure 20*).

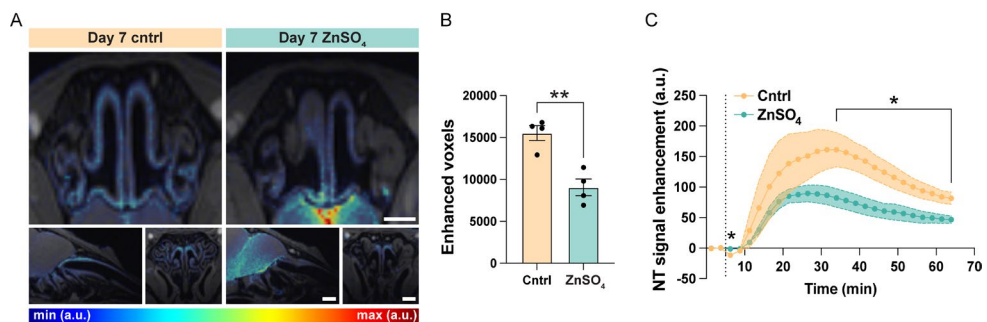


Figure 20. Nasal efflux is impaired by intranasal treatment with ZnSO₄.

(A) Representative images of the nasal turbinates (NT) at axial (top), sagittal (left bottom) and coronal (right bottom) views on day 7 at timepoint 18 of the experiment. Scale bars: 1 mm. (B) Number of nasal turbinate voxels that significantly enhanced following the GBCA injection. (C) Time – enhancement curves of the signal enhancement at the nasal turbinates of mice treated with ZnSO₄ or saline. Adapted from Paper III.

The results of **Paper III** establish the nasal route as an important CSF efflux pathway that can rapidly adapt to different pathophysiological challenges. Using multimodal in vivo and ex vivo imaging techniques, we were able to further characterize anatomical and functional aspects of this complex efflux pathway that extends from the cribriform plate to the lymph nodes of the cervical region.

We showed that the nasal efflux pathway can quickly respond to acute volumetric shifts of CSF and readily disseminate the fluid to downstream compartments. We

also validated, using light-sheet microscopy of optically cleared samples, the direct connection between the nasal area and the SCLNs, which constitute the primary drainage site for nasal efflux.

Interestingly, unlike other efflux pathways that have been shown to deteriorate in aging, such as the meningeal and nasopharyngeal lymphatics^{42,51,220}, CSF flow through the cribriform plate was preserved in 2-year-old mice, suggesting that this pathway remains functional throughout the lifespan of mice. While the downstream flow to the SCLNs has been reported to diminish in aging due to reduced contractility of the superficial cervical lymphatic vessels²²¹, the nasal turbinates constitute an outflow reservoir that can accommodate CSF flow.

Previous studies have linked AD to impaired CSF clearance by the nasal route¹⁴⁵. However, little is known about the impact of A β on the efflux pathways. Our co-injection experiments revealed that acute exposure to A β_{1-42} impaired efflux through the nasal pathway.

Finally, our DCE-MRI experiments expanded on previous findings regarding the disruption of nasal efflux following intranasal ZnSO₄ treatment, which damages the olfactory sensory neurons, a crucial component of the pathway²⁰⁰.

Taken together, these findings highlight the nasal pathway's unique ability to regulate CSF efflux under different situations. Future studies could harness this pathway to enhance CSF efflux in a variety of acute and chronic diseases.

$A\beta_{1-42}$ clearance pathways in the gyrencephalic brain (Paper IV)

The glymphatic system has been repeatedly shown to contribute to $A\beta$ clearance from the CNS^{71,72,110}. However, once in the CSF, $A\beta$ can still interact with the brain and the glymphatic system and the consequences of this interaction remain largely unknown. This study aimed to investigate the consequences of $A\beta$ recirculation in the CSF on glymphatic function and to further explore $A\beta$ distribution and clearance pathways. To this end, we used a pig model, which offers a larger, more complex brain structure similar to humans, to gain insights that may be more translatable to human physiology than those obtained from rodent studies^{164,168}.

Circulating $A\beta_{1-42}$ causes global impairment in glymphatic influx

To study the effects of $A\beta$ circulation in the CSF, pigs were co-injected in the CM with the fluorescent tracer BSA-647 and $A\beta_{1-42}$ HiLyte-555 or aCSF, which were allowed to circulate for 2 h (*Figure 21A*). The introduction of $A\beta_{1-42}$ into the CSF resulted in significant reductions in global CSF distribution and glymphatic influx. Whole brain imaging revealed marked decreases in tracer distribution across dorsal, lateral, and ventral surfaces in $A\beta_{1-42}$ injected animals compared to controls (*Figure 21B-F*). This impairment was further evident in cortical sections, where a 31% reduction in overall tracer influx was observed throughout the anteroposterior axis (*Figure 21G-I*).

$A\beta_{1-42}$ is retained at the proximal PVS influx sites

Closer examination of $A\beta_{1-42}$ distribution patterns revealed a distinctive accumulation at the proximal PVS sites. Confocal imaging of penetrating vessels revealed that while BSA-647 traveled from large vessels to downstream microvasculature, $A\beta_{1-42}$ appeared to be retained at the larger penetrating vessel influx sites.

Quantification of penetration depth along penetrating vessels demonstrated that $A\beta_{1-42}$ penetrated on average 150 μm less than BSA-647 (*Figure 22A-C*). This difference in penetration depth was intriguing, given that $A\beta_{1-42}$ has a significantly lower molecular weight than BSA-647 and would be expected to penetrate further based on size alone.

High-magnification confocal imaging of the microvasculature approximately 1.5 mm below the brain surface revealed a striking absence of $A\beta_{1-42}$ at this depth, while BSA-647 was present in the PVS of the microvasculature (*Figure 22D-F*).

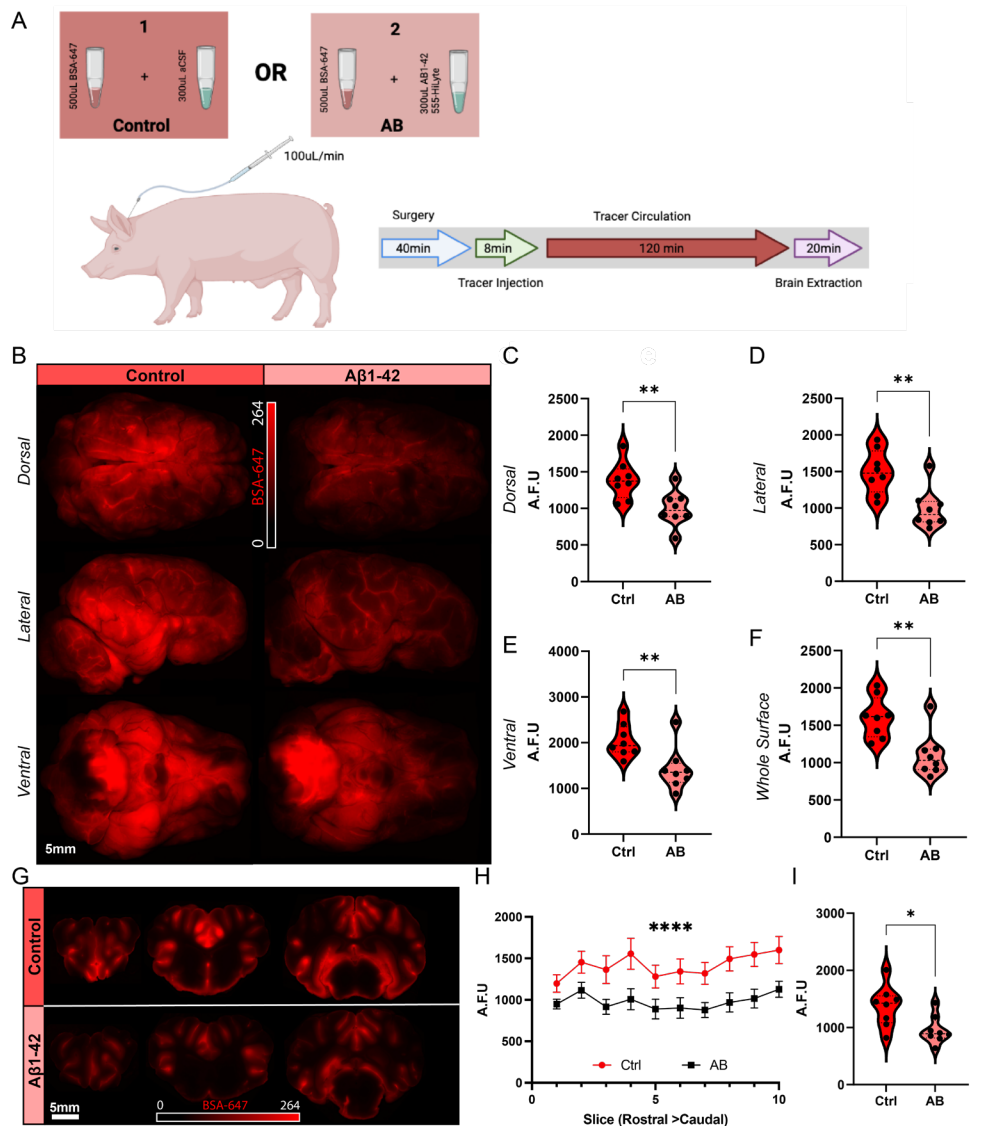


Figure 21. Glymphatic influx is impaired by $A\beta_{1-42}$ in the CSF.

(A) Schematic representation of the experimental setup. (B) Representative images of dorsal, lateral and ventral brain surfaces from control and $A\beta_{1-42}$ injected pigs. (C-F) Quantification of fluorescence intensity at dorsal (C), lateral (D), ventral (E) and all brain surfaces (F) between control and $A\beta_{1-42}$ injected animals. (G) Representative coronal cortical sections from control and $A\beta_{1-42}$ injected animals. (H) Quantification of fluorescence intensity in ten sections from rostral to caudal in control and $A\beta_{1-42}$ injected animals. (I) Quantification of average fluorescence intensity from all coronal slices between control and $A\beta_{1-42}$ injected animals. Adapted from Paper IV.

Furthermore, light-sheet microscopy of optically cleared pieces of pig cortex provided a comprehensive view of this phenomenon, showing widespread $A\beta_{1-42}$ entrapment across approximately 100 vessels in the given cortical area. All of these examined vessels exhibited substantial BSA-647 penetration along the PVS, with only shallow aggregation of $A\beta_{1-42}$ (*Figure 22G*).

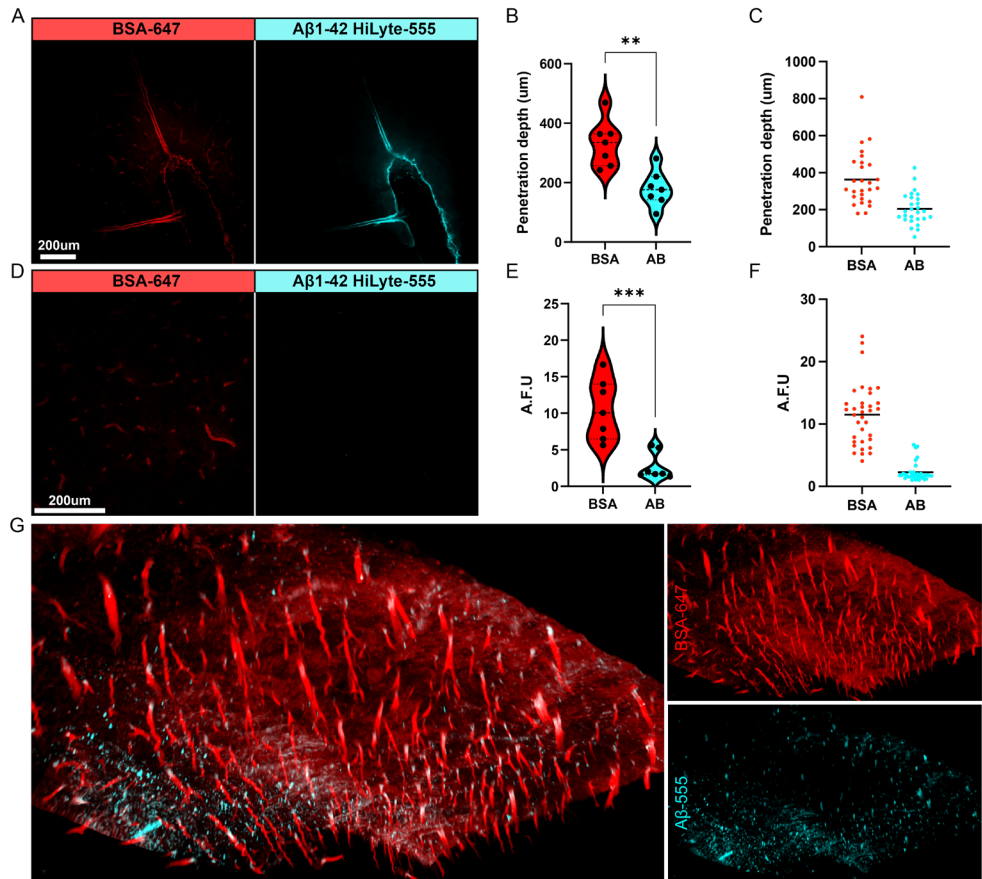


Figure 22. $A\beta_{1-42}$ aggregation at proximal PVS influx sites.

(A) Representative images of a sulcus showing the depth of penetration between BSA-647 and $A\beta_{1-42}$. (B-C) Quantification of tracer penetration depth along penetrating vessels for BSA-647 and $A\beta_{1-42}$ for each pig (B) and for all vessels analyzed (C). (D) Representative images approximately 1.5 mm below the brain surface showing BSA-647 in smaller PVS but absent of $A\beta_{1-42}$. (E-F) Quantification of tracer intensities in deep cortical regions for each pig (E) and for all regions analyzed (F). (G) Representative three-dimensional reconstruction image from light sheet microscopy showing widespread $A\beta_{1-42}$ aggregation in upper PVS and deeper BSA-647 penetration. Adapted from Paper IV.

A β ₁₋₄₂ co-localizes with elastin across the cerebral arterial wall

From our first observations of the large caliber vessels of the Circle of Willis, it was immediately noticeable that BSA-647 and A β ₁₋₄₂ seemed to have different localization across the vascular wall. High-magnification images of coronal sections revealed that while BSA-647 was primarily found in the outer vessel border at the level of the adventitia, A β ₁₋₄₂ showed a strong affinity for the inner vascular lumen with additional string-like distributions within the smooth muscle and adventitial layers of the vessel wall. Sections from the middle cerebral artery (MCA) were then stained for smooth muscle actin (SMA) to visualize the smooth muscle layer (tunica media) of the vessel. Analysis of the intensity profile of each fluorophore showed that BSA-647 localized to the adventitia layer while A β ₁₋₄₂ localized to the tunica intima, thereby confirming the previous observations (*Figure 23A-F*).

We then hypothesized that this A β ₁₋₄₂ localization might in fact relate to the localization of elastin elements in the vascular wall. Immunostaining against elastin confirmed that A β ₁₋₄₂ co-localized with elastin elements across the vascular wall. These included thin fibers running throughout the media and adventitia layers of the vessel, as well as the thick inner elastic lamina, located in close proximity to the endothelial cell basement membrane (*Figure 23G-H*).

Overall, the results of **Paper IV** show that the glymphatic system is significantly impaired by acute exposure to A β ₁₋₄₂. This observation is of great importance since the mechanisms around waste management following glymphatic clearance from the brain are still poorly understood. Once brain waste enters the perivenous space, it is expected to be cleared along the different efflux pathways⁷¹. However, the exact anatomical pathways of this transport remain a matter of debate, and it is still unclear whether these waste products can recirculate in the CSF compartment and for how long. A recent study proposed that waste products can follow bridging veins which eventually enter the dura. The arachnoid cuff exits that form around them may allow the exit of solutes from the subarachnoid space to the dura⁵³. Interestingly, this global reduction in glymphatic transport was only evident in the larger gyrencephalic brain of pigs. Previous studies in mice, as well as our own experiments had shown that co-injection of A β was not sufficient to impair the glymphatic system¹⁵³. While we cannot postulate what the case would be in humans, these results highlight the importance of the pig model to study the glymphatic system.

Based on our observation that A β ₁₋₄₂ does not penetrate as far into the PVS as the BSA-647 does, despite its reduced molecular weight, we were able to identify the distinct localization patterns of these two molecules across the vascular wall of large caliber arteries. Again, the use of the pig model with its large structures was invaluable in revealing these details.

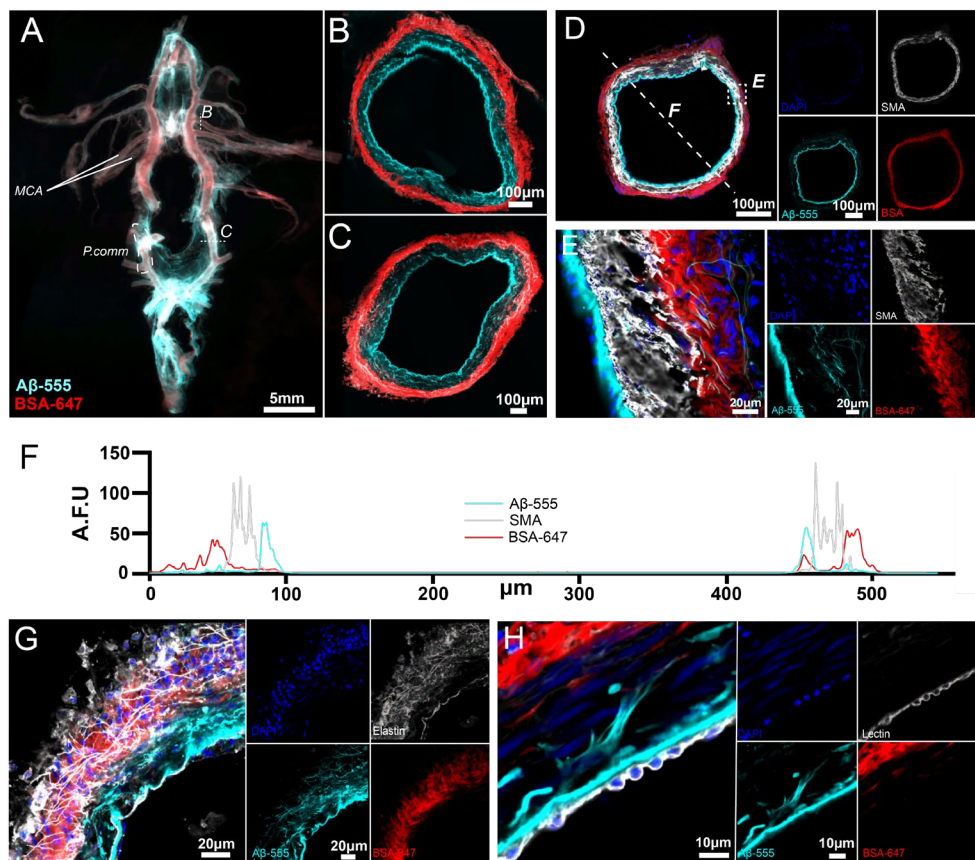


Figure 23. $A\beta_{1-42}$ co-localizes with elastin elements across the cerebral arterial wall.

(A) Representative image of dissected circle of Willis from an $A\beta_{1-42}$ injected pig. (B-C) Representative confocal images of MCA (B) and posterior communicating artery (C) sections from an $A\beta_{1-42}$ injected pig showing BSA-647 and $A\beta_{1-42}$ HiLyte-555 localizations along the vascular wall. (D) Representative confocal image of an MCA section from an $A\beta_{1-42}$ injected animal with immunohistochemical staining for SMA and dotted white line along which fluorophore intensities are plotted. (E) Higher magnification image from (D) of the vascular wall where SMA (white) denotes the tunica media of the vessel. BSA-647 (red) is localized to the adventitia, while $A\beta_{1-42}$ is localized towards the tunica intima. (F) Intensity plot from the MCA of an $A\beta_{1-42}$ injected animal showing differential peaks of fluorophore localizations across the vascular wall. (G) Representative high magnification confocal image of the MCA from an $A\beta_{1-42}$ injected animal with immunohistochemical staining for elastin (white) showing co-localization of $A\beta_{1-42}$ (cyan) and elastin (white) along the internal elastic lamina elastin fibers throughout the vascular wall. (H) High magnification confocal image from the vascular wall showing $A\beta_{1-42}$ (cyan) localized at the internal elastic lamina and the tunica media, in close proximity to the endothelial cell layer stained with lectin (white). Adapted from Paper IV.

Intriguingly, the elastin-based system that facilitates the transport of $A\beta$ across the vascular wall appeared to be specific to biologically relevant proteins. Indeed, only $A\beta_{1-42}$ and $A\beta_{1-40}$ exhibited this distribution, while biologically inert proteins such as BSA-647 and 10,000 MW dextran-555 were only localized to the outer vascular

wall. In an attempt to further characterize this pathway, transmission electron microscopy of MCA sections revealed a complex network of tributaries between smooth muscle cells that could be traced from the outer boundary of the tunica media down to the internal elastic lamina. This suggests a potential route for the transport of A β ₁₋₄₂ from the CSF and outer vascular boundary to more luminal sites in close proximity to endothelial cells. Since vascular endothelial cells and smooth muscle cells are known to express the low-density lipoprotein related receptor protein 1 (LRP1) that mediates the transport of A β across the BBB²²²⁻²²⁴, it can be postulated that this pathway facilitates the clearance of A β from the CSF to the blood. Whether this pathway also contributes to the clearance of other proteins such as α -synuclein as well as the degree of relative contribution compared to other clearance pathways remains to be investigated.

Conclusions and Future perspectives

This thesis aimed to address several aspects of CSF circulation and the glymphatic system in physiological and pathological situations. Much like the CSF field that extends to several different directions, this thesis also touched upon various topics; from the investigation of disease models and their impact on the glymphatic system to comparative studies and methodological refinement and from CSF efflux pathways to alternative clearance mechanisms of A β .

In **Paper I** we used a model of HF to study its impact on the glymphatic system. While the system has naturally been studied in a variety of neurological diseases, there are very few glymphatic studies done in disease models of other organs, such as diabetes. Interestingly, in that model of diabetes, a similar case of glymphatic mismatch was reported, with increased glymphatic influx and reduced glymphatic clearance^{196,197}. While in our study the increased glymphatic influx was accompanied by no difference in glymphatic clearance, these studies collectively suggest that the mechanisms regulating influx and clearance are not identical. Glymphatic function relies on a delicate balance among several fine-tuned factors, and changes in each of these parameters can exert partial effects on influx, clearance, or both. Therefore, it is crucial to comprehensively examine various drivers of the glymphatic system, as the interplay between them both in physiology and under different diseases is still not fully understood. At the same time, this study found that reduced CBF correlated with reduced glymphatic clearance, pointing towards CBF as a potential new regulator of glymphatic clearance. However, more studies are needed to investigate how exactly CBF exerts its effect on glymphatic clearance and whether this connection applies to other disease models as well as under physiological conditions. It is important to note that CBF was measured under anesthesia and emerging evidence suggests that the primary regulators of glymphatic flow might differ between sleep and anesthesia¹³⁷. Therefore, the role of CBF in glymphatic clearance should be further studied in sleeping mice with the use of MRI. While CBF changes cannot be easily induced due to autoregulatory mechanisms that normally maintain it within a certain range, its reduction in different disease models could still be used as a diagnostic marker for reduced glymphatic clearance. As a result, the widespread application of CBF measurement using MRI in clinical practice could offer a simple, non-invasive estimation of glymphatic clearance in diseases where CBF is compromised, such as AD, HF and diabetes. Finally, this study paves the way for future investigations into the effects

of cardiovascular and other diseases on the brain's clearance mechanisms, raising the awareness of different fields on the glymphatic system and its implications.

In **Paper II** we aimed to provide a comprehensive guide for selecting the most appropriate lectin and labeling method for different experimental setups. Out of the commonly used lectins that were tested, LEA lectin emerged as the ideal choice for labeling healthy cerebral vasculature on free-floating brain slices, with its specificity being on par with genetic labeling and a commonly used immunostaining marker. However, it should be used with caution in disease models, especially when neuroinflammation is expected or suspected, due to potential unspecific binding to activated microglia. On the other hand, when the experimental design allows it, transcatheter perfusion with WGA lectin can produce equally good results compared to histological application of LEA lectin. In conclusion, while lectins remain valuable tools for vascular labeling in glymphatic research, their application demands careful consideration of tissue type, physiological state, and experimental goals. These findings underscore the need for ongoing refinement of research methods as our understanding of the glymphatic system evolves. They also serve as a reminder that even well-established methods require periodic re-evaluation and validation across different experimental contexts. As the field progresses, continued method development and cross-validation will be essential to ensure robust, reproducible findings that expand our understanding of brain physiology and pathology.

In **Paper III** we delved into the functional characterization of the nasal CSF efflux pathway using a range of in vivo and ex vivo imaging techniques. We confirmed that this site of CSF drainage can dynamically adapt to acute volumetric shifts of CSF, while it also remains functional in aging. However, it is acutely impaired by exposure to circulating A β and when the olfactory sensory neurons are damaged. Further studies should try to unravel the mechanisms behind this A β -induced impairment and whether it is due to a mechanical blockade or a functional phenomenon specific to A β . Investigation of the efflux pathways in transgenic models of AD could be useful in this regard. Similarly, more work is needed to elucidate the role of olfactory sensory neurons in this pathway and identify whether CSF flows within the perineurium or within lymphatic vessels that cross the cribriform plate. Functional experiments using lymphatic reporter mouse lines as well as the application of vascular endothelial growth factor C (VEGFC), which promotes lymphangiogenesis could provide answers to these questions. Finally, we also reported that this pathway is conserved between mice and pigs, paving the way for investigation of the anatomical and functional aspects of this pathway in humans. While the CSF efflux pathways have been an area of increased research in the last few years, several key questions remain unanswered, such as their relative contribution to CSF efflux under physiological and pathological conditions. To this end, more in vivo studies are needed to investigate CSF in different pathways simultaneously and not in isolation. Additionally, their connections to the

glymphatic system have been seriously understudied. A recent study reported that improving the contractility of superficial cervical lymphatic vessels increased glymphatic clearance following an intraparenchymal injection of tracer²²¹, paving the way for therapeutic applications that target the efflux pathways to exert an effect on the glymphatic system. Since the nasal efflux pathway runs in close proximity to the nose, the intranasal route constitutes a promising candidate for drug delivery targeting the nasal efflux pathway and ultimately the glymphatic system.

In **Paper IV** we used the pig model that has been developed in our lab^{164,168} to study how the glymphatic system is affected by acute exposure to A β . We found that soluble A β caused a global impairment of glymphatic influx, providing insights into the consequences of A β recirculation in the CSF. This impairment of glymphatic influx that was observed in pigs, but not in mice, highlights the importance of studying these processes in the larger gyrencephalic brain of pigs that better resembles human physiology. Additionally, the identification of an elastin-based pathway that mediates A β transport across the vascular wall provides new insights into potential clearance mechanisms. This pathway, which appears to be specific for biologically relevant proteins, may serve to funnel waste from the CSF to vascular endothelial cells, where it can be cleared to the blood. Further work is needed to delineate the mechanisms of this transmural pathway as well as to identify the exact role of elastin in it. To this end, mice with elastin haploinsufficiency could be used to study how the reduction of vascular elastin affects A β circulation. These mice could also be crossed with transgenic AD mouse lines to investigate whether reduction of vascular elastin aggravates AD pathology. The existence of this pathway specifically for the transport of biologically relevant proteins also exposes potential caveats of glymphatic studies. Inert tracers that are commonly used to study CSF circulation might follow different paths compared to proteins that are actually cleared by the glymphatic system. Therefore, the use of biologically relevant proteins (conjugated with fluorophores or radio-labeled) should be an integral part of future CSF and glymphatic research. In conclusion, this study not only advances our understanding of brain waste clearance but also poses important questions about the clearance of waste once it (re)enters the CSF.

Reflection on methods and final remarks

The studies included in this thesis started amidst an ever-changing landscape of methods used to study CSF circulation and the glymphatic system. In many cases our methodology changed to comply with emerging advances in the field, while we also implemented well-established methods. The use of MRI (Papers I and III) has been pivotal for the expansion of our understanding of in vivo CSF dynamics. While the development and constant refinement of the sophisticated analysis pipelines can be challenging, each new application pushes the boundaries of the field a little further. Given the dependence of glymphatic influx measurements on tracer size,

we have tried to use both small GBCA and large fluorescent tracers in our studies (Papers I and III). The similar results that we reported highlight the efficacy of both methodologies and provide complementary insights into different aspects of glymphatic function and CSF efflux. Additionally, the use of light sheet microscopy (Papers I, III and IV) has opened new avenues for visualizing the system as a whole, unveiling previously hidden connections. Finally, the use of both mice and pigs (Papers III and IV) with their converging and conflicting findings highlights important translational insights. Since the methods to study the glymphatic system are constantly evolving, there is great need for comparative studies and for results that are consistent across different methodologies.

After more than a decade of intense glymphatic research, some of the early controversies that emerged regarding the role of sleep and AQP4 have now been elucidated, while others still remain^{17,139,225,226}. It is certain that future technological advances will allow us to dig deeper into the mechanisms and implications of this system. Despite opposing views, the discovery of the glymphatic system sparked an unparalleled interest in the field of CSF circulation, with thousands of studies constantly challenging the boundaries of our knowledge and opening new avenues for exploration.

References

1. Wright BLC, Lai JTF, Sinclair AJ. Cerebrospinal fluid and lumbar puncture: a practical review. *J Neurol*. 2012;259(8):1530-1545. doi:10.1007/s00415-012-6413-x
2. Finger S. *Minds Behind the Brain: A History of the Pioneers and Their Discoveries*. Oxford University Press; 2010. doi:10.1093/acprof:oso/9780195181821.001.0001
3. Herbowski L. The Maze of the Cerebrospinal Fluid Discovery. *Anat Res Int*. 2013;2013:1-8. doi:10.1155/2013/596027
4. Rubin RC, Henderson ES, Ommaya AK, Walker MD, Rall DP. The Production of Cerebrospinal Fluid in Man and Its Modification by Acetazolamide. *J Neurosurg*. 1966;25(4):430-436. doi:10.3171/jns.1966.25.4.0430
5. Lehtinen MK, Bjornsson CS, Dymecki SM, Gilbertson RJ, Holtzman DM, Monuki ES. The choroid plexus and cerebrospinal fluid: emerging roles in development, disease, and therapy. *J Neurosci*. 2013;33(45):17553-17559. doi:10.1523/JNEUROSCI.3258-13.2013
6. MacAulay N, Keep RF, Zeuthen T. Cerebrospinal fluid production by the choroid plexus: a century of barrier research revisited. *Fluids Barriers CNS*. 2022;19(1):26. doi:10.1186/s12987-022-00323-1
7. Faivre E, Paris F de médecine de. *Thèse Pour Le Doctorat En Médecine Des Granulations Méningiennes*. Rignoux; 1853. <https://books.google.se/books?id=xn2vYgEACAAJ>
8. Weed LH. THE CEREBROSPINAL FLUID. *Physiol Rev*. 1922;2(2):171-203. doi:10.1152/physrev.1922.2.2.171
9. Dandy WE. EXPERIMENTAL HYDROCEPHALUS. *Ann Surg*. 1919;70(2):129-142. doi:10.1097/00000658-191908000-00001
10. Frazier CH, Peet MM. FACTORS OF INFLUENCE IN THE ORIGIN AND CIRCULATION OF THE CEREBROSPINAL FLUID. *Am J Physiol Content*. 1914;35(3):268-282. doi:10.1152/ajplegacy.1914.35.3.268
11. de Rougemont J, Ames A, Nesbett FB, Hofmann HF. FLUID FORMED BY CHOROID PLEXUS: A TECHNIQUE FOR ITS COLLECTION AND A COMPARISON OF ITS ELECTROLYTE COMPOSITION WITH SERUM AND CISTERNAL FLUIDS. *J Neurophysiol*. 1960;23(5):485-495. doi:10.1152/jn.1960.23.5.485
12. HASSIN GB, OLDBERG E, TINSLEY M. CHANGES IN THE BRAIN IN PLEXECTOMIZED DOGS: WITH COMMENTS ON THE CEREBROSPINAL FLUID. *Arch Neurol Psychiatry*. 1937;38(6):1224-1239. doi:10.1001/archneurpsyc.1937.02260240104008

13. Milhorat TH, Hammock MK, Fenstermacher JD, Rall DP, Levin VA. Cerebrospinal Fluid Production by the Choroid Plexus and Brain. *Science* (80-). 1971;173(3994):330-332. doi:10.1126/science.173.3994.330
14. Milhorat TH. Choroid Plexus and Cerebrospinal Fluid Production. *Science* (80-). 1969;166(3912):1514-1516. doi:10.1126/science.166.3912.1514
15. Cserr HF. Physiology of the choroid plexus. *Physiol Rev.* 1971;51(2):273-311. doi:10.1152/physrev.1971.51.2.273
16. Hladky SB, Barrand MA. Fluid and ion transfer across the blood–brain and blood–cerebrospinal fluid barriers; a comparative account of mechanisms and roles. *Fluids Barriers CNS.* 2016;13(1):19. doi:10.1186/s12987-016-0040-3
17. Rasmussen MK, Mestre H, Nedergaard M. Fluid transport in the brain. *Physiol Rev.* 2022;102(2):1025-1151. doi:10.1152/physrev.00031.2020
18. Orešković D, Radoš M, Klarica M. Cerebrospinal fluid secretion by the choroid plexus? *Physiol Rev.* 2016;96(4):1661-1662. doi:10.1152/physrev.00021.2016
19. Oshio K, Watanabe H, Song Y, Verkman AS, Manley GT. Reduced cerebrospinal fluid production and intracranial pressure in mice lacking choroid plexus water channel Aquaporin-1. *FASEB J.* 2005;19(1):76-78. doi:10.1096/fj.04-1711fje
20. Jensen DB, Toft-Bertelsen TL, Barbuskaite D, et al. The Na⁺, K⁺, 2Cl⁻ Cotransporter, Not Aquaporin 1, Sustains Cerebrospinal Fluid Secretion While Controlling Brain K⁺ Homeostasis. *Adv Sci.* 2025;12(6):1-16. doi:10.1002/advs.202409120
21. Oernbo EK, Steffensen AB, Razzaghi Khamesi P, et al. Membrane transporters control cerebrospinal fluid formation independently of conventional osmosis to modulate intracranial pressure. *Fluids Barriers CNS.* 2022;19(1):65. doi:10.1186/s12987-022-00358-4
22. Aristotle., Thompson DW. *Historia Animalium*. The Clarendon Press; 1910. doi:10.5962/bhl.title.147382
23. Milhorat TH. The third circulation revisited. *J Neurosurg.* 1975;42(6):628-645. doi:10.3171/jns.1975.42.6.0628
24. Rocca J. Galen and the ventricular system. *J Hist Neurosci.* 1997;6(3):227-239. doi:10.1080/09647049709525710
25. Cotugno D. *De Ischiade Nervosa Commentarius*. Ex typographia Simoniana; 1779. <https://books.google.se/books?id=Yb3WvAEACAAJ>
26. Deisenhammer F, Sellebjerg F, Teunissen CE, Tumani H. Cerebrospinal fluid in clinical neurology. *Cerebrospinal Fluid Clin Neurol.* Published online January 1, 2015:1-441. doi:10.1007/978-3-319-01225-4/COVER
27. Cushing H. The third circulation and its channels. *Lancet.* 1925;2:851–857.
28. Weed LH. Meninges and Cerebrospinal Fluid. *J Anat.* 1938;72(Pt 2):181-215. http://link.springer.com/10.1007/978-1-4684-0150-9_3
29. Key A, Retzius G. *Studien in Der Anatomie Des Nervensystems Und Des Bindegewebes* . Samson & Wallin; 1875.
30. Vesalius A. *De Humani Corporis Fabrica* . Apud Joan. Tornaesium; 1552.

31. Pacchioni A, Schröck L, Muratori DM, Oddi N, Buagni GF. *Dissertatio Epistolaris de Glandulis Conglobatis Duræ Meningis Humanæ, Indeque Ortis Lymphaticis Ad Piam Meningem Productis. Lucæ Schrokio Viro Clarissimo Cæsareo-Leopoldine Naturæ Curiosorum Academiæ Præsidi &c. Antonius Pacchionus Regiensis, Physicus Ro. typis Io. Francisci Buagni; 1705.*
<https://books.google.se/books?id=uP8o4etilRkC>
32. Woollam DHM. The historical significance of the cerebrospinal fluid. *Med Hist.* 1957;1(2):91-114. doi:10.1017/S0025727300021025
33. Turner L. The Structure and Relationships of Arachnoid Granulations. In: *Ciba Foundation Symposium - The Cerebrospinal Fluid: Production, Circulation and Absorption.* Novartis Foundation Symposia. ; 1958:32-54.
doi:<https://doi.org/10.1002/9780470719077.ch3>
34. Butler AB, Dacey RG, Maffeo CJ, Mann JD, Johnson RN, Bass NH. Mechanisms of Cerebrospinal Fluid Absorption in Normal and Pathologically Altered Arachnoid Villi. In: *Neurobiology of Cerebrospinal Fluid 2.* Springer US; 1983:707-726.
doi:10.1007/978-1-4615-9269-3_45
35. The Oliver-Sharpey Lectures ON THE CEREBRO-SPINAL FLUID. *Lancet.* 1910;176(4531):1-8. doi:10.1016/S0140-6736(00)52276-4
36. Weed LH. The absorption of cerebrospinal fluid into the venous system. *Am J Anat.* 1923;31(3):191-221. doi:10.1002/aja.1000310302
37. Shah T, Leurgans SE, Mehta RI, et al. Arachnoid granulations are lymphatic conduits that communicate with bone marrow and dura-arachnoid stroma. *J Exp Med.* 2023;220(2). doi:10.1084/jem.20220618
38. Proulx ST. Cerebrospinal fluid outflow: a review of the historical and contemporary evidence for arachnoid villi, perineural routes, and dural lymphatics. *Cell Mol Life Sci.* 2021;78(6):2429-2457. doi:10.1007/s00018-020-03706-5
39. Schwalbe G. Die Arachnoidalraum ein Lymphraum und sein Zusammenhang mit den Perichoroidalraum.. *Zbl med Wiss Zentralblatt fur die medizinischen Wissenschafte.* 1869;7:465-467. Accessed February 11, 2025.
<https://cir.nii.ac.jp/crid/1571135651028186752.bib?lang=en>
40. Jacob L, de Brito Neto J, Lenck S, et al. Conserved meningeal lymphatic drainage circuits in mice and humans. *J Exp Med.* 2022;219(8). doi:10.1084/jem.20220035
41. Stanton EH, Persson NDÅ, Gomolka RS, et al. Mapping of CSF transport using high spatiotemporal resolution dynamic contrast-enhanced MRI in mice: Effect of anesthesia. *Magn Reson Med.* 2021;85(6):3326-3342. doi:10.1002/mrm.28645
42. Yoon JH, Jin H, Kim HJ, et al. Nasopharyngeal lymphatic plexus is a hub for cerebrospinal fluid drainage. *Nature.* Published online January 10, 2024.
doi:10.1038/s41586-023-06899-4
43. Decker Y, Krämer J, Xin L, et al. Magnetic resonance imaging of cerebrospinal fluid outflow after low-rate lateral ventricle infusion in mice. *JCI Insight.* 2022;7(3):1-13.
doi:10.1172/jci.insight.150881

44. Furukawa M, Shimoda H, Kajiwaru T, Kato S, Yanagisawa S. Topographic study on nerve-associated lymphatic vessels in the murine craniofacial region by immunohistochemistry and electron microscopy. *Biomed Res.* 2008;29(6):289-296. doi:10.2220/biomedres.29.289
45. Ma Q, Ineichen B V., Detmar M, Proulx ST. Outflow of cerebrospinal fluid is predominantly through lymphatic vessels and is reduced in aged mice. *Nat Commun.* 2017;8(1):1434. doi:10.1038/s41467-017-01484-6
46. Aspelund A, Antila S, Proulx ST, et al. A dural lymphatic vascular system that drains brain interstitial fluid and macromolecules. *J Exp Med.* 2015;212(7):991-999. doi:10.1084/jem.20142290
47. Ma Q, Decker Y, Müller A, Ineichen B V., Proulx ST. Clearance of cerebrospinal fluid from the sacral spine through lymphatic vessels. *J Exp Med.* 2019;216(11):2492-2502. doi:10.1084/jem.20190351
48. Bucchieri F, Farina F, Zummo G, Cappello F. Lymphatic vessels of the dura mater: a new discovery? *J Anat.* 2015;227(5):702-703. doi:10.1111/joa.12381
49. Sandrone S, Moreno-Zambrano D, Kipnis J, van Gijn J. A (delayed) history of the brain lymphatic system. *Nat Med.* 2019;25(4):538-540. doi:10.1038/s41591-019-0417-3
50. Louveau A, Smirnov I, Keyes TJ, et al. Structural and functional features of central nervous system lymphatic vessels. *Nature.* 2015;523(7560):337-341. doi:10.1038/nature14432
51. Ahn JH, Cho H, Kim JH, et al. Meningeal lymphatic vessels at the skull base drain cerebrospinal fluid. *Nature.* 2019;572(7767):62-66. doi:10.1038/s41586-019-1419-5
52. Louveau A, Herz J, Alme MN, et al. CNS lymphatic drainage and neuroinflammation are regulated by meningeal lymphatic vasculature. *Nat Neurosci.* 2018;21(10):1380-1391. doi:10.1038/s41593-018-0227-9
53. Smyth LCD, Xu D, Okar S V., et al. Identification of direct connections between the dura and the brain. *Nature.* 2024;627(8002):165-173. doi:10.1038/s41586-023-06993-7
54. Ringstad G, Eide PK. Cerebrospinal fluid tracer efflux to parasagittal dura in humans. *Nat Commun.* 2020;11(1):354. doi:10.1038/s41467-019-14195-x
55. Hett K, McKnight CD, Eisma JJ, et al. Parasagittal dural space and cerebrospinal fluid (CSF) flow across the lifespan in healthy adults. *Fluids Barriers CNS.* 2022;19(1):1-13. doi:10.1186/s12987-022-00320-4
56. Eide PK, Ringstad G. Cerebrospinal fluid egress to human parasagittal dura and the impact of sleep deprivation. *Brain Res.* 2021;1772(August):147669. doi:10.1016/j.brainres.2021.147669
57. Eide Therkelsen H, Enger R, Eide PK, Ringstad G. Evidence for cellular and solute passage between the brain and skull bone marrow across meninges: A systematic review. *J Cereb Blood Flow Metab.* Published online January 25, 2025. doi:10.1177/0271678X251316392
58. Papadopoulos Z, Smyth LCD, Smirnov I, Gibson DA, Herz J, Kipnis J. Differential impact of lymphatic outflow pathways on cerebrospinal fluid homeostasis. *J Exp Med.* 2025;222(2). doi:10.1084/jem.20241752

59. Rasmussen MK, Mestre H, Nedergaard M. The glymphatic pathway in neurological disorders. *Lancet Neurol.* 2018;17(11):1016-1024. doi:10.1016/S1474-4422(18)30318-1
60. Wiig H, Swartz MA. Interstitial fluid and lymph formation and transport: physiological regulation and roles in inflammation and cancer. *Physiol Rev.* 2012;92(3):1005-1060. doi:10.1152/physrev.00037.2011
61. Cserr HF, Harling-Berg CJ, Knopf PM. Drainage of brain extracellular fluid into blood and deep cervical lymph and its immunological significance. *Brain Pathol.* 1992;2(4):269-276. doi:10.1111/j.1750-3639.1992.tb00703.x
62. Abbott NJ. Evidence for bulk flow of brain interstitial fluid: significance for physiology and pathology. *Neurochem Int.* 2004;45(4):545-552. doi:10.1016/j.neuint.2003.11.006
63. Meng L, Hou W, Chui J, Han R, Gelb AW. Cardiac Output and Cerebral Blood Flow. *Anesthesiology.* 2015;123(5):1198-1208. doi:10.1097/ALN.0000000000000872
64. Williams LR, Leggett RW. Reference values for resting blood flow to organs of man. *Clin Phys Physiol Meas.* 1989;10(3):187-217. doi:10.1088/0143-0815/10/3/001
65. Hablitz LM, Nedergaard M. The glymphatic system. *Curr Biol.* 2021;31(20):R1371-R1375. doi:10.1016/j.cub.2021.08.026
66. Cserr HF. BULK FLOW OF CEREBRAL EXTRACELLULAR FLUID AS A POSSIBLE MECHANISM OF CSF-BRAIN EXCHANGE. In: *Fluid Environment of the Brain.* Elsevier; 1975:215-224. doi:10.1016/B978-0-12-197450-3.50018-7
67. Cserr HF, Cooper DN, Milhorat TH. Flow of cerebral interstitial fluid as indicated by the removal of extracellular markers from rat caudate nucleus. *Exp Eye Res.* 1977;25 Suppl:461-473. doi:10.1016/s0014-4835(77)80041-9
68. Cserr HF, Cooper DN, Suri PK, Patlak CS. Efflux of radiolabeled polyethylene glycols and albumin from rat brain. *Am J Physiol Physiol.* 1981;240(4):F319-F328. doi:10.1152/ajprenal.1981.240.4.F319
69. Rennels ML, Gregory TF, Blaumanis OR, Fujimoto K, Grady PA. Evidence for a "paravascular" fluid circulation in the mammalian central nervous system, provided by the rapid distribution of tracer protein throughout the brain from the subarachnoid space. *Brain Res.* 1985;326(1):47-63. doi:10.1016/0006-8993(85)91383-6
70. Rennels ML, Blaumanis OR, Grady PA. Rapid solute transport throughout the brain via paravascular fluid pathways. *Adv Neurol.* 1990;52:431-439. Accessed February 13, 2025. <https://pubmed.ncbi.nlm.nih.gov/2396537/>
71. Iliff JJ, Wang M, Liao Y, et al. A Paravascular Pathway Facilitates CSF Flow Through the Brain Parenchyma and the Clearance of Interstitial Solutes, Including Amyloid β . *Sci Transl Med.* 2012;4(147):1-12. doi:10.1126/scitranslmed.3003748
72. Nedergaard M. Garbage Truck of the Brain. *Science (80-).* 2013;340(6140):1529-1530. doi:10.1126/science.1240514

73. WOOLLAM DH, MILLEN JW. The perivascular spaces of the mammalian central nervous system and their relation to the perineuronal and subarachnoid spaces. *J Anat.* 1955;89(2):193-200.
<http://www.ncbi.nlm.nih.gov/pubmed/14367214><http://www.pubmedcentral.nih.gov/articlerender.fcgi?artid=PMC1244781>
74. Wardlaw JM, Benveniste H, Nedergaard M, et al. Perivascular spaces in the brain: anatomy, physiology and pathology. *Nat Rev Neurol.* 2020;16(3):137-153.
doi:10.1038/s41582-020-0312-z
75. Mestre H, Verma N, Greene TD, et al. Periarteriolar spaces modulate cerebrospinal fluid transport into brain and demonstrate altered morphology in aging and Alzheimer's disease. *Nat Commun.* 2022;13(1). doi:10.1038/s41467-022-31257-9
76. Zhang ET, Inman CB, Weller RO. Interrelationships of the pia mater and the perivascular (Virchow-Robin) spaces in the human cerebrum. *J Anat.* 1990;170:111-123.
<http://www.ncbi.nlm.nih.gov/pubmed/2254158><http://www.pubmedcentral.nih.gov/articlerender.fcgi?artid=PMC1257067>
77. Mestre H, Tithof J, Du T, et al. Flow of cerebrospinal fluid is driven by arterial pulsations and is reduced in hypertension. *Nat Commun.* 2018;9(1):4878.
doi:10.1038/s41467-018-07318-3
78. Smets NG, van der Panne SA, Strijkers GJ, Bakker ENTP. Perivascular spaces around arteries exceed perivenous spaces in the mouse brain. *Sci Rep.* 2024;14(1):17655. doi:10.1038/s41598-024-67885-y
79. Mestre H, Hablitz LM, Xavier ALR, et al. Aquaporin-4-dependent glymphatic solute transport in the rodent brain. *Elife.* 2018;7. doi:10.7554/eLife.40070
80. Jung JS, Bhat R V., Preston GM, Guggino WB, Baraban JM, Agre P. Molecular characterization of an aquaporin cDNA from brain: candidate osmoreceptor and regulator of water balance. *Proc Natl Acad Sci U S A.* 1994;91(26):13052-13056.
doi:10.1073/pnas.91.26.13052
81. Hasegawa H, Ma T, Skach W, Matthay MA, Verkman AS. Molecular cloning of a mercurial-insensitive water channel expressed in selected water-transporting tissues. *J Biol Chem.* 1994;269(8):5497-5500. doi:10.1016/s0021-9258(17)37486-0
82. Nagelhus EA, Ottersen OP. Physiological roles of aquaporin-4 in brain. *Physiol Rev.* 2013;93(4):1543-1562. doi:10.1152/physrev.00011.2013
83. Nielsen S, Nagelhus EA, Amiry-Moghaddam M, Bourque C, Agre P, Ottersen OP. Specialized membrane domains for water transport in glial cells: high-resolution immunogold cytochemistry of aquaporin-4 in rat brain. *J Neurosci.* 1997;17(1):171-180. doi:10.1523/JNEUROSCI.17-01-00171.1997
84. Eidsvaag VA, Enger R, Hansson HA, Eide PK, Nagelhus EA. Human and mouse cortical astrocytes differ in aquaporin-4 polarization toward microvessels. *Glia.* 2017;65(6):964-973. doi:10.1002/glia.23138
85. King LS, Kozono D, Agre P. From structure to disease: the evolving tale of aquaporin biology. *Nat Rev Mol Cell Biol.* 2004;5(9):687-698. doi:10.1038/nrm1469

86. Jorgačevski J, Zorec R, Potokar M. Insights into Cell Surface Expression, Supramolecular Organization, and Functions of Aquaporin 4 Isoforms in Astrocytes. *Cells*. 2020;9(12). doi:10.3390/cells9122622
87. De Bellis M, Pisani F, Mola MG, et al. Translational readthrough generates new astrocyte AQP4 isoforms that modulate supramolecular clustering, glial endfeet localization, and water transport. *Glia*. 2017;65(5):790-803. doi:10.1002/glia.23126
88. Strand L, Moe SE, Solbu TT, Vaadal M, Holen T. Roles of aquaporin-4 isoforms and amino acids in square array assembly. *Biochemistry*. 2009;48(25):5785-5793. doi:10.1021/bi802231q
89. Neely JD, Christensen BM, Nielsen S, Agre P. Heterotetrameric composition of aquaporin-4 water channels. *Biochemistry*. 1999;38(34):11156-11163. doi:10.1021/bi990941s
90. Landis DMD, Reese TS. Arrays of particles in freeze-fractured astrocytic membranes. *J Cell Biol*. 1974;60(1):316-320. doi:10.1083/jcb.60.1.316
91. Verbavatz JM, Ma T, Gobin R, Verkman AS. Absence of orthogonal arrays in kidney, brain and muscle from transgenic knockout mice lacking water channel aquaporin-4. *J Cell Sci*. 1997;110 (Pt 2(22):2855-2860. doi:10.1242/jcs.110.22.2855
92. Wolburg H, Wolburg-Buchholz K, Fallier-Becker P, Noell S, Mack AF. Structure and functions of aquaporin-4-based orthogonal arrays of particles. *Int Rev Cell Mol Biol*. 2011;287:1-41. doi:10.1016/B978-0-12-386043-9.00001-3
93. de Bellis M, Cibelli A, Mola MG, et al. Orthogonal arrays of particle assembly are essential for normal aquaporin-4 expression level in the brain. *Glia*. 2021;69(2):473-488. doi:10.1002/glia.23909
94. Crane JM, Verkman AS. Determinants of aquaporin-4 assembly in orthogonal arrays revealed by live-cell single-molecule fluorescence imaging. *J Cell Sci*. 2009;122(Pt 6):813-821. doi:10.1242/jcs.042341
95. Suzuki H, Nishikawa K, Hiroaki Y, Fujiyoshi Y. Formation of aquaporin-4 arrays is inhibited by palmitoylation of N-terminal cysteine residues. *Biochim Biophys Acta*. 2008;1778(4):1181-1189. doi:10.1016/j.bbamem.2007.12.007
96. Smith AJ, Yao X, Dix JA, et al. Test of the 'glymphatic' hypothesis demonstrates diffusive and aquaporin-4-independent solute transport in rodent brain parenchyma. *Elife*. 2017;6:1-16. doi:10.7554/eLife.27679
97. Hablitz LM, Vinitsky HS, Sun Q, et al. Increased glymphatic influx is correlated with high EEG delta power and low heart rate in mice under anesthesia. *Sci Adv*. 2019;5(2). doi:10.1126/sciadv.aav5447
98. Plá V, Bork P, Harnpramukul A, et al. A real-time in vivo clearance assay for quantification of glymphatic efflux. *Cell Rep*. 2022;40(11). doi:10.1016/j.celrep.2022.111320
99. Yao X, Hrabětová S, Nicholson C, Manley GT. Aquaporin-4-Deficient Mice Have Increased Extracellular Space without Tortuosity Change. *J Neurosci*. 2008;28(21):5460-5464. doi:10.1523/JNEUROSCI.0257-08.2008
100. Gomolka RS, Hablitz LM, Mestre H, et al. Loss of aquaporin-4 results in glymphatic system dysfunction via brain-wide interstitial fluid stagnation. *Elife*. 2023;12:1-25. doi:10.7554/eLife.82232

101. Bojarskaite L, Nafari S, Ravnanger AK, et al. Role of aquaporin-4 polarization in extracellular solute clearance. *Fluids Barriers CNS*. 2024;21(1):28. doi:10.1186/s12987-024-00527-7
102. Furman CS, Gorelick-Feldman DA, Davidson KGV, et al. Aquaporin-4 square array assembly: Opposing actions of M1 and M23 isoforms. *Proc Natl Acad Sci U S A*. 2003;100(23):13609-13614. doi:10.1073/pnas.2235843100
103. Hablitz LM, Plá V, Giannetto M, et al. Circadian control of brain glymphatic and lymphatic fluid flow. *Nat Commun*. 2020;11(1):4411. doi:10.1038/s41467-020-18115-2
104. Zeppenfeld DM, Simon M, Haswell JD, et al. Association of perivascular localization of aquaporin-4 with cognition and Alzheimer disease in aging brains. *JAMA Neurol*. 2017;74(1):91-99. doi:10.1001/jamaneurol.2016.4370
105. Smith AJ, Jin BJ, Ratelade J, Verkman AS. Aggregation state determines the localization and function of M1- and M23-aquaporin-4 in astrocytes. *J Cell Biol*. 2014;204(4):559-573. doi:10.1083/jcb.201308118
106. Ciappelloni S, Bouchet D, Dubourdieu N, et al. Aquaporin-4 Surface Trafficking Regulates Astrocytic Process Motility and Synaptic Activity in Health and Autoimmune Disease. *Cell Rep*. 2019;27(13):3860-3872.e4. doi:10.1016/j.celrep.2019.05.097
107. Jessen NA, Munk ASF, Lundgaard I, Nedergaard M. The Glymphatic System: A Beginner's Guide. *Neurochem Res*. 2015;40(12):2583-2599. doi:10.1007/s11064-015-1581-6
108. Neely JD, Amiry-Moghaddam M, Ottersen OP, Froehner SC, Agre P, Adams ME. Syntrophin-dependent expression and localization of Aquaporin-4 water channel protein. *Proc Natl Acad Sci U S A*. 2001;98(24):14108-14113. doi:10.1073/pnas.241508198
109. Amiry-Moghaddam M, Otsuka T, Hurn PD, et al. An alpha-syntrophin-dependent pool of AQP4 in astroglial end-feet confers bidirectional water flow between blood and brain. *Proc Natl Acad Sci U S A*. 2003;100(4):2106-2111. doi:10.1073/pnas.0437946100
110. Xie L, Kang H, Xu Q, et al. Sleep Drives Metabolite Clearance from the Adult Brain. *Science (80-)*. 2013;342(6156):373-377. doi:10.1126/science.1241224
111. Miyakoshi LM, Stæger FF, Li Q, et al. The state of brain activity modulates cerebrospinal fluid transport. *Prog Neurobiol*. 2023;229:102512. doi:10.1016/j.pneurobio.2023.102512
112. Bojarskaite L, Vallet A, Bjørnstad DM, et al. Sleep cycle-dependent vascular dynamics in male mice and the predicted effects on perivascular cerebrospinal fluid flow and solute transport. *Nat Commun*. 2023;14(1). doi:10.1038/s41467-023-36643-5
113. Holth JK, Fritschi SK, Wang C, et al. The sleep-wake cycle regulates brain interstitial fluid tau in mice and CSF tau in humans. *Science (80-)*. 2019;363(6429):880-884. doi:10.1126/science.aav2546

114. Kang JE, Lim MM, Bateman RJ, et al. Amyloid- β Dynamics Are Regulated by Orexin and the Sleep-Wake Cycle. *Science* (80-). 2009;326(5955):1005-1007. doi:10.1126/science.1180962
115. Deng S, Hu Y, Chen S, et al. Chronic sleep fragmentation impairs brain interstitial clearance in young wildtype mice. *J Cereb Blood Flow Metab.* 2024;(130). doi:10.1177/0271678X241230188
116. Shokri-Kojori E, Wang GJ, Wiers CE, et al. β -Amyloid accumulation in the human brain after one night of sleep deprivation. *Proc Natl Acad Sci.* 2018;115(17):4483-4488. doi:10.1073/pnas.1721694115
117. Eide PK, Vinje V, Pripp AH, Mardal K andre, Ringstad G. Sleep deprivation impairs molecular clearance from the human brain. *Brain.* 2021;144(3):863-874. doi:10.1093/brain/awaa443
118. Miao A, Luo T, Hsieh B, et al. Brain clearance is reduced during sleep and anesthesia. *Nat Neurosci.* Published online May 13, 2024. doi:10.1038/s41593-024-01638-y
119. Kroesbergen E, Riesselmann L V, Gomolka RS, et al. Glymphatic clearance is enhanced during sleep. 2024;1910280. doi:10.1101/2024.08.24.609514
120. Fultz NE, Bonmassar G, Setsompop K, et al. Coupled electrophysiological, hemodynamic, and cerebrospinal fluid oscillations in human sleep. *Science* (80-). 2019;366(6465):628-631. doi:10.1126/science.aax5440
121. Jiang-Xie LF, Drieu A, Bhasi K, Quintero D, Smirnov I, Kipnis J. Neuronal dynamics direct cerebrospinal fluid perfusion and brain clearance. *Nature.* 2024;627(8002):157-164. doi:10.1038/s41586-024-07108-6
122. Murdock MH, Yang C yi, Sun N, et al. Multisensory gamma stimulation promotes glymphatic clearance of amyloid. *Nature.* 2024;627(8002):149-156. doi:10.1038/s41586-024-07132-6
123. Hadaczek P, Yamashita Y, Mirek H, et al. The “Perivascular Pump” Driven by Arterial Pulsation Is a Powerful Mechanism for the Distribution of Therapeutic Molecules within the Brain. *Mol Ther.* 2006;14(1):69-78. doi:10.1016/j.ymthe.2006.02.018
124. Stoodley MA, Brown SA, Brown CJ, Jones NR. Arterial pulsation—dependent perivascular cerebrospinal fluid flow into the central canal in the sheep spinal cord. *J Neurosurg.* 1997;86(4):686-693. doi:10.3171/jns.1997.86.4.0686
125. Iliff JJ, Wang M, Zeppenfeld DM, et al. Cerebral Arterial Pulsation Drives Paravascular CSF–Interstitial Fluid Exchange in the Murine Brain. *J Neurosci.* 2013;33(46):18190-18199. doi:10.1523/JNEUROSCI.1592-13.2013
126. Mortensen KN, Sanggaard S, Mestre H, et al. Impaired Glymphatic Transport in Spontaneously Hypertensive Rats. *J Neurosci.* 2019;39(32):6365-6377. doi:10.1523/JNEUROSCI.1974-18.2019
127. Rey J, Sarntinoranont M. Pulsatile flow drivers in brain parenchyma and perivascular spaces: a resistance network model study. *Fluids Barriers CNS.* 2018;15(1):20. doi:10.1186/s12987-018-0105-6
128. Asgari M, de Zélicourt D, Kurtcuoglu V. Glymphatic solute transport does not require bulk flow. *Sci Rep.* 2016;6(1):38635. doi:10.1038/srep38635

129. Kedarasetti RT, Drew PJ, Costanzo F. Arterial pulsations drive oscillatory flow of CSF but not directional pumping. *Sci Rep.* 2020;10(1):10102. doi:10.1038/s41598-020-66887-w
130. van Veluw SJ, Hou SS, Calvo-Rodriguez M, et al. Vasomotion as a Driving Force for Paravascular Clearance in the Awake Mouse Brain. *Neuron.* 2020;105(3):549-561.e5. doi:10.1016/j.neuron.2019.10.033
131. Mateo C, Knutsen PM, Tsai PS, Shih AY, Kleinfeld D. Entrainment of Arteriole Vasomotor Fluctuations by Neural Activity Is a Basis of Blood-Oxygenation-Level-Dependent “Resting-State” Connectivity. *Neuron.* 2017;96(4):936-948.e3. doi:10.1016/j.neuron.2017.10.012
132. Munting LP, Bonnar O, Kozberg MG, et al. Spontaneous vasomotion propagates along pial arterioles in the awake mouse brain like stimulus-evoked vascular reactivity. *J Cereb Blood Flow Metab.* 2023;43(10):1752-1763. doi:10.1177/0271678X231152550
133. Holstein-Rønsbo S, Gan Y, Giannetto MJ, et al. Glymphatic influx and clearance are accelerated by neurovascular coupling. *Nat Neurosci.* 2023;26(6):1042-1053. doi:10.1038/s41593-023-01327-2
134. Kiviniemi V, Wang X, Korhonen V, et al. Ultra-fast magnetic resonance encephalography of physiological brain activity – Glymphatic pulsation mechanisms? *J Cereb Blood Flow Metab.* 2016;36(6):1033-1045. doi:10.1177/0271678X15622047
135. Helakari H, Korhonen V, Holst SC, et al. Human NREM Sleep Promotes Brain-Wide Vasomotor and Respiratory Pulsations. *J Neurosci.* 2022;42(12):2503-2515. doi:10.1523/JNEUROSCI.0934-21.2022
136. Tuunanen J, Helakari H, Huotari N, et al. Cardiovascular and vasomotor pulsations in the brain and periphery during awake and NREM sleep in a multimodal fMRI study. *Front Neurosci.* 2024;18(October). doi:10.3389/fnins.2024.1457732
137. Hauglund NL, Andersen M, Tokarska K, et al. Norepinephrine-mediated slow vasomotion drives glymphatic clearance during sleep. *Cell.* Published online January 2025:1-17. doi:10.1016/j.cell.2024.11.027
138. Berridge CW, Waterhouse BD. The locus coeruleus–noradrenergic system: modulation of behavioral state and state-dependent cognitive processes. *Brain Res Rev.* 2003;42(1):33-84. doi:10.1016/S0165-0173(03)00143-7
139. Bohr T, Hjorth PG, Holst SC, et al. The glymphatic system: Current understanding and modeling. *iScience.* 2022;25(9):1-33. doi:10.1016/j.isci.2022.104987
140. Ramos M, Burdon Bechet N, Battistella R, et al. Cisterna magna injection in rats to study glymphatic function. In: *Methods in Molecular Biology.* Vol 1938. ; 2019:97-104. doi:10.1007/978-1-4939-9068-9_7
141. Xavier ALR, Hauglund NL, von Holstein-Rathlou S, et al. Cannula Implantation into the Cisterna Magna of Rodents. *J Vis Exp.* 2018;2018(135). doi:10.3791/57378
142. Sweeney AM, Plá V, Du T, et al. In Vivo Imaging of Cerebrospinal Fluid Transport through the Intact Mouse Skull using Fluorescence Macroscopy. *J Vis Exp.* 2019;(149). doi:10.3791/59774

143. Lilius TO, Rosenholm M, Klinger L, et al. SPECT/CT imaging reveals CNS-wide modulation of glymphatic cerebrospinal fluid flow by systemic hypertonic saline. *iScience*. Published online 2022;105250. doi:10.1016/j.isci.2022.105250
144. Iliff JJ, Lee H, Yu M, et al. Brain-wide pathway for waste clearance captured by contrast-enhanced MRI. *J Clin Invest*. 2013;123(3):1299-1309. doi:10.1172/JCI67677
145. De Leon MJ, Li Y, Okamura N, et al. Cerebrospinal fluid clearance in Alzheimer disease measured with dynamic PET. *J Nucl Med*. 2017;58(9):1471-1476. doi:10.2967/jnumed.116.187211
146. Faghih MM, Keith Sharp M. Mechanisms of tracer transport in cerebral perivascular spaces. *J Biomech*. 2021;118:110278. doi:10.1016/j.jbiomech.2021.110278
147. Faghih MM, Sharp MK. Is bulk flow plausible in perivascular, paravascular and paravenous channels? *Fluids Barriers CNS*. 2018;15(1):17. doi:10.1186/s12987-018-0103-8
148. Vinje V, Eklund A, Mardal KA, Rognes ME, Støverud KH. Intracranial pressure elevation alters CSF clearance pathways. *Fluids Barriers CNS*. 2020;17(1). doi:10.1186/s12987-020-00189-1
149. Bedussi B, Almasian M, de Vos J, VanBavel E, Bakker ENTP. Paravascular spaces at the brain surface: Low resistance pathways for cerebrospinal fluid flow. *J Cereb Blood Flow Metab*. 2018;38(4):719-726. doi:10.1177/0271678X17737984
150. Raghunandan A, Ladron-De-guevara A, Tithof J, et al. Bulk flow of cerebrospinal fluid observed in periarterial spaces is not an artifact of injection. *Elife*. 2021;10:1-15. doi:10.7554/eLife.65958
151. Bèchet NB, Kylkilahti TM, Mattsson B, Petrasova M, Shanbhag NC, Lundgaard I. Light sheet fluorescence microscopy of optically cleared brains for studying the glymphatic system. *J Cereb Blood Flow Metab*. 2020;40(10):1975-1986. doi:10.1177/0271678X20924954
152. Kress BT, Iliff JJ, Xia M, et al. Impairment of paravascular clearance pathways in the aging brain. *Ann Neurol*. 2014;76(6):845-861. doi:10.1002/ana.24271
153. Peng W, Achariyar TM, Li B, et al. Suppression of glymphatic fluid transport in a mouse model of Alzheimer's disease. *Neurobiol Dis*. 2016;93(3):215-225. doi:10.1016/j.nbd.2016.05.015
154. Ishida K, Yamada K, Nishiyama R, et al. Glymphatic system clears extracellular tau and protects from tau aggregation and neurodegeneration. *J Exp Med*. 2022;219(3). doi:10.1084/jem.20211275
155. Xue Y, Liu X, Koundal S, et al. In vivo T1 mapping for quantifying glymphatic system transport and cervical lymph node drainage. *Sci Rep*. 2020;10(1):14592. doi:10.1038/s41598-020-71582-x
156. Lee H, Xie L, Yu M, et al. The effect of body posture on brain glymphatic transport. *J Neurosci*. 2015;35(31):11034-11044. doi:10.1523/JNEUROSCI.1625-15.2015
157. Smith AJ, Verkman AS. The "glymphatic" mechanism for solute clearance in Alzheimer's disease: Game changer or unproven speculation? *FASEB J*. 2018;32(2):543-551. doi:10.1096/fj.201700999

158. Gakuba C, Gaberel T, Goursaud S, et al. General Anesthesia Inhibits the Activity of the “Glymphatic System.” *Theranostics*. 2018;8(3):710-722. doi:10.7150/thno.19154
159. Abbott NJ, Pizzo ME, Preston JE, Janigro D, Thorne RG. The role of brain barriers in fluid movement in the CNS: is there a ‘glymphatic’ system? *Acta Neuropathol*. 2018;135(3):387-407. doi:10.1007/s00401-018-1812-4
160. Xu Z, Xiao N, Chen Y, et al. Deletion of aquaporin-4 in APP/PS1 mice exacerbates brain A β accumulation and memory deficits. *Mol Neurodegener*. 2015;10(1):58. doi:10.1186/s13024-015-0056-1
161. Feng W, Zhang Y, Wang Z, et al. Microglia prevent beta-amyloid plaque formation in the early stage of an Alzheimer’s disease mouse model with suppression of glymphatic clearance. *Alzheimers Res Ther*. 2020;12(1):125. doi:10.1186/s13195-020-00688-1
162. Harrison IF, Ismail O, Machhada A, et al. Impaired glymphatic function and clearance of tau in an Alzheimer’s disease model. *Brain*. 2020;143(8):2576-2593. doi:10.1093/brain/awaa179
163. Howells DW, Porritt MJ, Rewell SSJ, et al. Different Strokes for Different Folks: The Rich Diversity of Animal Models of Focal Cerebral Ischemia. *J Cereb Blood Flow Metab*. 2010;30(8):1412-1431. doi:10.1038/jcbfm.2010.66
164. Bèchet NB, Shanbhag NC, Lundgaard I. Glymphatic pathways in the gyrencephalic brain. *J Cereb Blood Flow Metab*. 2021;41(9):2264-2279. doi:10.1177/0271678X21996175
165. Johnston M, Zakharov A, Papaiconomou C, Salmasi G, Armstrong D. Evidence of connections between cerebrospinal fluid and nasal lymphatic vessels in humans, non-human primates and other mammalian species. *Cerebrospinal Fluid Res*. 2004;1(1):2. doi:10.1186/1743-8454-1-2
166. Johnston M, Zakharov A, Koh L, Armstrong D. Subarachnoid injection of Microfil reveals connections between cerebrospinal fluid and nasal lymphatics in the non-human primate. *Neuropathol Appl Neurobiol*. 2005;31(6):632-640. doi:10.1111/j.1365-2990.2005.00679.x
167. Goulay R, Flament J, Gauberti M, et al. Subarachnoid Hemorrhage Severely Impairs Brain Parenchymal Cerebrospinal Fluid Circulation in Nonhuman Primate. *Stroke*. 2017;48(8):2301-2305. doi:10.1161/STROKEAHA.117.017014
168. Bèchet NB, Shanbhag NC, Lundgaard I. Direct Cannula Implantation in the Cisterna Magna of Pigs. *J Vis Exp*. 2021;2021:1-12. doi:10.3791/62641
169. Kameya N, Sakai I, Saito K, et al. Evolutionary changes leading to efficient glymphatic circulation in the mammalian brain. *Nat Commun*. 2024;15(1):10048. doi:10.1038/s41467-024-54372-1
170. Eide PK, Ringstad G. MRI with intrathecal MRI gadolinium contrast medium administration: a possible method to assess glymphatic function in human brain. *Acta Radiol Open*. 2015;4(11):205846011560963. doi:10.1177/2058460115609635
171. Ringstad G, Vatnehol SAS, Eide PK. Glymphatic MRI in idiopathic normal pressure hydrocephalus. *Brain*. 2017;140(10):2691-2705. doi:10.1093/brain/awx191

172. Ringstad G, Valnes LM, Dale AM, et al. Brain-wide glymphatic enhancement and clearance in humans assessed with MRI. *JCI Insight*. 2018;3(13). doi:10.1172/jci.insight.121537
173. Eide PK, Pripp AH, Berge B, Hrubos-Strøm H, Ringstad G, Valnes LM. Altered glymphatic enhancement of cerebrospinal fluid tracer in individuals with chronic poor sleep quality. *J Cereb Blood Flow Metab*. Published online 2022:0271678X2210907. doi:10.1177/0271678x221090747
174. Eide PK, Lashkarivand A, Hagen-Kersten ÅA, et al. Intrathecal Contrast-Enhanced Magnetic Resonance Imaging of Cerebrospinal Fluid Dynamics and Glymphatic Enhancement in Idiopathic Normal Pressure Hydrocephalus. *Front Neurol*. 2022;13(April):1-21. doi:10.3389/fneur.2022.857328
175. Eide PK, Ringstad G. Functional analysis of the human perivascular subarachnoid space. *Nat Commun*. 2024;15(1):2001. doi:10.1038/s41467-024-46329-1
176. Botta D, Hutuca I, Ghoul E El, et al. Emerging non-invasive MRI techniques for glymphatic system assessment in neurodegenerative disease. *J Neuroradiol*. 2025;52(3):101322. doi:10.1016/j.neurad.2025.101322
177. Waymont JMJ, Valdés Hernández M del C, Bernal J, et al. Systematic review and meta-analysis of automated methods for quantifying enlarged perivascular spaces in the brain. *Neuroimage*. 2024;297(May):120685. doi:10.1016/j.neuroimage.2024.120685
178. Kamagata K, Saito Y, Andica C, et al. Noninvasive Magnetic Resonance Imaging Measures of Glymphatic System Activity. *J Magn Reson Imaging*. 2024;59(5):1476-1493. doi:10.1002/jmri.28977
179. Taoka T, Masutani Y, Kawai H, et al. Evaluation of glymphatic system activity with the diffusion MR technique: diffusion tensor image analysis along the perivascular space (DTI-ALPS) in Alzheimer's disease cases. *Jpn J Radiol*. 2017;35(4):172-178. doi:10.1007/s11604-017-0617-z
180. Wright AM, Wu Y, Feng L, Wen Q. Diffusion magnetic resonance imaging of cerebrospinal fluid dynamics: Current techniques and future advancements. *NMR Biomed*. 2024;37(9):1-33. doi:10.1002/nbm.5162
181. Taoka T, Ito R, Nakamichi R, Nakane T, Kawai H, Naganawa S. Diffusion Tensor Image Analysis ALong the Perivascular Space (DTI-ALPS): Revisiting the Meaning and Significance of the Method. *Magn Reson Med Sci*. 2024;23(3):rev.2023-0175. doi:10.2463/mrms.rev.2023-0175
182. Georgiopoulos C, Werlin A, Lasic S, et al. Diffusion tensor imaging along the perivascular space: the bias from crossing fibres. *Brain Commun*. 2024;6(6):1-11. doi:10.1093/braincomms/fcae421
183. Ringstad G. Glymphatic imaging: a critical look at the DTI-ALPS index. *Neuroradiology*. 2024;66(2):157-160. doi:10.1007/s00234-023-03270-2
184. Nedergaard M, Goldman SA. Glymphatic failure as a final common pathway to dementia. *Science (80-)*. 2020;370(6512):50-56. doi:10.1126/science.abb8739
185. Hardy JA, Higgins GA. Alzheimer's disease: the amyloid cascade hypothesis. *Science*. 1992;256(5054):184-185. doi:10.1126/science.1566067

186. Busche MA, Hyman BT. Synergy between amyloid- β and tau in Alzheimer's disease. *Nat Neurosci.* 2020;23(10):1183-1193. doi:10.1038/s41593-020-0687-6
187. Cui H, Wang W, Zheng X, et al. Decreased AQP4 Expression Aggravates α -Synuclein Pathology in Parkinson's Disease Mice, Possibly via Impaired Glymphatic Clearance. *J Mol Neurosci.* 2021;(0123456789). doi:10.1007/s12031-021-01836-4
188. Zou W, Pu T, Feng W, et al. Blocking meningeal lymphatic drainage aggravates Parkinson's disease-like pathology in mice overexpressing mutated α -synuclein. *Transl Neurodegener.* 2019;8(1):7. doi:10.1186/s40035-019-0147-y
189. Sundaram S, Hughes RL, Peterson E, et al. Establishing a framework for neuropathological correlates and glymphatic system functioning in Parkinson's disease. *Neurosci Biobehav Rev.* 2019;103:305-315. doi:10.1016/j.neubiorev.2019.05.016
190. Malkani R, Attarian H. Sleep in Neurodegenerative Disorders. *Curr Sleep Med Reports.* 2015;1(2):81-90. doi:10.1007/s40675-015-0016-x
191. Mendelsohn AR, Larrick JW. Sleep Facilitates Clearance of Metabolites from the Brain: Glymphatic Function in Aging and Neurodegenerative Diseases. *Rejuvenation Res.* 2013;16(6):518-523. doi:10.1089/rej.2013.1530
192. Hirose M, Asano M, Watanabe-Matsumoto S, et al. Stagnation of glymphatic interstitial fluid flow and delay in waste clearance in the SOD1-G93A mouse model of ALS. *Neurosci Res.* 2021;171:74-82. doi:10.1016/j.neures.2020.10.006
193. Liu H, Chen L, Zhang C, et al. Glymphatic influx and clearance are perturbed in Huntington's disease. *JCI Insight.* Published online September 3, 2024. doi:10.1172/jci.insight.172286
194. Bae YJ, Choi BS, Kim JM, Choi JH, Cho SJ, Kim JH. Altered glymphatic system in idiopathic normal pressure hydrocephalus. *Parkinsonism Relat Disord.* 2021;82(October 2020):56-60. doi:10.1016/j.parkreldis.2020.11.009
195. Fournier AP, Gauberti M, Quenault A, Vivien D, Macrez R, Docagne F. Reduced spinal cord parenchymal cerebrospinal fluid circulation in experimental autoimmune encephalomyelitis. *J Cereb Blood Flow Metab.* 2019;39(7):1258-1265. doi:10.1177/0271678X18754732
196. Jiang Q, Zhang L, Ding G, et al. Impairment of the glymphatic system after diabetes. *J Cereb Blood Flow Metab.* 2017;37(4):1326-1337. doi:10.1177/0271678X16654702
197. Boyd ED, Zhang L, Ding G, et al. The Glymphatic Response to the Development of Type 2 Diabetes. *Biomedicines.* 2024;12(2):401. doi:10.3390/biomedicines12020401
198. Kritsilis M, Vanherle L, Rosenholm M, et al. Loss of glymphatic homeostasis in heart failure. *Brain.* Published online December 18, 2024. doi:10.1093/brain/awae411
199. Vanherle L, Lidington D, Uhl FE, et al. Restoring myocardial infarction-induced long-term memory impairment by targeting the cystic fibrosis transmembrane regulator. *eBioMedicine.* 2022;86:104384. doi:10.1016/j.ebiom.2022.104384
200. Norwood JN, Zhang Q, Card D, Craine A, Ryan TM, Drew PJ. Anatomical basis and physiological role of cerebrospinal fluid transport through the murine cribriform plate. *Elife.* 2019;8:1-32. doi:10.7554/eLife.44278

201. in 't Zandt R, Mahmutovic Persson I, Tibiletti M, von Wachenfeldt K, Parker GJM, Olsson LE. Contrast enhanced longitudinal changes observed in an experimental bleomycin-induced lung fibrosis rat model by radial DCE-MRI at 9.4T. Wu M, ed. *PLoS One*. 2024;19(9):e0310643. doi:10.1371/journal.pone.0310643
202. Rasche V, de Boer RW, Holz D, Proksa R. Continuous radial data acquisition for dynamic MRI. *Magn Reson Med*. 1995;34(5):754-761. doi:10.1002/mrm.1910340515
203. Heiberg E, Sjögren J, Ugander M, Carlsson M, Engblom H, Arheden H. Design and validation of Segment - freely available software for cardiovascular image analysis. *BMC Med Imaging*. 2010;10(1):1. doi:10.1186/1471-2342-10-1
204. Gottschalk M. Look-Locker FAIR TrueFISP for arterial spin labelling on mouse at 9.4 T. *NMR Biomed*. 2020;33(3):1-11. doi:10.1002/nbm.4191
205. Gottschalk M, Swanberg K. kswanberg/rcbFLOW: rcbFLOWv1.0.0. Published online June 2024. <https://doi.org/10.5281/zenodo.11475856>
206. Schindelin J, Arganda-Carreras I, Frise E, et al. Fiji: an open-source platform for biological-image analysis. *Nat Methods*. 2012;9(7):676-682. doi:10.1038/nmeth.2019
207. Renier N, Wu Z, Simon DJ, Yang J, Ariel P, Tessier-Lavigne M. iDISCO: A Simple, Rapid Method to Immunolabel Large Tissue Samples for Volume Imaging. *Cell*. 2014;159(4):896-910. doi:10.1016/j.cell.2014.10.010
208. Qiu C, Winblad B, Marengoni A, Klarin I, Fastbom J, Fratiglioni L. Heart failure and risk of dementia and Alzheimer disease: A population-based cohort study. *Arch Intern Med*. 2006;166(9):1003-1008. doi:10.1001/archinte.166.9.1003
209. Vogels RLC, Scheltens P, Schroeder-Tanka JM, Weinstein HC. Cognitive impairment in heart failure: A systematic review of the literature. *Eur J Heart Fail*. 2007;9(5):440-449. doi:10.1016/j.ejheart.2006.11.001
210. Cermakova P, Eriksdotter M, Lund LH, Winblad B, Religa P, Religa D. Heart failure and Alzheimer's disease. *J Intern Med*. 2015;277(4):406-425. doi:10.1111/joim.12287
211. Roy B, Woo MA, Wang DJJ, Fonarow GC, Harper RM, Kumar R. Reduced regional cerebral blood flow in patients with heart failure. *Eur J Heart Fail*. 2017;19(10):1294-1302. doi:10.1002/ehf.874
212. Alosco ML, Hayes SM. Structural brain alterations in heart failure: a review of the literature and implications for risk of Alzheimer's disease. *Heart Fail Rev*. 2015;20(5):561-571. doi:10.1007/s10741-015-9488-5
213. Mueller K, Thiel F, Beutner F, et al. Brain Damage With Heart Failure. *Circ Res*. 2020;126(6):750-764. doi:10.1161/CIRCRESAHA.119.315813
214. Pavan C, L R Xavier A, Ramos M, et al. DNase Treatment Prevents Cerebrospinal Fluid Block in Early Experimental Pneumococcal Meningitis. *Ann Neurol*. 2021;90(4):653-669. doi:10.1002/ana.26186
215. Munk AS, Wang W, Bèchet NB, et al. PDGF-B Is Required for Development of the Glymphatic System. *Cell Rep*. 2019;26(11):2955-2969.e3. doi:10.1016/j.celrep.2019.02.050

216. Minamikawa T, Miyake T, Takamatsu T, Fujita S. A new method of lectin histochemistry for the study of brain angiogenesis. *Histochemistry*. 1987;87(4):317-320. doi:10.1007/BF00492584
217. Simionescu M, Simionescu N, Palade GE. Differentiated microdomains on the luminal surface of capillary endothelium: distribution of lectin receptors. *J Cell Biol*. 1982;94(2):406-413. doi:10.1083/jcb.94.2.406
218. Battistella R, Kritsilis M, Matuskova H, et al. Not All Lectins Are Equally Suitable for Labeling Rodent Vasculature. *Int J Mol Sci*. 2021;22(21):11554. doi:10.3390/ijms222111554
219. Todorov MI, Paetzold JC, Schoppe O, et al. Machine learning analysis of whole mouse brain vasculature. *Nat Methods*. 2020;17(April). doi:10.1038/s41592-020-0792-1
220. Da Mesquita S, Louveau A, Vaccari A, et al. Functional aspects of meningeal lymphatics in ageing and Alzheimer's disease. *Nature*. 2018;560(7717):185-191. doi:10.1038/s41586-018-0368-8
221. Du T, Raghunandan A, Mestre H, et al. Restoration of cervical lymphatic vessel function in aging rescues cerebrospinal fluid drainage. *Nat Aging*. Published online August 15, 2024. doi:10.1038/s43587-024-00691-3
222. Pflanzner T, Janko MC, André-Dohmen B, et al. LRP1 mediates bidirectional transcytosis of amyloid- β across the blood-brain barrier. *Neurobiol Aging*. 2011;32(12):2323.e1-2323.e11. doi:10.1016/j.neurobiolaging.2010.05.025
223. Kanekiyo T, Liu CC, Shinohara M, Li J, Bu G. Lrp1 in brain vascular smooth muscle cells mediates local clearance of Alzheimer's amyloid- β . *J Neurosci*. 2012;32(46):16458-16465. doi:10.1523/JNEUROSCI.3987-12.2012
224. Storck SE, Meister S, Nahrath J, et al. Endothelial LRP1 transports amyloid- β 1-42 across the blood-brain barrier. *J Clin Invest*. 2016;126(1):123-136. doi:10.1172/JCI81108
225. Hladky SB, Barrand MA. *The Glymphatic Hypothesis: The Theory and the Evidence*. Vol 19. BioMed Central; 2022. doi:10.1186/s12987-021-00282-z
226. Mestre H, Mori Y, Nedergaard M. The Brain's Glymphatic System: Current Controversies. *Trends Neurosci*. 2020;43(7):458-466. doi:10.1016/j.tins.2020.04.003

Acknowledgements

Completing a PhD is often described as a solitary journey, and in many ways, it truly is. Despite being part of a bustling university and a lively academic community, each PhD experience is uniquely personal, shaped by individual challenges, triumphs, doubts, and hopefully some discoveries. Over the years, there were several moments of struggle and uncertainty about the next steps. In these difficult moments, it's easy to question yourself and wonder if this long road will ultimately be worth it. Reflecting back now, however, I realize that what made this journey truly meaningful wasn't just the science, it was the people who surrounded me along the way.

First of all, I want to thank my supervisor, Iben Lundgaard, for giving me the opportunity to work in this fascinating field and for providing me with the freedom and trust to pursue my ideas and develop as a scientist. Thank you for believing in me. Your encouragement and willingness to listen when things got tough made all the difference. I also wish to thank my co-supervisor, Anja Meissner, for our productive meetings and your insightful ideas.

To my fellow PhD students in the lab, with whom I shared countless chats and cups of coffee over the years, along with many celebrations and moments of frustration, thank you. Marta, for all the cozy dinners and for always being up for an adventure; Roberta, for all the fun times at conferences; Nic, for the enjoyable sauna chats and beers in Malmö. Tekla, thank you for always being there and keeping our group active and Na, thank you for your inspiring dedication. Sharing our struggles and successes created a sense of community that made even the hardest days feel manageable. I'm so glad that I had the chance to work alongside you all, and even happier that I still have you in my life outside the lab.

Nagesh, thank you for teaching me so much and always believing in me. This thesis wouldn't be possible without you. Kelley, thank you for your scientific rigor, the inspiring scientific discussions, and for the even more meaningful lunch chats on the balcony. Jari, thank you for the collaboration and support. I am sure that each of you will succeed in your next steps, whatever they may be.

To the amazing team of the Lundgaard lab: Sam, Chenchen, Denys, Xuanhui, Oksana, Max, Emily, Arzu, Shiqiao, and everyone else who passed from our lab over the years, thank you for creating a cozy environment that I will definitely miss.

Lotte, thank you for our wonderful collaboration and great chats both inside and outside BMC. René, thank you for introducing me to the world of MRI and for brightening up those endless hours with interesting conversations. Michael and Sebastian, thank you for training me and for always being willing to help whenever I bugged you with troubleshooting questions.

To all the fantastic collaborators who made this work possible, and especially to Marko Rosenholm, Yuan Yao and Kimberly Boster, for their critical assistance. Special thanks also go to Maiken Nedergaard for her invaluable knowledge and insightful comments.

Working in Lund and living in Copenhagen might seem like an odd decision at first glance. Although crossing national borders, the distance itself isn't that great (or can be, depending on the whims of the railway system). Although I was sometimes frustrated by this commute, especially after long days in the lab, I never doubted the decision to live on the other side of Øresund. For this, I must thank my friends, the ones who make my everyday life in Copenhagen such an amazing experience. These people who patiently listened to me talking about obscure topics they knew little about, who offered distractions when I desperately needed a break from my own thoughts, and who reminded me that life exists beyond papers and deadlines. Your support kept me grounded in reality and provided much-needed balance during intense periods. Most of all, thank you for making Copenhagen the place that I can call home.

I also wish to thank my friends in Greece, who have been part of my life throughout this journey, and all previous ones, and whom I greatly miss. You make every trip back home filled with beautiful memories. Even though our daily lives are less intertwined than they once were, I still feel close to you all, and I'm glad that Copenhagen has now become part of your lives too.

Στην οικογένειά μου, σας ευχαριστώ για την αγάπη και την υποστήριξή σας, που αποτέλεσαν το θεμέλιο μου καθ' όλη τη διάρκεια αυτής της διαδικασίας. Μαμά και μπαμπά, είμαι βαθιά ευγνώμων που με ενθαρρύνετε σε κάθε νέο βήμα της πορείας μου. Γιορτάζατε κάθε μικρή νίκη με γνήσιο ενθουσιασμό και σταθήκατε δίπλα μου στις στιγμές απογοήτευσης ή δυσκολίας. Μου υπενθυμίζατε συνεχώς ότι η αξία μου δε περιορίζεται σε ακαδημαϊκά επιτεύγματα. Σας ευχαριστώ και τους δύο που με κάνατε τον άνθρωπο που είμαι σήμερα.

To Lily, my partner throughout this journey and in life, none of this would have been possible without your love and support. Thank you for always believing in me and standing by my side during both the good times and the challenging ones. I look forward to seeing where life takes us next.

So, in the end, despite all its ups and downs, this PhD journey has absolutely been worth it. Not just because of what I've learned academically, but because of all of you who made this experience rewarding and unforgettable.